Improving culvert performance

Reducing energy losses by streamlining the entrance and exit of culverts.

Jordy van Vliet

TUDelft

Witteveen + Bos

Improving culvert performance

Reducing energy losses by streamlining the entrance and exit of culverts.

By
Jordy van Vliet

To obtain the degree Master of Science
at the Delft University of Technology,
in Civil Engineering specialised in Water Management.
To be defended publicly on March 19th, 2024

Student number:	4705440
Project duration:	January, 2023 - March, 2024
Graduation committee:	
Prof.dr.ir. R. Uijlenhoet	TU Delft - Water Resources
Dr.ir. O.A.C. Hoes	TU Delft - Water Resources
Prof.dr.ir. W.S.J. Uijttewaal	TU Delft - Environmental Fluid Mechanics
PhD.ir. D. Wüthrich	TU Delft - Hydraulic Structures and Flood Risk
Ir. A.L. de Jongste	Witteveen+Bos
Ing. M. Heinhuis	Hoogheemraadschap Delfland
Cover:	Artwork created with Artifical Inteligence engine.

An electronic version of this thesis is available at http://repository.tudelft.nl/.

Preface

This thesis is the final deliverable of my graduation research for the Master of Science in Civil Engineering at Delft University of Technology. Conducted in collaboration with Witteveen+Bos, this research leverages their expertise in OpenFOAM modelling. The overarching objective is to investigate the feasibility of fitting a profile onto existing culverts and bridges to mitigate energy losses, consequently extending their lifespan, and preventing premature replacements.

I want to express my sincere gratitude to everyone who played a crucial role in the development and completion of my master thesis. First and foremost, I extend my heartfelt thanks to Olivier Hoes. Our initial contact over a year ago marked the beginning of an inspiring journey. His enthusiasm for the social relevance of the research problem was contagious, and I am truly grateful for his unwavering support. Olivier consistently made time to address my queries and provided valuable feedback that significantly shaped the outcome of this thesis.

I would also like to express my special thanks to the entire team at Witteveen+Bos. Your warm welcome made me feel an integral part of both the company and the group. I am particularly grateful to Leon de Jongste for his guidance in navigating the complexities of the OpenFOAM software. Our weekly meetings about my progress were instrumental in refining the direction of my research. To Remko Uijlenhoet, I extend my appreciation for serving as the chair of my committee. Your insights and guidance were pivotal in ensuring the academic rigour of my thesis. Maurits Ertsen, thank you for your thoughtful feedback on my draft version, enhancing the overall flow of my thesis. A special mention goes to Davide Wüthrich and Wim Uijttewaal for generously sharing your expertise on energy losses and turbulence modelling. Your insights greatly enriched the depth of my research.

Finally, my sincere thanks to Martijn Heinhuijs of Hoogheemraadschap Delfland for being a valuable contact in exploring the practical applications of my idea. Your support has added a practical dimension to my academic pursuits.

I am profoundly grateful to each one of you for your contributions, guidance, and encouragement throughout this journey. Your collective efforts have been instrumental in the successful completion of my master thesis.

Besides my graduation committee, I would like to thank my family, friends, and colleagues for keeping me motivated and giving me the support I needed during this research. It means a great deal to me!

Jordy van Vliet

Krimpen aan de Lek, March 2024

Summary

In Dutch polders, numerous structures like bridges, weirs, culverts, and pumping stations have been constructed over centuries to manage water levels. These structures play a crucial role in maintaining water levels within predefined targets. The flat topography of the Dutch landscape combined with the collective impact of head losses, induced by these structures may result in flooding of polders during high runoff scenarios. Over time, culverts and bridges may underperform due to alterations in the water system, increased pressure from climate change, evolved design rules, insufficient maintenance, and shifts in land use.

A challenge is the potential hydraulic underperformance of structures and the need for their premature replacement, which is costly. Waiting until the end of their technical lifespan may contribute to floods. Therefore this thesis focuses on improving existing structures to mitigate the need for replacement, specifically by streamlining inlet and outlet openings to reduce energy losses. This leads to the research question of this thesis: *"How can the head loss over existing (too tight) culverts be minimised by adding an inlet or outlet profile and does this lead to a substantial enhancement in the performance of these culverts, providing a practical option to postpone the replacement of underperforming culverts?"*

To answer this question, the problem is explored by looking into the fundamentals of energy losses, including entrance losses, friction losses, and exit losses. This gives an understanding of the conditions under which these losses manifest. However, these basic calculations have inherent limitations due to their reliance on predefined coefficients. This renders them inadequate for evaluating the effects of introducing new profiles onto an existing structure.

To overcome this, a flume experiment has been performed to verify whether it is possible to measure water level differences for various profiles at the culvert entrance and exit. With a 3D Computational Fluid Dynamics (CFD) model (OpenFOAM), flows around different culverts are simulated. The results of the CFD model are compared to the flume experiment, after which the CFD model is used to simulate a variety of scenarios, with different profiles, culvert dimensions, velocities, and water depths.

As such, this thesis addresses challenges and uncertainties in quantifying head losses in culvert structures through experimental methods and CFD modelling. Experimental setups struggle with controlling all flow-influencing parameters, while CFD modelling offers flexibility but requires careful consideration of uncertainties and limitations. The discussion emphasizes the complexities of comparing experimental and model results, highlighting trade-offs and uncertainties in each approach.

The conclusion answers the central research question, confirming that specific profiles added to culverts can significantly reduce entrance losses up to 65%, thereby lowering headwaters for a constant discharge.

The recommendations section outlines possibilities for further research, including optimizing profile dimensions and conducting sensitivity analyses of influential parameters. Practical recommendations involve aligning large-diameter concrete culverts with the socket end in the flow direction and integrating groove or rounded profiles during construction for cost-effective inlet loss reduction.

Table of Contents

1. Introduction

1.1 Problem statement

In Dutch polders, a high density of bridges, weirs, culverts, and pumping stations can be found. Culverts in particular are very common, see Figure 1. Over the past centuries, these structures have been constructed to enable human activities. Dutch water boards make use of these structures to manage water levels within polders. To maintain water levels at pre-defined targets, water is let in when the water level falls below the target and is drained if it is above the target (*'Streefpeil'* in Dutch).

Figure 1: Allotment of meadows in the Krimpenerwaard, with all entrances to the meadow patches each having a culvert under the road indicated by the red stripes (Swart, S, 2021).

The Dutch landscape is very flat and thus reducing the hydraulic losses per structure is important. The cumulative effect of a series of structures in a watercourse can cause high water levels upstream in the polder as shown in Figure 2. Due to energy losses, the headwater depth is higher than the tailwater depth. The energy loss depends on the dimensions and shape of the structure. In practice, culverts and bridges are designed with a per-structure water level difference of just a few millimetres between the head and tailwater.

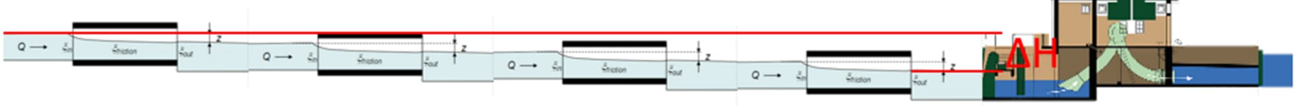

Figure 2: Water level difference across 4 structures, with pumping station on the right-hand side (Waterschap AGV, n.d.).

Over time, culverts and bridges may undergo a decline in performance, even if they were adequately dimensioned during the design phase. This deterioration could lead to an undesirable increase in the water level difference. Many existing culverts and bridges in the Netherlands are expected to underperform in the near future due to factors such as:

1. **Alterations in the water system:** Changes in the network of canals and the construction of new dams or canals can disrupt the original hydraulic balance.
2. **Increased pressure on existing water system:** Due to climate change more frequent heavy showers are predicted in which more water will precipitate in a shorter time frame which leads to an increased discharge demand (IPCC, 2021).
3. **Evolved design rules:** Old culverts and bridges are dimensioned with different design rules which may no longer align with contemporary standards.
4. **Insufficient maintenance:** Lack of capacity for maintenance can result in the accumulation of sludge or debris in the structure. This reduces the flow area in the structure and thus the flow capacity.
5. **Shift in land use from rural to urban:** Urbanisation leads to more impermeable surfaces causing faster and increased runoff from precipitation to the water system.

These factors indicate a growing need to replace structures before reaching the end of their technical and economic lifespan, which means replacement comes earlier than foreseen. All water boards have a yearly reservation to replace structures prematurely. However, a too-early replacement of many under-dimensioned structures with a larger one is simply too expensive. Conversely, delaying replacement until the end of their lifespan raises the risk of contributing to significant floods caused by underperforming structures. Extending the lifespan of these structures without the need for replacement by minimizing their head loss, could potentially prevent substantial expenses associated with updating water systems.

1.2 Objective and research question

The primary goal of this thesis is to investigate whether reducing energy losses around culverts can extend the lifespan of structures and prevent early replacement. The focus of the study is on streamlining existing culverts to minimize inlet and exit losses. Given that these culverts are already constructed, the approach involves introducing supplementary profiles to enhance hydraulic performance without altering their base structure. This leads to the following research question:

"How can the head loss over existing (too tight) culverts be minimised by adding an inlet or outlet profile and does this lead to a substantial enhancement in the performance of these culverts, providing a practical option to postpone the replacement of underperforming culverts?"

Initially, the locations where energy is dissipated around a culvert are explored to gain insight into where and why energy is lost, for this analysis the energy balance is employed.

Next, an analysis of all registered culverts in the Netherlands is performed from which the most common culvert type is found. This serves as a reference throughout the thesis to illustrate the impact of various solutions. Subsequently, the functioning of Dutch polders is explored to shed light on the issue of head loss in Dutch polders and the influence of culverts.

To address the research question an analysis of previous research on the streamlining of culverts is performed. By analysing three papers by Jaeger et al. (2020), Nassralla (2015) and Nam et al. (2013) insight into promising profiles is gained. This is followed by the synthesis of different culvert profiles that are used throughout the thesis.

To assess whether the hydraulic behaviour of culverts can be measured in practice, experiments were conducted in a TU-Delft flume. Various profiles were introduced at the rectangular culvert's entrance and exit under different discharge conditions. The objectives of the flume experiment are twofold: to confirm whether alterations in geometry affect the flow and to determine if a reduction in head loss is achievable.

Following this, the study delves into the application of Computational Fluid Dynamics (CFD) to evaluate its suitability for simulating flow around rectangular culverts. Additionally, it aims to investigate how different flow velocities and profiles influence fluid behaviour.

The data from the flume experiment and the CFD simulation are then compared to verify the functionality of the CFD model. This involves comparing empirical results and visual cues, demonstrating the potential for software analysis of hydraulic parameters, including discharge, water depth, velocity, and profile, without the need for physical experiments in a flume.

Lastly, simulations for circular culverts with varying diameters and profiles at the inlet and outlet are conducted, adjusting discharge and water depths. The objective is to discern the circumstances under which the use of profiles proves advantageous and to what extent they contribute to the mitigation of losses.

1.3 Structure of thesis

This thesis is set out as follows. Section 2 delineates the thematic framework: Section 2.1 commences with a general introduction of energy losses around culverts, succeeded by the common culvert dimensions and material in Section 2.2. Subsequently, Section 2.3 explains how a Dutch polder system operates, thereby clarifying the problem statement. Section 2.4 conducts a literature review on culvert streamlining. Lastly, Section 2.5 synthesizes the profiles that are used throughout the thesis.

Section 3 unfolds the empirical investigations: Section 3.1 commences with a description of the flume experiment conducted on a rectangular culvert, detailing the experimental setup, methodologies for data quantification, results, and reflective analysis. Section 3.2 addresses the (CFD) model employed for a rectangular culvert, highlighting its configuration, methods for result quantification, obtained results, and insights. Section 3.3 compares outcomes from both the flume experiment and the CFD model, juxtaposing visual observations and quantitative findings of the head losses around a culvert. To deepen insights, Section 3.4 presents a CFD model developed for a circular culvert, unveiling results obtained across various combinations of culvert diameters, profile shapes and velocities.

Section 4 contains the discussion, interpreting the results while addressing the limitations of the model and the study. Concluding remarks are provided in Section 5, followed by recommendations for future research and implications of culverts in practice in Section 6.

2. Culverts

2.1 Energy losses around culverts

To comprehend the energy dissipation around a culvert, an energy balance is employed to identify the points where losses occur. A more in-depth analysis of local and minor losses is presented in Appendix A. This examination will focus on the submerged flow of a culvert, a scenario that occurs during high-flow conditions.

The total energy head loss (ΔH_L) due to flow passing through the culvert is made up of the entrance loss (ΔH_e), the friction losses through the barrel (ΔH_f), and the exit loss (ΔH_o). The total head loss is summarized in equation (1). The total energy loss is formulated as a product of the coefficient for entrance, friction and exit loss and the culvert velocity. This ensures the summation of loss coefficients, as all losses are expressed using the culvert velocity.

$$\Delta H_L = \Delta H_e + \Delta H_f + \Delta H_o = \left(k_e + f * \frac{L}{D_{culvert}} + k_o\right) * \frac{v_{culvert}^2}{2g} = \sum \xi \frac{v_{culvert}^2}{2g} \quad (1)$$

$\Delta H_{e,f,o}$:	Energy loss of the entrance, friction, and exit.	[m]
$k_{e,o}$:	Loss coefficient for the entrance and exit	[-]
f:	Darcy-Weisbach friction factor	[-]
L:	Length of the culvert	[m]
$D_{culvert}$:	Diameter of the culvert	[m]
$v_{culvert}$:	Average velocity in the culvert	[m/s]
g:	Acceleration due to gravity	[m/s^2]
ξ	Sum of all loss coefficients	[-]

Equation (1) is graphed across a spectrum of loss coefficients (ξ) that are realistically encountered in the field, spanning from 0.8 to 1.6. For the culvert velocity, a range from 0 to 1 m/s is used which are again realistic values. This offers insights into the impact of the loss coefficient on head loss across different culvert velocities.

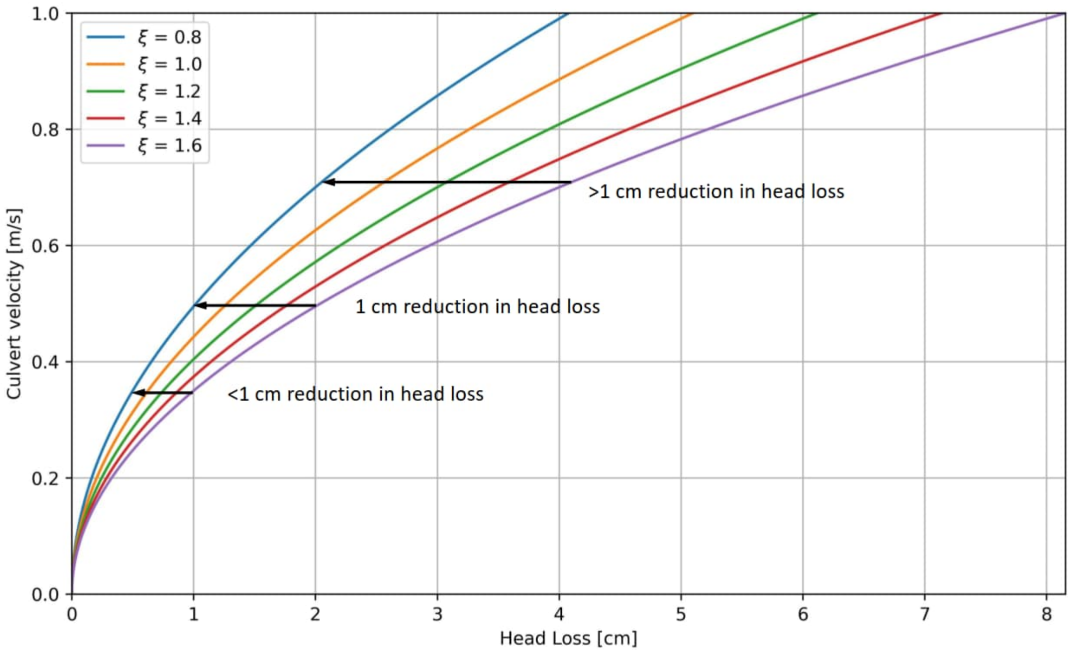

Figure 3: Plot of equation (1) for a range of loss coefficients (ξ) [0.8 - 1.6] for a culvert velocity from 0 to 1 m/s, in which the head loss across the culvert is expressed in cm.

Figure 3 illustrates the non-linear relation between culvert velocity and head loss. Moreover, increasing the loss coefficient increases the head loss for a given velocity. This suggests two potential approaches for reducing head loss, a reduction of the velocity and a reduction in the loss coefficient. Within the context of polder water systems, where culverts are integral components for draining excess water, reducing flow velocity is impractical, as it risks flooding within the polder. Therefore, focusing on minimizing the loss coefficient presents a more viable solution. If for example the loss coefficient is reduced from 1.6 to 0.8 the effect on the head loss is dependent on the culvert velocity. For higher culvert velocities the reduction in head loss is larger as demonstrated by the black arrows in Figure 3, thus reducing the loss coefficient is especially useful at hight flow velocities, which are exactly the instances in which flooding occurs.

To achieve a reduction in the loss coefficient, a deeper understanding of the factors influencing the loss coefficient is crucial. In Figure 4 a cross section of a culvert is shown in which six sections of importance are marked regarding the losses around a culvert. This figure includes the Energy Grade Line (EGL) which indicates the total energy head (H). The Hydraulic Grade Line (HGL) indicates the pressure head (h). The orange lines indicate the expression of the kinetic energy ($\frac{v_i^2}{2g}$), which is the difference between the total energy head and the pressure head.

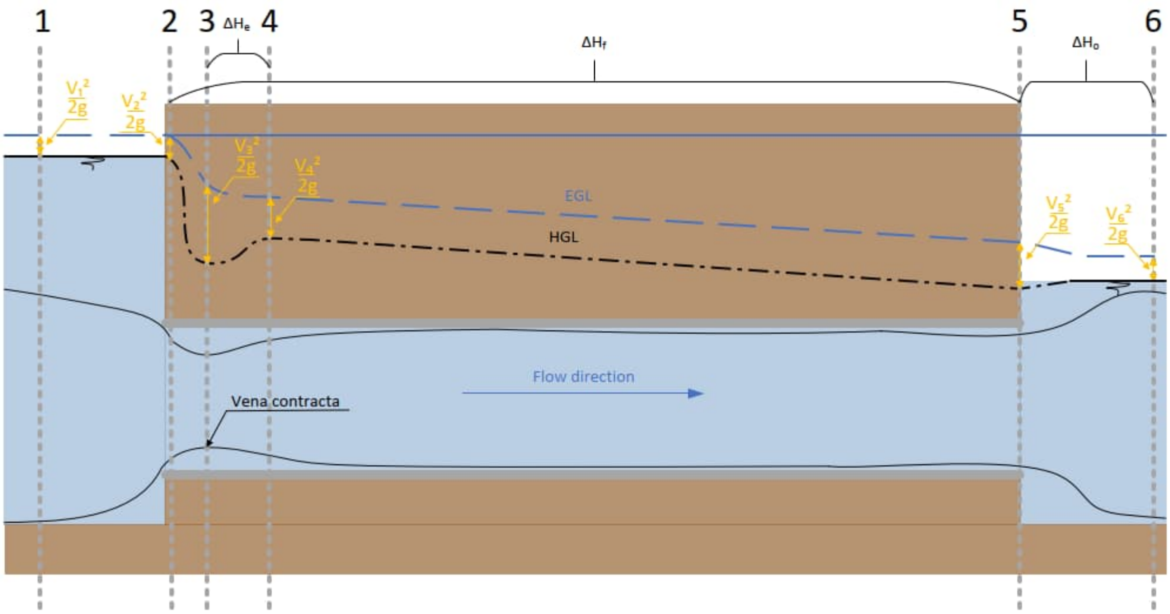

Figure 4: Cross section of a submerged culvert with six different locations in which the flow losses are indicated. EGL is the Energy Grade Line. HGL is the Hydraulic Grade Line. The orange lines indicate the velocity head. The grade lines and therefore the velocity head are exaggerated and not to scale, facilitating clearer observation of the processes in a culvert.

The entrance loss (ΔH_e) is located at the upstream end of the culvert between sections 3 and 4, where the flow undergoes deceleration downstream of the vena contracta. Illustrated in Figure 4 by a decline in velocity head, transitioning from $\frac{v_3^2}{2g}$ to $\frac{v_4^2}{2g}$. The large velocity head at section 3 originates from the accelerating flow caused by the contraction.
The Friction loss in the culvert occurs between sections 2 and 5 as denoted by the downward-sloping Hydraulic Gradient Line (HGL) and Energy Gradient Line (EGL) depicted in Figure 4, symbolised by ΔH_f.

Lastly, the exit loss (ΔH_o) occurs between sections 5 and 6 where a sudden expansion leads to a reduction in fluid velocity, inducing energy losses. The energy losses are caused by the decelerating flow as well as eddies that extract energy from the flow. The decrease in kinetic energy causes a corresponding increase in potential energy which results in an overall drop in total energy, as indicated in Figure 4.

2.2 The common culvert

In this section the results of a statistical analysis of all culverts in the Netherlands are shown, this includes information about the common culvert and culvert shapes found. For more statistics on Dutch culverts, readers can refer to Appendix B.

The dataset compiled from the 21 waterboards[1] across the Netherlands reveals the registration of 590,000 culverts, with complete data available for 500,000 culverts, as illustrated in Figure 5 (left). The abundance of culverts can be explained by the fact that it is not uncommon to find 400 culverts within a single polder in Dutch landscapes, as illustrated in Figure 5 (right). The combined length of all Dutch culverts exceeds 8000 kilometres.

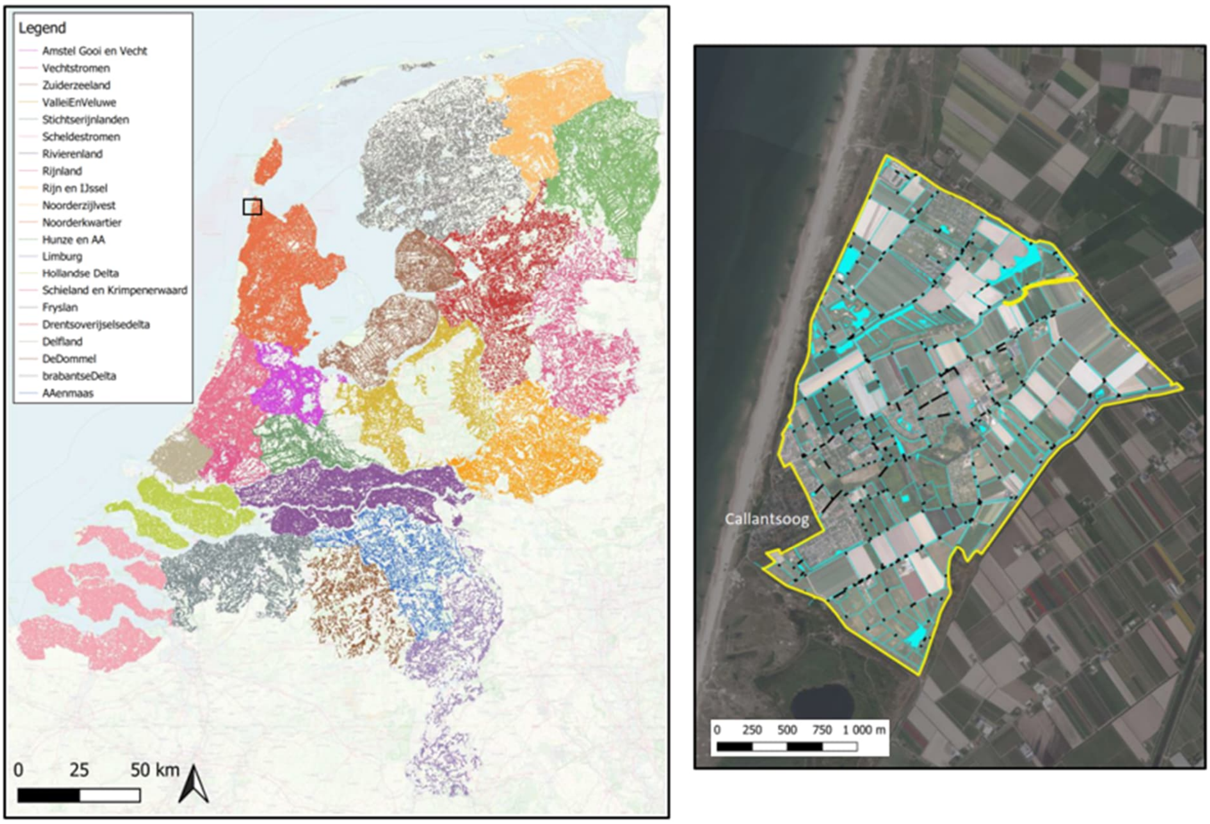

Figure 5: The left image shows a map of the Netherlands in which culverts of the 21 waterboards are shown, the different colours highlight the different waterboards of the Netherlands. The empty spots in the centre of the Netherlands are the Utrechtse Heuvelrug and Veluwe, these are the two high-lying sandy areas of the Netherlands without surface water. The black square indicates the location of the zoomed frame on the right, a polder near Callantsoog is shown which has 400 culverts in an area of 700 hectares.

[1] The 21 waterboards of The Netherlands: Hoogheemraadschap De Stichtse Rijnlanden, Hoogheemraadschap Hollands Noorderkwartier, Hoogheemraadschap van Delfland, Hoogheemraadschap van Rijnland, Hoogheemraadschap van Schieland en de Krimpenerwaard, Waterschap Aa en Maas, Waterschap Amstel, Gooi en Vecht, Waterschap Brabantse Delta, Waterschap De Dommel, Waterschap Drents Overijsselse Delta, Waterschap Hollandse Delta, Waterschap Hunze en Aa's, Waterschap Limburg, Waterschap Noorderzijlvest, Waterschap Rijn en IJssel, Waterschap Rivierenland, Waterschap Scheldestromen, Waterschap Vallei en Veluwe, Waterschap Vechtstromen, Waterschap Zuiderzeeland and Wetterskip Fryslân.

Regarding the shape of the culvert itself, circular is the most common shape (93%), followed by rectangular (5,3%), whereas shapes such as arch, elliptical, and triangular are far less common as shown in Figure 6 (Rahman, n.d.).

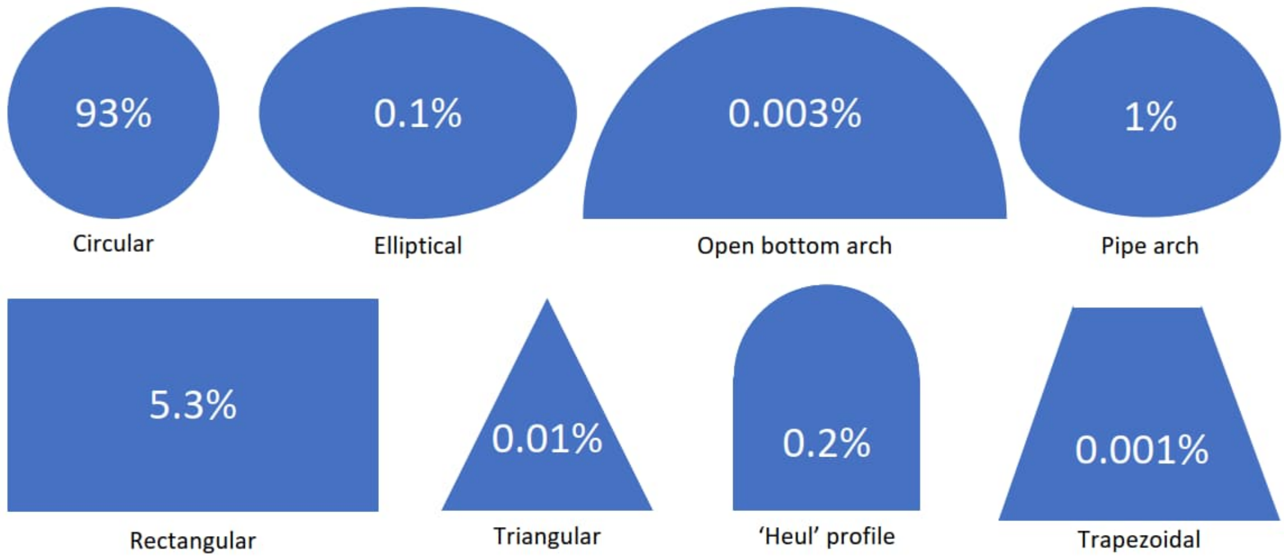

Figure 6: Culvert shapes employed in Dutch polders, based on all useable data collected from all waterboards. The percentage in the shape indicates the relative times a shape occurs based on available data (502,409 culverts).

Furthermore, other lessons are drawn from the culvert data which are summarised below.

- Circular culverts with a diameter of 0.3, 0.5, and 0.6 meters are most employed, accounting for respectively 16, 28 and 13% of the circular culvert data.
- The most common length of a circular culvert is eight meters (13,000 culverts or 3% of all circular culverts).
- The most common length of a non-circular culvert is six meters (3,291 culverts or 3% of all non-circular culverts).
- 50% of circular culverts have a length smaller than 10 meters.
- Length data is missing for 62,413 culverts or 11% of all culverts.
- Shape data is missing for 86,614 culverts or 15% of all culverts.

To conclude, the focus of this thesis is on a circular culvert as these are the most prevalent. The common Dutch culvert is a circular culvert with a diameter of 0.5 meters, a length of 8 meters and made of PVC.

2.3 The Dutch polder system

In this section, the Dutch polder system is explained, which underscores the necessity of designing culverts for minimal head losses. Appendix C shows an example calculation that illustrates the influence of the number of culverts on the available head loss.
Dutch polders consist of water level compartments ('peilvakken' in Dutch) which are connected by watercourses, these compartments are shown in Figure 7 for the Oude Leede area. In each compartment, the responsible waterboard is committed to maintaining the water level at a pre-agreed level ('streefpeil'). Determining an optimal water level is challenging due to the diverse land uses each requiring a different groundwater level. The most optimal water level is a compromise, given that different land uses are spread within a compartment and the ground elevation is not uniform (Rijkswaterstaat, n.d.).

Figure 7: The left figure shows the water level compartments, indicated by the black lines and the different coloured shapes. In the shape, the agreed water level ('streefpeil') is mentioned. The area indicated is located Southeast of Delft around the A13 highway and Oude Leede (right) (Delfland, n.d.).

Overall the difference in water level between adjacent compartments is approximately between 20 and 60 cm as demonstrated in Figure 7 (left). Within this range, it is crucial to account for all losses to prevent unwanted water interaction between compartments.
One of the losses considered is friction in the watercourse. In practise watercourses are designed to a water level slope of approximately 4 cm per kilometre watercourse. In other words, a watercourse of 1 km has a friction head loss of 4 cm.
Additionally, structures such as culverts or bridges are designed for a maximum head loss of 4 to 5 mm per structure (Cultuurtechnisch Vademecum, 2000). For example, 10 bridges in series causes a cumulative head loss of 4 to 5 cm.
Weirs are employed to separate the water level compartment, these must remain in free flow, for this an additional height is needed to prevent the weir from becoming a submerged weir. The design discharge guideline for a Dutch polder is 10 m^3 min^{-1} $(100\ ha)^{-1}$ (Cultuurtechnisch Vademecum, 2000).

In Figure 8, three compartments are visualised in different flow conditions, for this a water level difference of 20 cm between the compartments is shown which shows the difficulty to manage head losses for small water level differences. In Figure 8A no water is flowing through the system. The water level across the compartment is constant since no energy losses occur. Figure 8B shows design flow conditions, in which energy losses occur in the system, these lead to a slight rise in the headwater level. The headwater rise however is small enough to keep the weirs in free-flowing condition.

Figure 8C shows extreme runoff conditions in combination with poorly designed culverts, here the headwater level of the downstream compartment 1 rises to such an extent that the tailwater of compartment 2 is influenced. The weir is not separating the water level between the compartments leading to floods in the upstream compartments 2 and 3. These floods occur because the discharge exceeds the capacity of the existing structures, resulting in an energy loss across the structures that is too large.

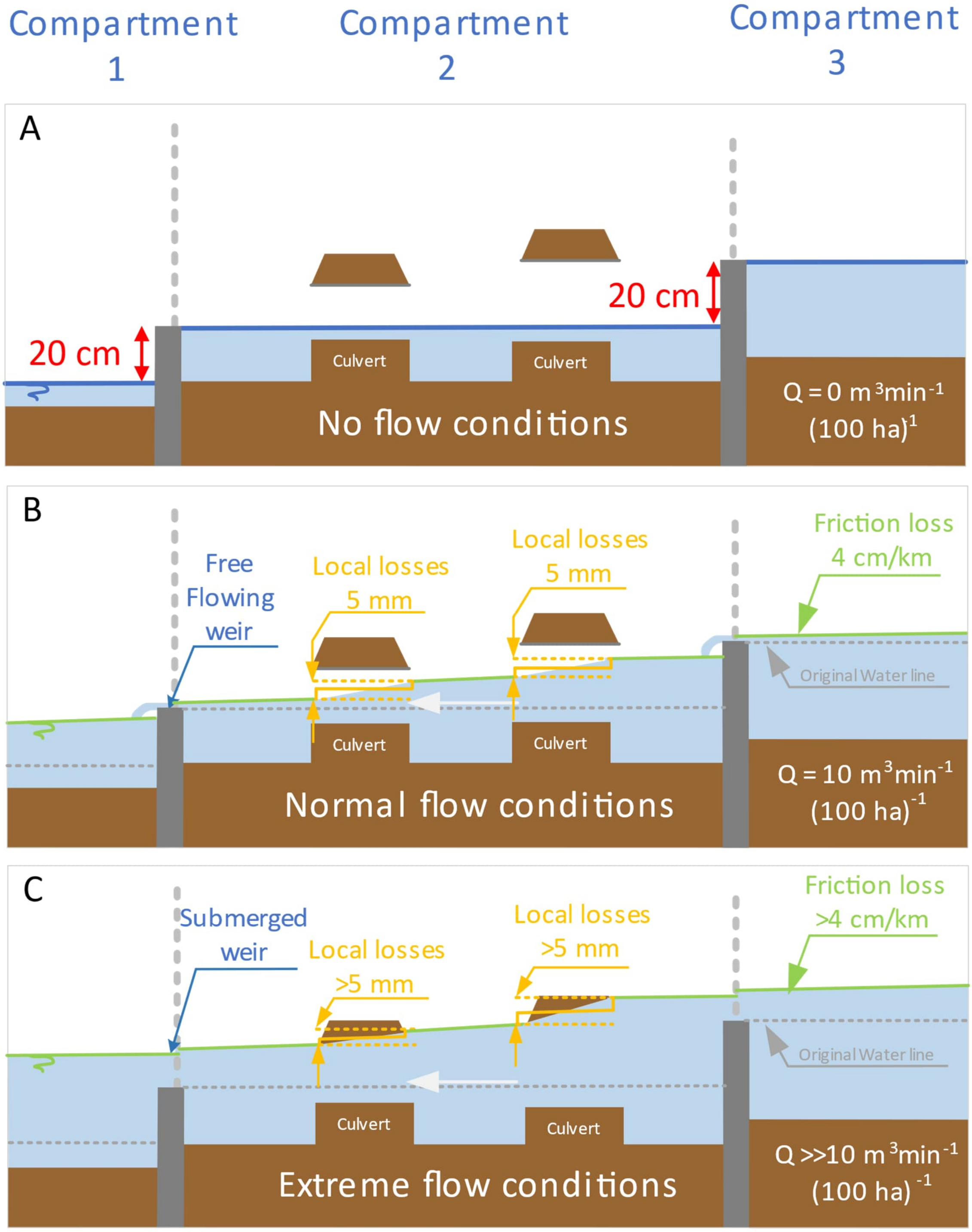

Figure 8: A) No flow conditions show that weirs are effective in separating the compartment water level. An example of 20 cm has been given. B) Normal flow conditions show an increase in the headwater of compartment 2. However, the weir is still free-flowing and separates the water levels between the compartments. C) Extreme flow conditions increase the water level in Compartment 1 and turns the weir into a submerged weir, which influences the water level in Compartment 2 and subsequently Compartment 3. Water level differences are not to scale and are dramatized to aid in visualising the differences.

2.4 Literature review

In this section previous research that has been performed on reducing losses around culverts is investigated, this lays the foundation for further research on this topic.
To start with the research of Jaeger et al. (2020), who's research aimed to improve the discharge capacity of existing culverts by adapting the water level downstream of the culvert. Raising the water level above the height of the outlet utilizes the entire cross-sectional area of the culvert for water flow. While it has been observed that this solution enhances culvert performance in certain cases, its application is not viable for Dutch polders. This is because raising the water level contradicts the restrictions imposed by the limited allowable head loss, rendering it impractical. Moreover, most culverts already operate in full flow conditions during high flow conditions since rainfall runoff raises the overall water level in the polder.
The study explored inlet modifications influencing culvert performance by CFD modelling and scaled experiments. These findings indicated that by adjusting the entrance design by using large rounded or 45° chamfer profiles, water flow increased while maintaining stable headwater levels. The study suggests that a rounded corner with a radius (r) of $0.2 * Width_{culvert}$ improved the flow rate by up to 20%. For chamfer edges with length (l), $0.25 * Width_{culvert}$ similar improvements are found, see Figure 9.

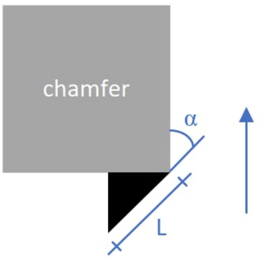

Figure 9: Notation of the length and angle of the chamfered edge, adapted from Table 3.1 (Jeager et al, 2020) Blue arrow indicates the flow direction, one side of the inlet structure is shown.

These experiments addressed scaled rectangular culverts in 2D scenarios. Scaling affects the hydraulic conditions and therefore the results (Novk and Belka, 1981). Furthermore, the transferability of his results to circular culverts is uncertain but essential since it is found that circular culverts are most common. Additionally, the study did not determine the exact loss coefficients for the different profiles, which means that the application of these profiles is difficult to quantify.

The research by Nassralla (2015) explores the impact of various profiles downstream and upstream of a circular culvert on the flow. Through 400 runs with varying angles and contraction ratios, the study identifies optimal configurations for minimizing losses during the transition from a free-surface channel to a pipe culvert and vice versa, as shown in Figure 10.

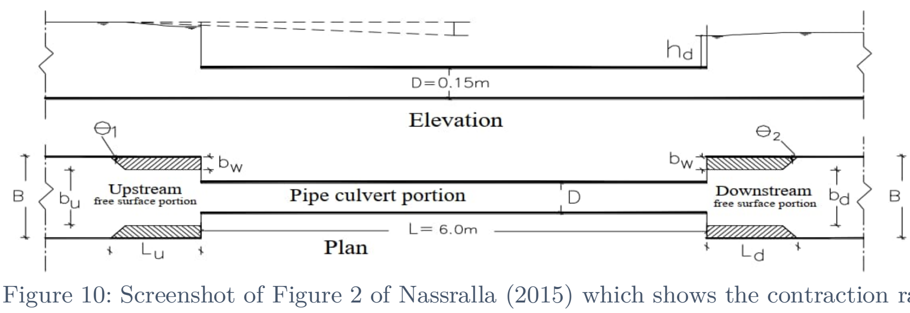

Figure 10: Screenshot of Figure 2 of Nassralla (2015) which shows the contraction ratio (b_u/D), angle θ_1 and θ_2, diameter D and the water depth above the culvert height h_d.

The findings include that increasing the width contraction ratio (b_u/D) reduces the entrance loss. This can be explained since the velocity difference before and within the structure decreases. Consequently, this diminishes the extent of deceleration downstream of the vena contracta and thus decreases the entrance loss.
The suggested improvements regarding the inlet and outlet profile of the culvert, conclude that the smallest entrance loss is found for $\theta_1 = 15°$, whereas $\theta_1 = 90°$ gives the highest entrance loss. Similarly for the exit losses, the θ_2=90° angle causes the largest losses, where the optimum was found for θ_2=60° (submergence ratios of $\frac{h_d}{D} = 0.2$) and θ_2=30° (submergence ratios of $\frac{h_d}{D} > 0.2$). This signifies that adding an angle to the in and outlet of the culvert can reduce the loss coefficient. Moreover, it confirms that the largest losses are found for square-edged culverts.
For lower values of Froude number ($Fr < 0.15$), the angle of sidewalls and the value of contraction ratios at the inlet and outlet of the pipe culvert had a small effect on local head loss. This implies that for the profiles to effectively reduce head loss, the flow velocity must be sufficiently high, which is the case during high runoff conditions.
The study indicated that raising the tailwater level led to a rise in exit loss, with minimal effects on entrance loss. This can be explained by the dissipation of the velocity head from the culvert during the sudden expansion with a larger cross-section. As a result, it increases the contrast between the velocity within the culvert and downstream of it, causing a greater reduction in velocity head and ultimately contributing to an increased exit loss. However, raising the tailwater level is unwanted in a Dutch polder due to the limited height available for head losses.

Experiments by Nam et al. (2013) investigated the influence of symmetry on head loss. A free-surface channel to a conduit was studied using diverse discharge levels and dimensions of a rectangular conduit attached to the downstream end of a free-surface channel as shown in Figure 11.

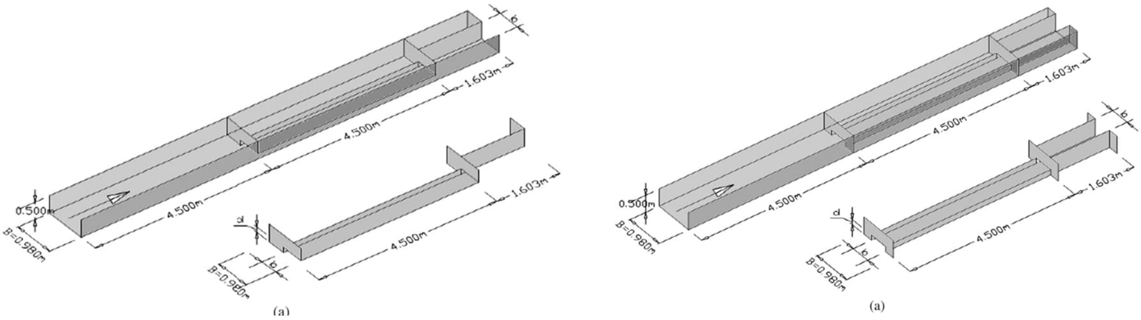

Figure 11: Screenshots of Figures 1 and 2 of Nam et al. (2013) which show an asymmetric channel on the left and a symmetric channel on the right.

The study produced analytical equations for the local head-loss coefficient in both symmetric and asymmetric rectangular culverts. It was observed that asymmetric culverts exhibit a 15% greater loss coefficient compared to their symmetric counterparts. Moreover, the asymmetric configuration consistently displayed higher maximum flow velocities during the transition from free surface to conduit. This suggests that the culvert's placement in the watercourse influences the loss coefficient and should be considered. In Dutch polders, culverts are usually symmetrically placed. However, when improvements are needed, ensuring symmetry within the watercourse can be one of the factors in reducing the loss coefficient.

The way a culvert is positioned into the watercourse also influences the local losses as proposed by Idel'chik (1960), and the U.S. Army Corps of Engineers (2016). The findings of these works include loss coefficients for differently shaped culverts (Appendix D). An example of the inlet loss coefficient (k_e) of different circular culvert is shown in Figure 12. Exit loss coefficients (k_o) are assumed to be constant at k_o = 1.

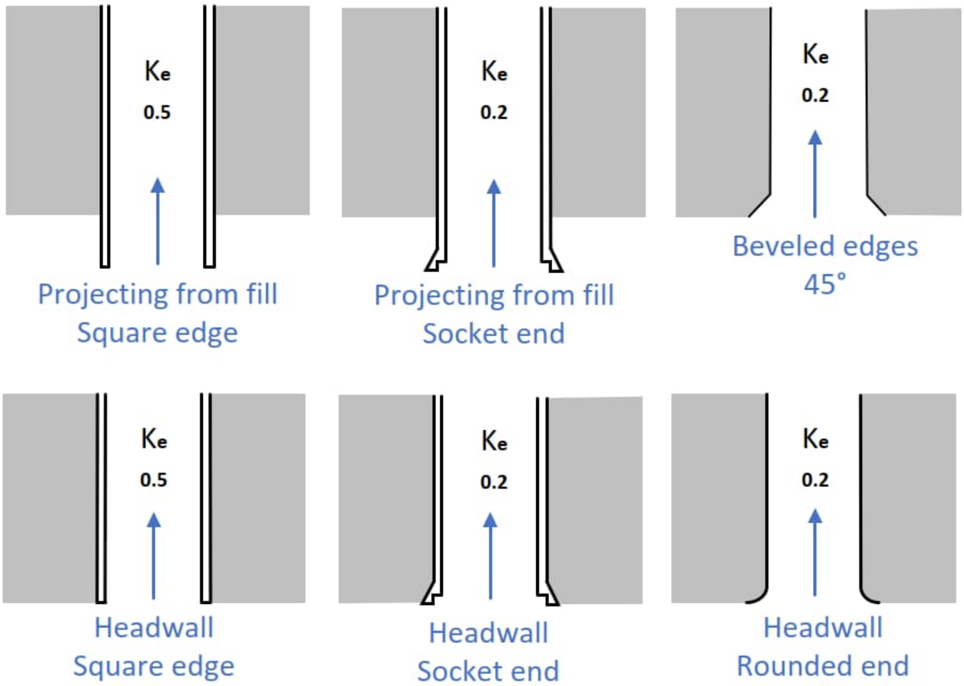

Figure 12: Different shaped circular culvert entrances, and their inlet loss coefficient adapted from Appendix D.

The applicability of these shapes is constrained by the fact that this thesis aims to add profiles to pre-existing structures, whereas Figure 12 shows that these shapes are an integral part of the structure, which might exhibit a different response for the loss coefficient. Nevertheless, these shapes provide valuable insights into the impact of such configurations on local losses. A notable observation from Figure 12, indicates that the inlet loss coefficient is 0.5 for both the headwall with a square edge and the one projecting from the fill. One could assume that the inlet loss for the projecting culvert is greater due to a larger volume of water being part of the recirculation zone and the necessity for water to change direction to a greater extent when compared to the 90° angle of the square edge.

2.5 Synthesis of applicable culvert profiles

Utilizing insights gathered from the literature review, various profiles have been formulated. These profiles are employed throughout this thesis and have been implemented in both rectangular and circular culverts. A cross-section of each of these profiles is presented below, along with an explanation of why these profiles were selected.

Square-edged inlet with headwall
The first profile that is defined is the most basic shape, a square-edged inlet with a headwall and serves as the base case against which all other profiles are compared. This shape is typically found and has not been streamlined in any way, see Figure 13. The shape is characterized by 90° angles at both ends of the culvert.

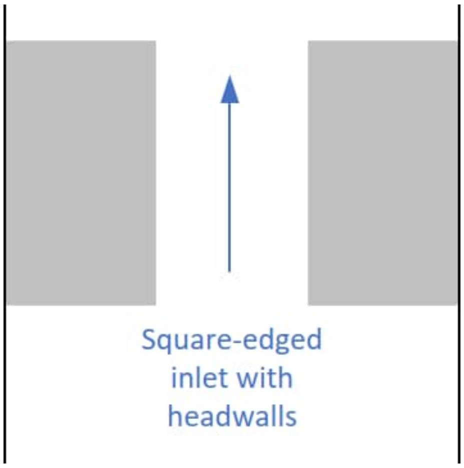

Figure 13: Square-edged inlet with headwall, characterised by 90° angles. The blue arrow indicates the flow direction.

Inlet with 45° wing walls
The simplest improvement to the inlet side is to add a 45° angle onto the inlet side of the structure (Figure 14).
Contrary to suggested by Jaeger et al. (2020) the profile has been applied to the full width of the watercourse. The principle is that the flow is guided to the contraction and reduces the possibility for recirculating flow zones to form.

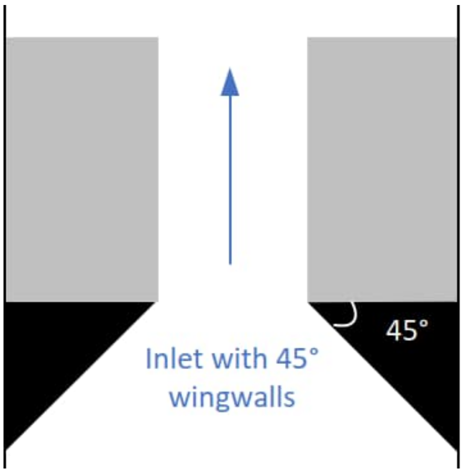

Figure 14: Addition of a 45° angle onto the inlet side of the structure. The blue arrow indicates the flow direction.

Gradual widening of the outlet

To minimize exit losses, a 2-meter-long guide is employed to streamline the sudden expansion at the outlet, as seen in Figure 15. This approach is based on the understanding that the flow from a sudden expansion requires approximately 8 to 10 times the width of the canal to properly widen. The design aims to strike a balance, creating an outlet adaptation that remains compact enough to occupy a small footprint. The primary goal is to prevent the formation of recirculation zones that can extract energy from the main flow.

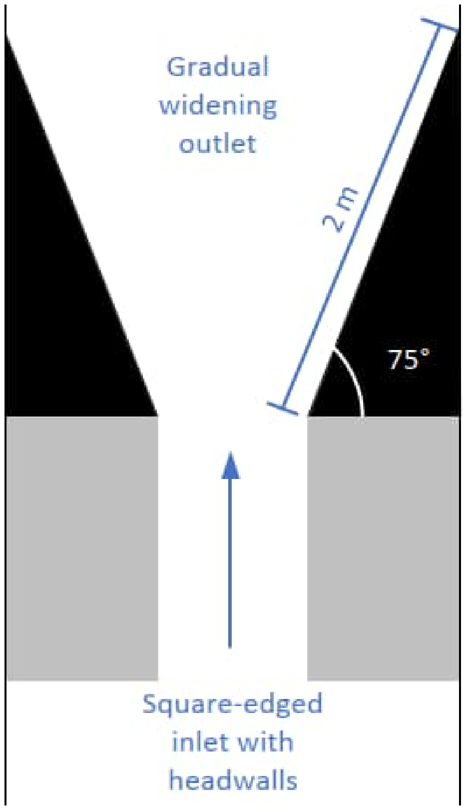

Figure 15: Inlet 90 degrees, with a widening at the outlet. The blue arrow indicates the flow direction.

Half round inlet

The next profile utilizes rounded corners, the application however is different than normally applied since the profile is added onto the culvert structure, as shown in Figure 16.

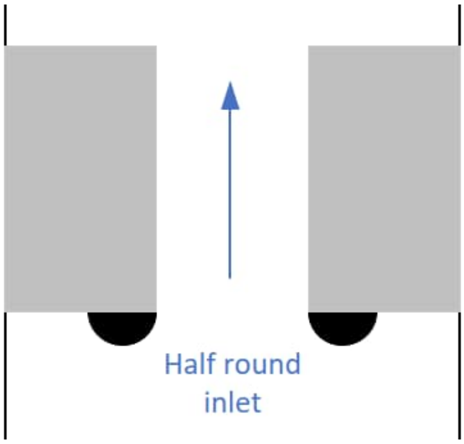

Figure 16: Half-round shaped culvert inlet. The blue arrow indicates the flow direction.

Groove end inlet with headwall
The groove end inlet suggested by Smith et al. (1995) consists of a short length of larger diameter pipe which projects upstream of the culvert. The principle is that the contraction happens before the culvert and aligns the streamlines with the culvert wall upon entry thereby decreasing entrance loss. The groove end inlet is shown in Figure 17.

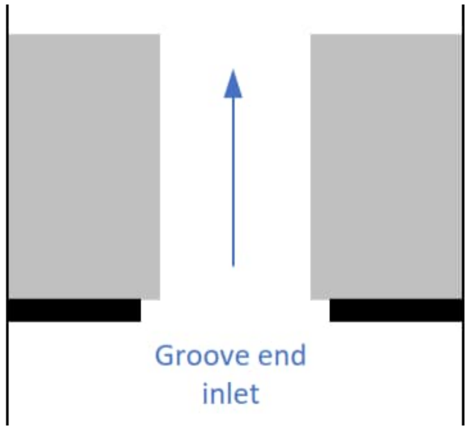

Figure 17: Groove end inlet geometry. The blue arrow indicates the flow direction.

Inlet with 45° wing walls and gradual widening outlet
This profile is a combination of a gradual contraction using a 45° wing wall and a gradual widening of the outlet objectively reducing the entrance and exit loss by streamlining both ends of the culvert as shown in Figure 18.

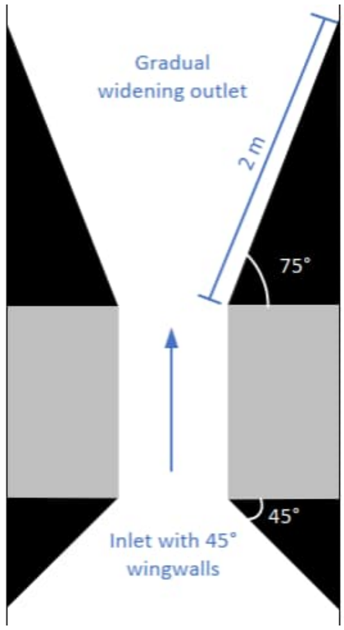

Figure 18: Inlet and outlet improvement using a 45 ° angle for the inlet and a 75° angle for the outlet. The blue arrow indicates the flow direction.

3.1 Flume experiment - rectangular culvert

In this section, the flume experiment is discussed. The experiments in the flume are conducted to verify whether alterations to the inlet and outlet geometry influence the flow and whether a reduction in the water level is measurable.

3.1.1 Setup of the flume experiment

The flume experiment was conducted in a TU-Delft flume constructed of concrete with a length (40 m), width (1.5 m) and height (1.3 m). At the upstream end, a stilling well provided a uniform velocity distribution over the cross-section as indicated in Figure 19. At 18 meters from the inlet, a 2-meter-long rectangular wooden structure with a contraction ratio of 3:1 was symmetrically placed resulting in a culvert width of 0.5 meters. By incorporating a realistic contraction ratio and opting for a rectangular culvert, the simplicity of the experimental setup was ensured. At the downstream end of the flume, a movable weir controlled the tailwater level in the flume between fully open and 10 cm closed.

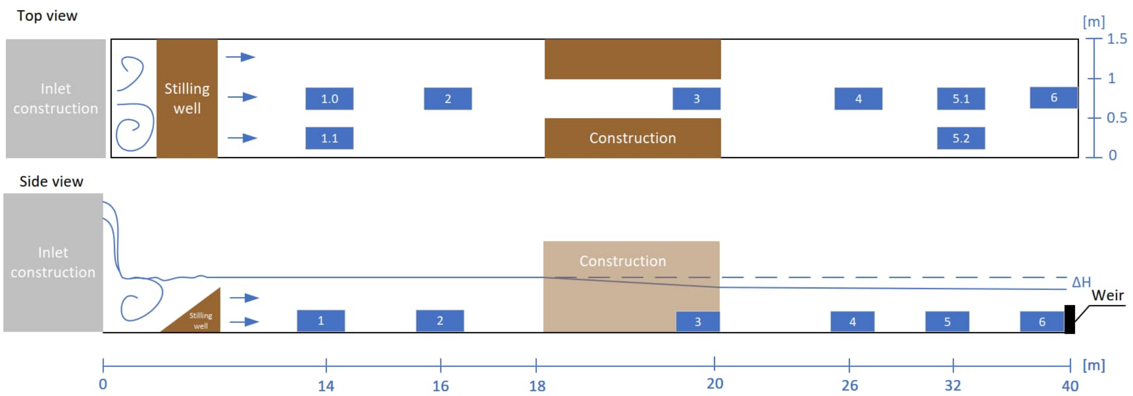

Figure 19: Top and side view of flume experiment: The left side shows the inlet construction with the stilling well to the right. The locations of the pressure sensors are indicated by the blue squares, these are located at the bottom of the flume. Between 18 and 20 meters the culvert is shown, at the end of the flume a moveable weir is shown.

To gauge the water level along the flume, eight locations (see Figure 19) were equipped with a pressure sensor with an accuracy of ± 5 mm (TD-Divers, van Essen instruments).
Velocity was determined using an Acoustic Digital Current meter with an accuracy of ± 0.25 cm/s (ADC from OTT Hydromet). At locations 1.0 and 3, the velocity was measured at 0.4 times the water depth (0.4H) in relation to the bed, as suggested by Pradhan et al. (2015) for obtaining the depth-averaged velocity.
In-situ depth measurements were conducted using a ruler with an accuracy of ±1mm. Velocity and depth measurements were then used to calculate the discharge, with an accuracy of ± 5-10% according to Le Coz et al. (2014).
To align the pressure sensors with each other, the flume was filled to a depth of 10 cm at the farthest upstream sensor location. After a waiting period of 2 minutes, during which the time was documented, this moment was identified as the baseline. The calibration procedure considers both the culvert slope and atmospheric pressure. The sensors were set to record data at one-second intervals.
Initially, a constant discharge was created in the flume, verified using the velocity area method. Subsequently, various profiles were introduced around the culvert, followed by a 5-minute waiting period to allow the water to reach a new equilibrium as suggested by Jeager et al. (2020). The time was recorded, and a 30-second measurement was taken, with the average value representing the water depth for that specific scenario.

3.1.2 Employed profiles in the flume experiment

The flume experiment incorporated a range of inlet and outlet profiles to examine their influence on hydraulic performance. The profiles used in the experiment are depicted in Figure 20, providing a visual representation of the configurations subjected to testing. These diverse profiles were synthesised from section 2.5 and provide a mix of inlet and outlet adjustments.

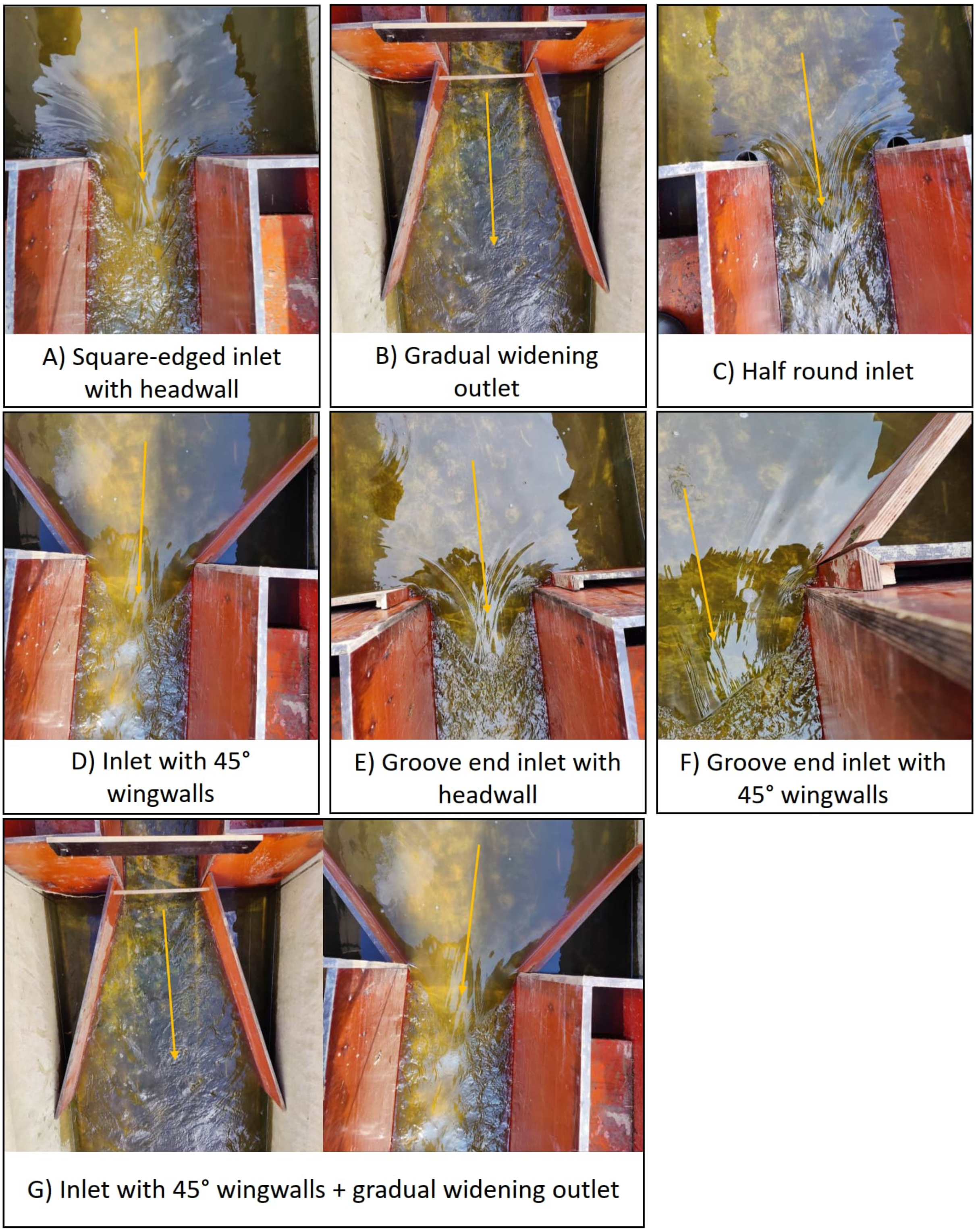

Figure 20: Top view of the profiles that are employed in the flume experiment, synthesised from section 2.5. Orange arrows indicate flow direction.

3.1.3 Quantifying the results of the flume experiment

To evaluate the influence of various profiles under different conditions, the water level difference across the structure is calculated. Specifically, Locations 1 and 3 (Figure 21) are strategically situated at the furthest distance from the culvert to ensure a consistent flow pattern. Utilizing depth and velocity measurements, the discharge is determined.

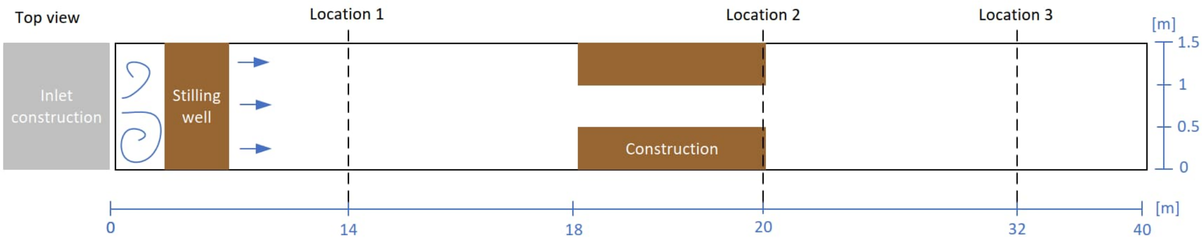

Figure 21: Locations 1 and 3 are used to calculate the water level difference across the culvert.

The findings are analysed across several dimensions. Initially, the visual cues are described such as alterations in the flow patterns and areas where water level fluctuations are noticeable. Subsequently, the water level differences across various culvert velocities are graphed, aiding in the visualization of how profiles influence the water level difference. Finally, the uncertainty in the results is explored, considering the precision of the measurements.

3.1.4 Results and reflection

In this section, the results of the flume experiment are shown and reflected on. First, the visual results are shown, followed by the water level difference across the structure for the various profiles. For detailed results on measured water level differences and velocity, please refer to Appendix E

Visual results

At the flume inlet (location 1, Figure 21), a uniform velocity was measured across the width, which was measured using the Acoustic Digital Current (ADC) meter. This observation confirms the effective operation of the stilling well.

At the culvert entrance, a contraction led to a noticeable drop in the water level, depicted in Figure 22 (left). The increased velocity, in accordance with Bernoulli's equation, caused the decrease in water level. Conversely, at the culvert exit, a slight rise in water level occurred due to flow deceleration.

Additionally, at the culvert's exit, as the stream expanded the Coanda effect caused the flow to align to one side (Panitz & Wasan, 1972). Using the ADC large velocities along one flume wall and negative velocities along the opposite wall are measured, which is shown in Figure 22 right. Downstream of the culvert the flow gradually widens but does not reach the full width of the flume. This would require increased friction or a longer downstream section of the flume.

Figure 22: Left: Water level drop at the entrance of the culvert. Right: Exit of the culvert with flow lines that visualise the Coanda effect.

Experimental measurement results – water level difference
During the flume experiment, different scenarios were tested. From these scenarios, the water level difference across the culvert is calculated between locations 1 and 3 (Figure 21) and plotted in Figure 23.

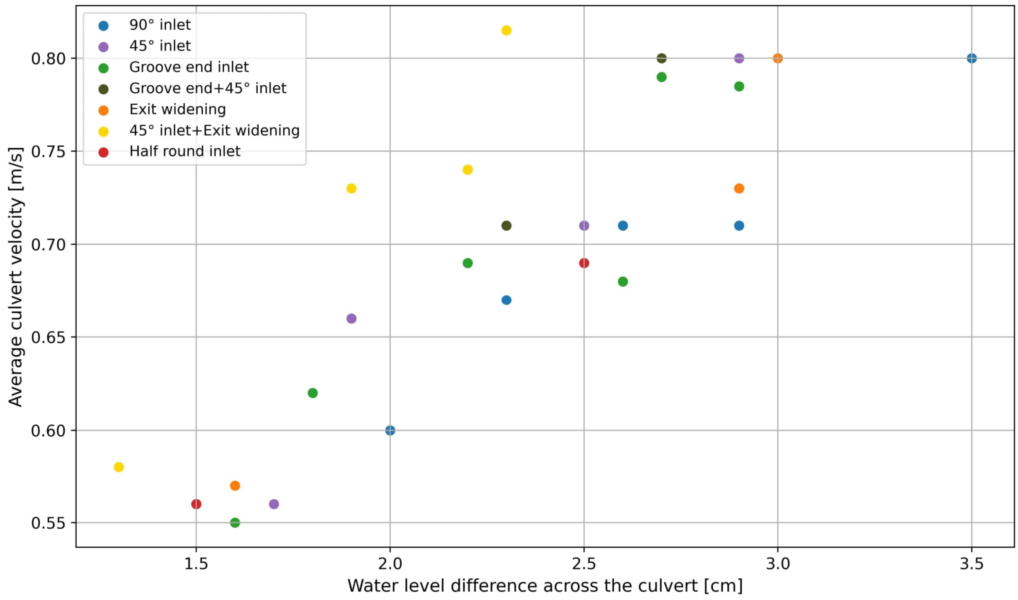

Figure 23: Results of the flume experiment, in which the average culvert velocity and the water level difference are plotted for the various experiments, with the legend indicating the culvert profiles.

From Figure 23 the average value is deduced for each profile as well as the minimum and maximum value, which are presented in Table 1. Moreover, the results in Figure 23 show an upward trend for water level difference and culvert velocity, which backs up equation (1), where the water level difference increases for higher culvert velocities.

Table 1: Water level differences across culvert profiles in flume experiment: average, minimum, and maximum values extracted from Figure 23.

	Profile	Average water level difference [cm]	Minimum water level difference [cm]	Maximum water level difference [cm]
A	Square-edged inlet with headwall	2.7	2	3.5
B	Gradual widening outlet	2.5	1.6	3
C	Half round inlet	2.0	1.5	2.5
D	Inlet with 45° wingwalls	2.2	1.7	2.9
E	Groove end inlet with headwall	2.0	1.5	2.9
F	Groove end inlet with 45° wingwalls	2.2	1.5	2.7
G	Inlet 45° wingwalls + gradual widening outlet	1.9	1.3	2.3

Table 1 shows that for the average, minimum and maximum values, the reference profile A is the worst performing. Whereas the other profiles decrease the water level difference across the culvert.

Comparison of all experiments – water level differences

Next, five scenarios with different discharge and water depth, and thus different culvert velocities are compared. The water level differences across the culvert between locations 1 and 3 of Figure 21 are summarized for each experiment in Table 2, providing insights into the reduction in the water level difference resulting from the addition of a profile.

Table 2: Water level difference [cm] for various profiles for different culvert velocities.

	Discharge [m3/s]	**0,076**	**0,1**	**0,12**	**0,075**	**0,094**
	Culvert depth [cm]	**27**	**30**	**34**	**21**	**24**
	Culvert velocity [m/s]	**0.56**	**0.67**	**0.71**	**0.72**	**0.78**
A	Square-edged inlet with headwall	2.0	2.3	2.6	2.9	3.5
B	Gradual widening outlet	1.6			2.9	3.0
C	Half round inlet	1.5			2.5	
D	Inlet with 45° wingwalls	1.7	1.9	2.2	2.5	2.9
E	Groove end inlet with headwall	1.6	1.8	2.2	2.6	2.8
F	Groove end inlet with 45° wingwalls	1.5			2.3	2.7
G	Inlet 45° wingwalls + gradual widening outlet	1.3		1.9	2.2	2.3

From Table 2, it is noticeable that the water level difference is largest for the square-edged inlet (profile A) which is the shape that is not streamlined. All other solutions show a decrease in water level difference in comparison to profile A. To quantify the difference, profile A is used as a reference to calculate the relative difference in Table 3.

Table 3: Relative reduction of water level difference with respect to profile A, adapted from Table 2.

	Discharge [m3/s]	**0,076**	**0,1**	**0,12**	**0,075**	**0,094**
	Culvert depth [cm]	**27**	**30**	**34**	**21**	**24**
	Culvert velocity [m/s]	**0.56**	**0.67**	**0.71**	**0.72**	**0.78**
A	Square-edged inlet with headwall	-	-	-	-	-
B	Gradual widening outlet	-20%			0%	-14%
C	Half round inlet	-25%			-14%	
D	Inlet with 45° wingwalls	-15%	-17%	-15%	-14%	-17%
E	Groove end inlet with headwall	-20%	-22%	-15%	-10%	-20%
F	Groove end inlet with 45° wingwalls	-25%			-21%	-23%
G	Inlet 45° wingwalls + gradual widening outlet	-35%		-27%	-24%	-34%

From Table 3, profile G gives the highest reduction in water level difference, this is the profile with an entrance and exit profile applied. Looking at profile B, where the exit loss is reduced by gradually widening the outlet the reduction is minimal. Moreover, all inlet-improved profiles showed a reduction between 10 and 25%, these results were anticipated since a reduction in entrance loss was intended.

Uncertainty in flume experiment

The assumption is made that the water level converges and remains stable. Data from the pressure sensors is used to calculate the standard deviation from the last minute of the measurement campaign (60 values). The average standard deviation for all sensors and cases is 0.2 cm, where the range is 0.1 – 0.4 cm, this would suggest that a stable water level is measured. On the other hand, looking at the differences between the minimum and maximum values in the same minute this is on average 0.9 cm with a range between 0.4–2.2 cm. This would suggest a bad precision of the pressure sensors, considering that the measured water level difference is in the same order of magnitude. Moreover, when the results between adjacent pressure sensors (1.0 and 1.1 or 5.1 and 5.2, from Figure 19) are compared a small variation is present of on average 0.3 cm, with a range between -0.3 to 1.8 cm. This means that either the water level between two adjacent sensors varies or the calibration of these sensors is insufficient. If the difference had been constant over time, it could be related to the sideward slope of the flume. However, the difference varies over time which suggests that the calibration is not accurate.

Assuming a constant discharge for the 5 different scenarios is justified as the deviation from the average discharge is between -5 and 6% which is between the suggested deviation of ± 5-10% by Le Coz et al. (2014).

3.2 CFD model – rectangular culvert

3.2.1 OpenFOAM

OpenFOAM is an open-source Computational Fluid Dynamics (CFD) software package used for simulating fluid flow. Using a suite of solvers and libraries different fluid flow problems (e.g. laminar flows, turbulent, multiphase, and compressible flows) can be addressed. It enables the analysis of fundamental principles, including mass continuity, momentum conservation, and energy conservation. Fluid motion is solved using the Navier-Stokes equations (OpenFOAM, n.d.). By defining the geometry of the flume, specifying boundary conditions, and selecting appropriate turbulence models and numerical schemes, OpenFOAM can simulate the flow patterns, velocity profiles, and pressure distributions within the flume.

3.2.2 Setup of the CFD model

The important principles of the CFD model are briefly described below. For a comprehensive understanding of how the CFD software OpenFOAM operates, along with the workflow and parameters necessary to replicate the model results, the reader is referred to the detailed guide in Appendix F.

The dimensions of the CFD model closely correspond to those of the flume experiment, facilitating direct comparison between the responses of the model and the flume to any alterations made within the model. This feature simplifies the process of comparing results at a later stage. To streamline modelling time, the upstream section of the culvert was shortened by 12 meters, as it was observed that the flow developed rapidly in this section. The model height is kept as low as possible to simulate the air-water interface while minimizing computational cells for air as they are not of interest. Therefore the model height is kept to the expected water level plus 20 cm. The culvert itself remains at the same location and retains identical dimensions as in the flume.
To account for different material properties, the mesh was divided into patches, allowing for the application of boundary conditions like friction and discharge, shown in Figure 24.

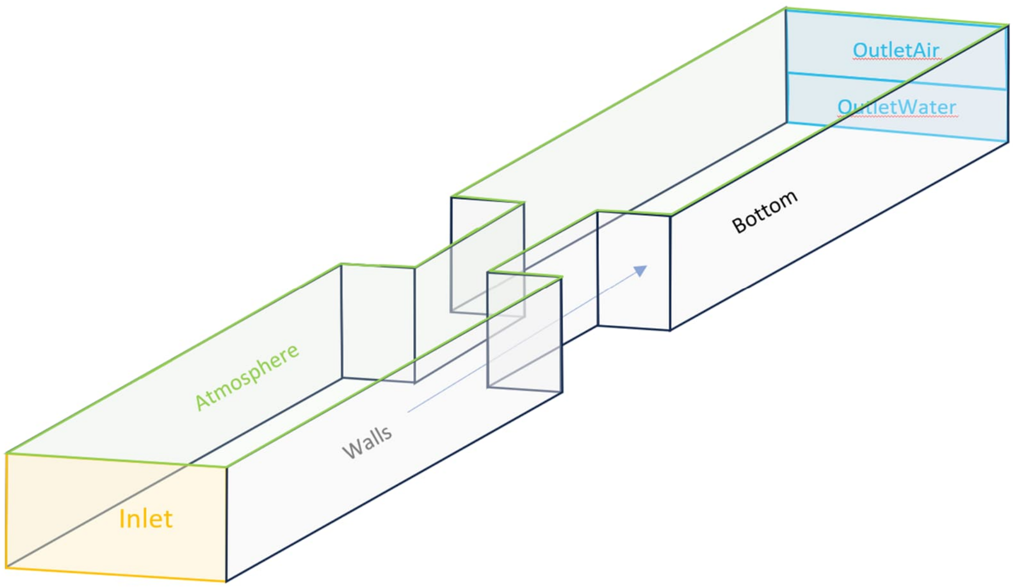

Figure 24: Basic layout of CFD model using the patches, *Inlet*, *Atmosphere*, *Walls*, *Bottom*, *OutletAir* and *OutletWater*. Blue arrow indicates flow direction.

The inlet and outlet patches were adapted from Broecker et al. (2019) and determine how water enters and leaves the model. The inlet patch was used to let water enter the model with a constant discharge. The unknown upstream water level was allowed to develop during the run time of the model as shown in Figure 25 (left). The outlet patch was split into a water and air phase, *outletWater* and *outletAir* as shown in Figure 25 (right). The water level at the outlet side was fixed by the height of the *outletWater* patch. In this way the downstream water level is controlled at a fixed depth, replicating real-world scenarios where the tailwater depth is fixed because of the boundary condition of the downstream watercourse. Furthermore, the discharge from the outlet patch was identical to the discharge at the inlet to have a stable discharge throughout the model.

Figure 25: Visual representation of the inlet patch boundary on the left, which shows a variable water level and a fixed discharge into the model. The right image shows the outlet patch boundary which uses the height of the *OutletWater* patch to fix the water level, using an identical discharge out of the model to have a constant discharge throughout the model.

3.2.3 Quantifying the model results

To quantify the effect of the different profiles in various scenarios, the work of Nortier & de Koning (2000) introduces a loss coefficient for the entrance and exit loss. Appendix A presents a concise study on energy losses around a culvert. It combines the background and derivation of local and friction losses, supplemented by a numerical example utilizing the average culvert. Rewriting equations (19) and (32) for locations 1, 2 and 3 illustrated in Figure 26 yields the entrance loss coefficient (k_e) in equation (2) and the exit loss coefficient (k_o) in equation (3). Locations 1 and 3 are positioned at the largest distance from the culvert to ensure a return to a flow pattern as uniform as feasible. Similarly, location 2, situated at the downstream end of the culvert, adheres to the same principle.

Figure 26: Locations 1, 2 and 3 are used as a reference for equations (2) and (3), in which the loss coefficients for the entrance and exit losses are calculated.

$$k_e = \frac{\Delta H_e}{\frac{v_2^2}{2g}} = \frac{H_1 - H_2}{\frac{v_2^2}{2g}} = \frac{\left(h_1 + \frac{v_1^2}{2g}\right) - \left(h_2 + \frac{v_2^2}{2g}\right)}{\frac{v_2^2}{2g}} \qquad (2)$$

$$k_o = \frac{\Delta H_o}{\frac{v_2^2}{2g}} = \frac{H_2 - H_3}{\frac{v_2^2}{2g}} = \frac{\left(h_2 + \frac{v_2^2}{2g}\right) - (h_3 + \frac{v_3^2}{2g})}{\frac{v_2^2}{2g}} \qquad (3)$$

With

$h_{1,2,3}$:	Hydrostatic head at locations 1, 2 and 3	[m]
$v_{1,2,3}$:	Average velocity at cross-sections 1, 2 and 3	[m/s]
g:	Acceleration due to gravity	[m/s^2]
$\Delta H_{e,o}$:	Difference in energy head at the entrance and exit	[m]
$k_{e,o}$:	Entrance and exit loss coefficient	[-]

It is important to observe that these equations do not account for friction loss. Nam et al. (2013) have demonstrated that the impact of friction loss is deemed negligible in short smooth culverts, contributing to 2 to 3% of the total head loss between locations 1 and 3.
The water level and average velocity were determined using the OpenFOAM model at the final time step (4000 seconds), ensuring parameter convergence. This involved extracting cross-sections at locations 1, 2, and 3 from Figure 26 and integrating the average velocity across these cross-sections, thus accommodating variations in cell size along each cross-section.

3.2.4 Results and reflection

In this section, the outcomes derived from the CFD model are presented. Initially, the convergence of the model is demonstrated, followed by the outcomes of the loss coefficient calculations and the water level difference across the culvert. Detailed results for each CFD model run are shown in Appendix G.1. Lastly, the uncertainties are brought into perspective.

Model convergence

Post-processing of the model results reveals convergence to a quasi-stable state for both water level and velocity after 800 to 1000 seconds, as depicted in Figure 27. This is essential since the model is used to predict the water levels and velocity.
During the last 100 seconds of the simulation, the water level exhibits a standard deviation of 0.2 mm, suggesting a stable state and implying that the model has reached stability. Likewise, the velocity converges, stabilizing in the flow direction with an average standard deviation of 0.01 m/s over the same time interval, see Figure 27 right.

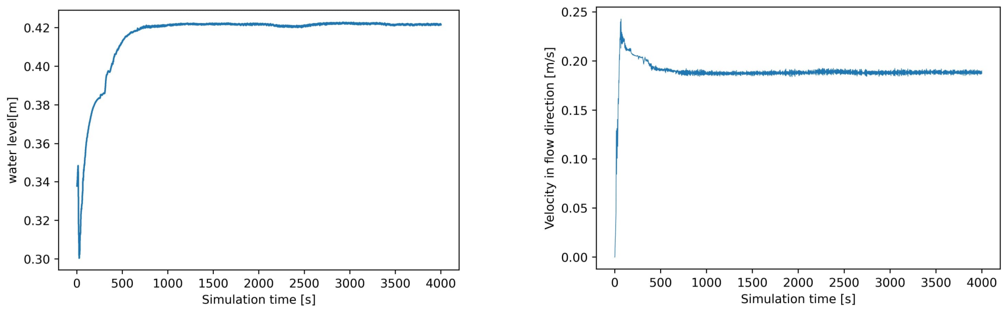

Figure 27: Left: Graph of the water level over time for an upstream probe location, showing a steady water level after about 900 seconds. Right: Graph of velocity in the flow direction for an upstream probe location.

Experimental measurement results – water level difference

Similarly, for the flume experiment the water level difference across the culvert is set out for the CFD results in Figure 28, from which the reduction in water level can be deduced.

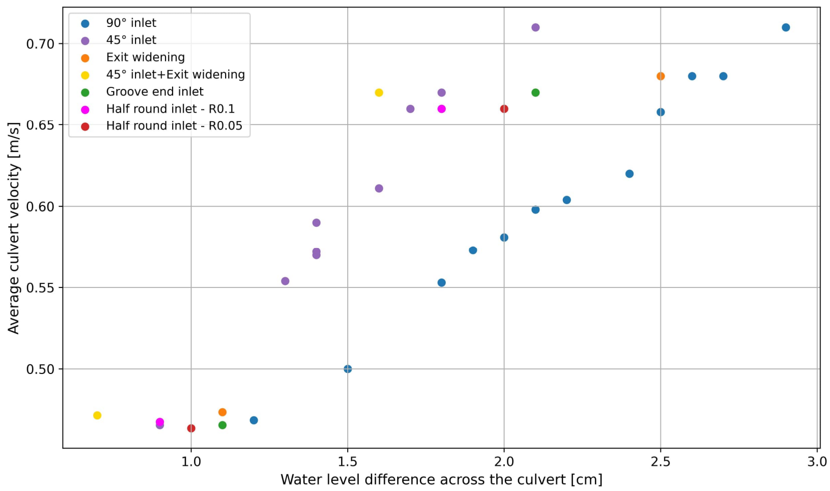

Figure 28: Results of the CFD model for the rectangular culvert, in which the average culvert velocity and the water level difference are plotted for the various culvert profiles.

From Figure 28 it is evident that the 90° inlet marked in blue exhibits the largest water level difference for a specific culvert velocity. Notably, all improved culverts display a decrease in the water level difference, as they are positioned left of the blue data points.

Experimental measurement results – loss coefficient

The loss coefficients corresponding to both entrance and exit loss are plotted against the culvert velocity for various profile shapes (Figure 29). This demonstrates whether a correlation between the loss coefficient and the culvert velocity exists for the various profiles.

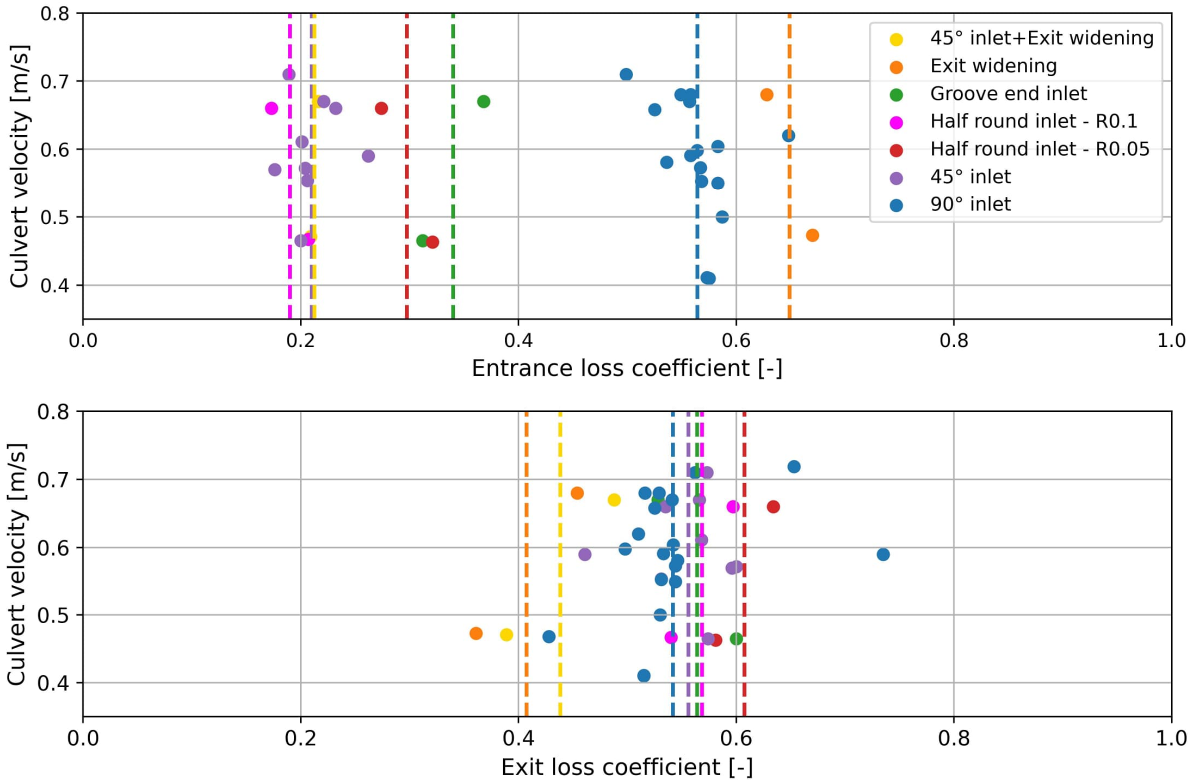

Figure 29: Plot of the loss coefficient of the rectangular culvert obtained through CFD analysis plotted against culvert velocity. The vertical lines indicate the average value for the corresponding profile. The top graph displays the entrance loss coefficient for different profiles, while the bottom graph illustrates the exit loss coefficient.

Figure 29 illustrates the influence of the profile applied to the rectangular culvert on the entrance loss coefficient. Distinct clusters are evident, with the blue and orange clusters featuring a 90° inlet and exhibiting the highest loss coefficient. Conversely, the 45°, half-round, and groove end profiles display lower entrance loss coefficients, aligning with expectations of an improved inlet profile. Furthermore, the exit loss coefficient records its lowest values when the exit is widened, as indicated by the observations in orange and yellow. For the inlet-improved culverts, the exit loss coefficient remains constant.

The average value is calculated from the observed values in Figure 29, which are summarized in Table 4. By employing the square-edged inlet (A) as a reference, the percentage change in the loss coefficients shows the relative influence of the profile on the loss coefficient. This provides valuable insights into the performance differences across the profiles considered.

Table 4: Average entrance loss coefficient ($\boldsymbol{K_e}$), and average exit loss coefficient ($\boldsymbol{K_o}$) calculated from Figure 29, for each of the different profiles in a rectangular culvert. The last column contains the sum of the loss coefficients. The percentage difference with respect to profile A is given between brackets.

	Profiles	**Average $\boldsymbol{K_e}$ [-], (Percentage difference relative to profile A)**	**Average $\boldsymbol{K_o}$ [-], (Percentage difference relative to profile A)**	**$\boldsymbol{K_e + K_o}$ [-], (Percentage difference relative to profile A)**
A	Square-edged inlet with headwall	0.6	0.5	1.1
B	Gradual widening outlet	0.7, (+8%)	0.4, (-23%)	1.1, (0%)
C1	Half round – radius 0.05 m	0.3, (-50%)	0.6, (+13%)	0.9, (-18%)
C2	Half round – radius 0.1 m	0.2, (-68%)	0.6, (+8%)	0.8, (-31%)
D	Inlet with 45° wingwalls	0.2, (-65%)	0.6, (+6%)	0.8, (-30%)
E	Groove end inlet	0.3, (-43%)	0.6, (+6%)	0.9, (-18%)
G	Inlet 45° wingwalls + gradual widening outlet	0.2, (-65%)	0.4, (-17%)	0.6, (-41%)

From Table 4, the following observations are made:

- All inlet-improved culverts show a decrease in inlet coefficient by up to 68%.
- All inlet-improved culvert showed an increase in exit loss (between 6–13%), this is due to the increased velocity within the culvert, resulting in a greater difference in velocity head between the culvert and downstream area.
- Case B reduces the exit coefficient by 23% when the outlet is adapted, however leading to an increase in the inlet coefficient by 8%, which could be caused by the increase in velocity at location 2 and therefore a larger velocity difference with respect to location 1(Figure 26).
- Case G exhibits similar performance for the inlet coefficient of profile D, with a reduction equal to -65%. However, while the outlet coefficient is also reduced (-17%), it is less than that in Case B (-23%) where only the outlet was reduced. This difference (23-17 = 6 %) is equal to the increase in outlet coefficient observed in case D, which was caused by an improvement of the inlet.

Uncertainty of the model results

To understand the precision of the calculated loss coefficients from Figure 29, the range is noted in Table 5, which shows that the range for both inlet and outlet coefficient are maximally 0.1 (except for the exit loss coefficient of profile A, which is 0.3), demonstrating that the CFD model produces precise results for a more or less constant discharge and water depth combination.

Table 5: Range of the loss coefficient from Figure 29.

	Profiles	**Range K_e [min-max]**	**Range K_o [min - max]**
A	Square-edged inlet with headwall	0.5–0.6	0.4–0.7
B	Gradual widening outlet	0.6–0.7	0.4–0.5
C1	Half round – radius 0.05 m	0.3–0.3	0.6–0.6
C1	Half round – radius 0.1 m	0.2–0.2	0.5–0.6
D	Inlet with 45° wingwalls	0.2–0.3	0.5–0.6
E	Groove end inlet	0.3–0.4	0.5–0.6
G	Inlet 45° wingwalls + gradual widening outlet	0.2–0.2	0.4–0.5

As noted before, the average water level is calculated from the last 100 seconds of the simulation. From this a standard deviation of 0.2 mm is found for the water level at the different probe locations. Regarding the velocity in the flow direction an average standard deviation of 0.01 m/s is found for the various probe locations.

3.3 Comparison of flume and CFD model

To compare results between the flume experiment and the CFD model, it is necessary to establish comparable conditions. The discharge and downstream water level (which determine the velocity) of the flume experiment were used as an input for the CFD model. Data on water depth and velocity were collected at eight identical locations (as depicted in Figure 19) for both experiment and model scenarios.
Based on two criteria the results were compared. First, a qualitative analysis of the visual results was performed, considering aspects such as flow lines, water level drops and overall flow behaviour. Following this, the average water level difference for various profiles was examined to assess whether the experiment and model demonstrated similar performance. This comparison aids in verifying the model results against experimental data confirming whether CFD can be used to model culvert flow.

3.3.1 Visual results

Visual observations obtained from the flume experiment are recognized within the simulation model. Specifically, the water level drop at the entrance of the flume (Figure 30, left) is observed within the OpenFOAM simulation as demonstrated in Figure 30 (right).

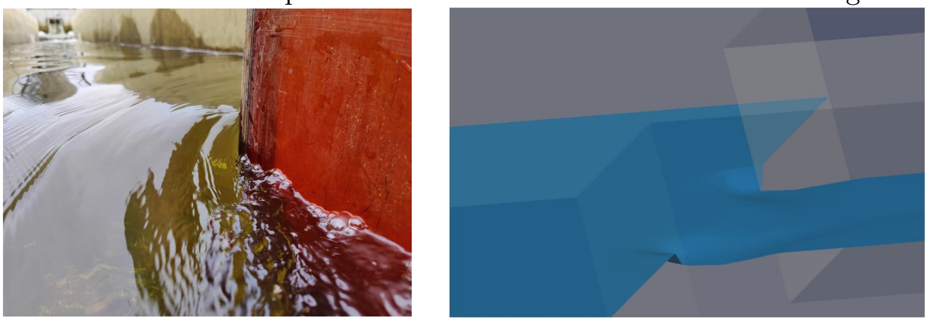

Figure 30: Water level drop at the entrance of the culvert. The left image shows the flume result, and the right image shows the OpenFOAM model result.

The Coanda effect, which was observed in the flume and is shown in Figure 22, can also be seen in the OpenFOAM simulation presented in Figure 31. Here the flow attached to the left wall of the flume downstream of the culvert. The opposite side of the flume showed a return flow which is also visible in the flow lines in Figure 31.

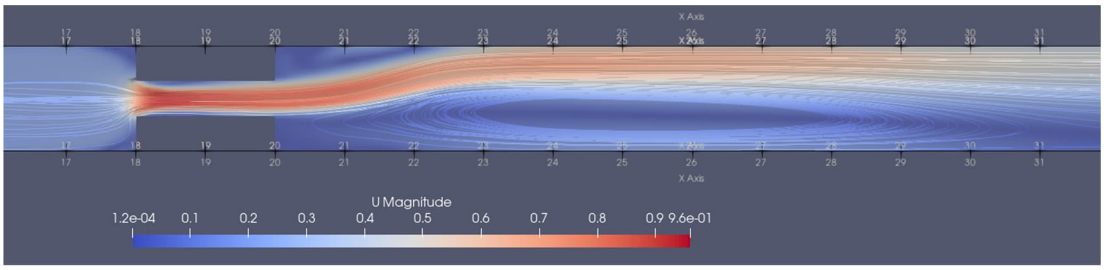

Figure 31: Coanda effect in OpenFOAM simulation, top view with velocity magnitude [m/s].

3.3.2 Comparison of CFD and flume results

A comparison can be made between the flume and CFD simulations to see the difference in water level across the culvert for various shapes and different culvert velocities. Using the uncertainties in the results the results can be put into perspective.

Initially, the water level difference across the culvert is computed for both the flume and CFD models. Subsequently, comparable cases are selected based on the measured water depth at locations 1 and 2 (Figure 26) and culvert velocity. From these cases, the water level differences are plotted in Figure 32. To account for the uncertainty in the water level difference, error bars are plotted. For the flume experiment, the error bars originate from the difference between the measurement locations, range 1.4 to 2.9 cm. For the results obtained from CFD simulations, the estimated error margins are 5% for the differences in water levels, which vary between 0.07 and 1.5 cm. This estimation reflects the simplifications inherent in the modelling process and the impact of rounding, highlighting the difficulty in accurately determining uncertainties without a comprehensive uncertainty analysis.

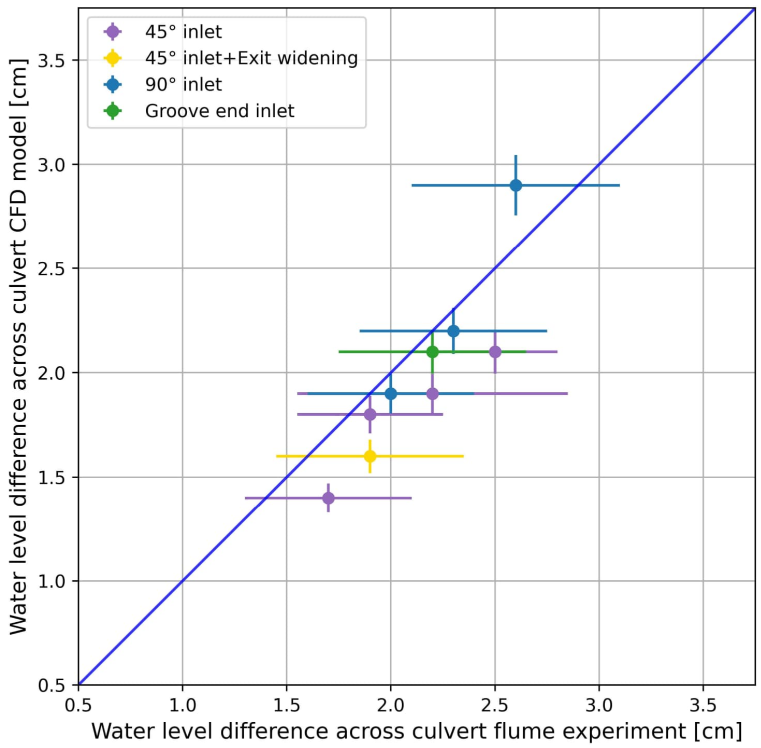

Figure 32: The plot depicts the water level difference across the culvert. The y-axis represents the water level difference of the CFD model, while the x-axis represents the water level difference of the flume experiment. The blue line signifies a perfect match where the water level is equal for both. The horizontal and vertical lines indicate the error margin.

What stands out in the findings presented in Figure 32 is the significant role of uncertainty in the flume experiment. This uncertainty allows for all results to align with the blue line, indicating a perfect agreement when this uncertainty is considered. For the cases showed an exact match in velocity could not be found. In scenarios where the observations fall beneath the line, the CFD model yielded a lower velocity, leading to diminished water level differences and consequently, positions below the ideal line. Furthermore, the portrayed water level differences are towards the upper range of what is typically observed in real-world scenarios, thereby ensuring a sufficiently large difference for measurement.

3.4 CFD model – circular culvert

3.4.1 Setup of the CFD model

After confirming that OpenFOAM can simulate fluid flow around culverts with diverse inlet and outlet profiles the software was utilized to examine the impact of culvert shape, profile, discharge, and water depth on the loss coefficient. Appendix G.2 provides a comprehensive overview of the model runs.

All models employed a circular fully submerged culvert, as circular culverts are most common and a submerged culvert mirrors real-world conditions during peak discharge. The culvert was positioned at the channel bottom, representing the typical installation method in water courses as shown in Figure 33 and explained in Appendix B.2.

Figure 33: Left image shows a culvert installed in the field, where the culvert is placed at the bottom of the watercourse. The right image shows the model equivalent, with the culvert also placed on the bottom.

[1] Profile influence on the loss coefficient for various culvert velocities

First, five different profiles (A, B, C, D, E from Figure 20) have been modelled for a culvert with a diameter of 0.5 meters. A downstream water depth of 0.6 and 1.1 meters was employed with a discharge of 0.125 m^3/s and 0.19 m^3/s, resulting in culvert velocities of 0.6 and 1 m/s. This results in four variations which are shown in Table 6. The purpose of these four scenarios was to assess the impact of profile shape on the loss coefficient under varying conditions of culvert velocity and downstream water depth.

Table 6: Four scenarios tested, using the discharge and downstream water depth to control the culvert velocity.

Profile shape	Discharge [m^3/s]	Downstream water depth [m]	Culvert velocity [m/s]
A, B, C, D, E	0.125	0.6	0.6
A, B, C, D, E	0.19	0.6	1
A, B, C, D, E	0.125	1.1	0.6
A, B, C, D, E	0.19	1.1	1

[2] Culvert velocity impact on loss coefficient for various culvert diameters
Thirdly, three different culvert velocities (0.35, 0.8 and 1.1 m/s) have been applied to a square-edged inlet (profile A) with a diameter of 0.3, 0.5 and 0.8 meters and a tailwater depth of 1.2 meters. Uniform culvert velocities for different diameters were achieved by adjusting the discharge in the model, see Table 7. The objective was to evaluate the impact of culvert velocity on the loss coefficient for varying culvert diameters.

Table 7: Three different culvert velocities for three different culvert diameters (0.3, 0.5, 0.8) achieved by adjusting the discharge.

Culvert velocity [m/s]	**Discharge for Ø 0.3-meter culvert [m³/s]**	**Discharge for Ø 0.5-meter culvert [m³/s]**	**Discharge for Ø 0.8-meter culvert [m³/s]**
0.35	0.03	0.07	0.18
0.8	0.06	0.16	0.40
1.1	0.08	0.22	0.55

Combined with the situation in which a discharge of 0.125 m3/s has been applied to a square-edged inlet (profile A) with a diameter of 0.3, 0.5 and 0.8 meters and a tailwater depth of 1.2 meters (Table 8). The purpose was to investigate the effects of culvert diameter on the loss coefficient under similar discharge conditions.

Table 8: Constant culvert discharge for three culvert diameters (0.3, 0.5, 0.8).

Culvert discharge [m³/s]	**Culvert velocity for Ø 0.3-meter culvert [m/s]**	**Culvert velocity for Ø 0.5-meter culvert [m/s]**	**Culvert velocity for Ø 0.8-meter culvert [m/s]**
0.125	1.8	0.6	0.3

[3] Diameter and depth influence on loss coefficient for various culvert velocities.
Next, six distinct combinations of diameter and tailwater depth are employed with a square-edged inlet (profile A). The specifics of these variations are outlined in Table 9, where the culvert velocity range tested is provided. These scenarios give insight into the influence of both diameter and tailwater depth on the loss coefficient. These diameters were chosen since they are most common in The Netherlands, while the selected velocities encompass a range of higher velocities commonly encountered in Dutch culverts.

Table 9: Six diameter and depth combinations of the square edged inlet, indicated in the table is the range of culvert velocities employed.

	Tailwater depth [m]		
	0.6	**1.1**	**1.2**
Diameter, Ø 0.3 m	[1.1 – 1.4]		[0.4 – 1.8]
Diameter, Ø 0.5 m	[0.4 – 1]	[0.6 – 1]	[0.4 – 1.1]
Diameter, Ø 0.8 m			[0.3 – 1.1]

3.4.2 Results and reflection

This section investigates the effect of an additional profile on circular culverts, followed by an examination of the influence of culvert diameter and tailwater depth on the loss coefficient. Finally, a reflective analysis of the results is provided.

[1] Profile influence on the loss coefficient for various culvert velocities

In Figure 34, the results of Table 6 of the entrance and exit loss coefficient are plotted against the culvert velocity for the various profiles using different colours.

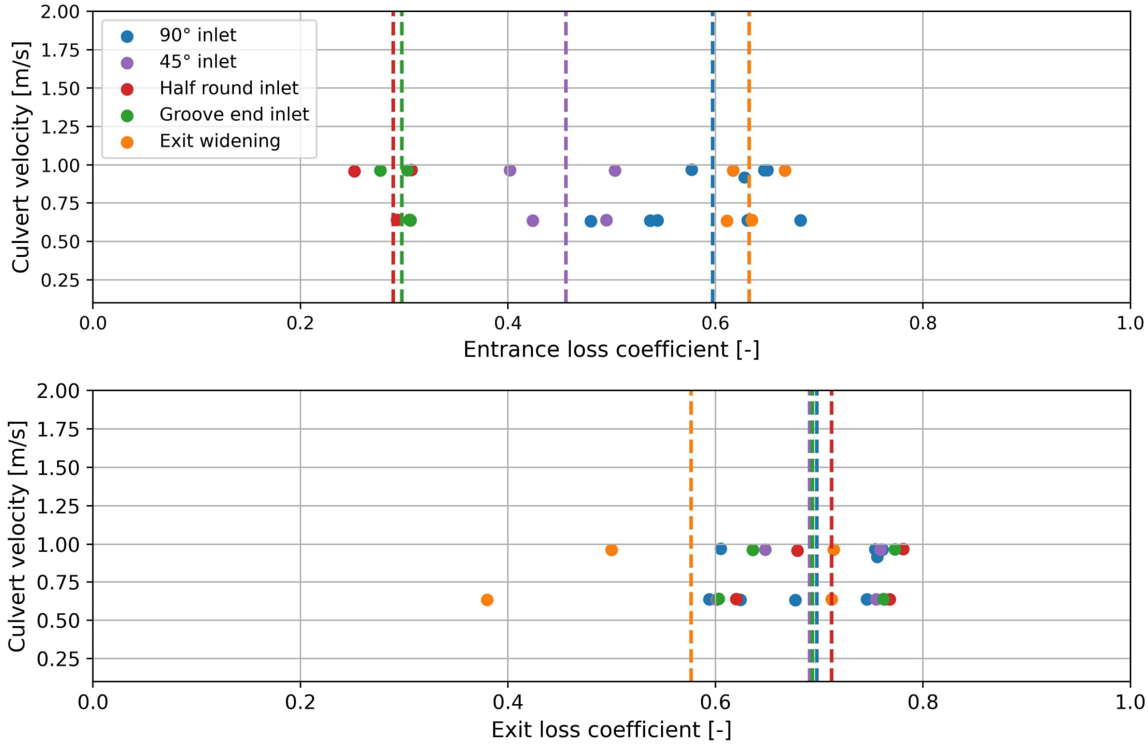

Figure 34: Results of the CFD model of the loss coefficients for the circular culvert. The top graph shows the entrance loss coefficient plotted against the culvert velocity for various profile shapes. The bottom graph shows the results for the exit loss coefficient. The vertical lines indicate the average loss coefficient per profile shape.

From Figure 34 the inlet loss coefficient illustrates distinct clusters, with the blue and orange clusters featuring a 90° inlet profile and exhibiting the highest entrance loss coefficient. Conversely, the 45° (purple), half-round (red), and groove end (green) profiles display lower entrance loss coefficients, aligning with expectations of an inlet improved profile. Furthermore, the exit loss coefficient records its lowest values when the exit is widened, as indicated by the observations in orange. However, a large spread is found for these results, which is attributed to the downstream water depth, which will be investigated in depth in the next section. The exit loss coefficient is on average constant for the inlet improved culverts, as noted by the vertical lines around 0.7.

The average value is calculated from the observed values in Figure 34. Using the square-edged inlet (profile A) as a reference, the percentage change in the loss coefficients is calculated. These results are presented in Table 10. This provides valuable insights into the performance differences across the profiles considered. To gain insight into the uncertainty the range of minimum and maximum values are summarised in Table 11.

Table 10: Results of the loss coefficient, and relative influence in comparison to profile A for the CFD model which uses a circular culvert of diameter 500 mm.

	Profile	**Average K_e [-], (Percentage difference relative to profile A)**	**Average K_o [-], (Percentage difference relative to profile A)**	**K_e + K_o [-], (Percentage difference relative to profile A)**
A	Square-edged inlet with headwall	0.6	0.7	1.3
B	Gradual widening outlet	0.6, (+2%)	0.6, (-19%)	1.2, (-10%)
C	Half round – diameter 0.15 m	0.3, (-53%)	0.7, (-1%)	1.0, (-25%)
D	Inlet with 45° wingwalls	0.5, (-26%)	0.7, (-4%)	1.1, (-14%)
E	Groove end inlet	0.3, (-52%)	0.7, (-4%)	1.0, (-26%)

Table 11: Range of the loss coefficients found in Figure 35, for the different profile shapes.

	Profile	**Range K_e (min-max) [-]**	**Range K_o (min -max) [-]**
A	Square-edged inlet with headwall	0.5–0.7	0.6–0.8
B	Gradual widening outlet	0.6–0.7	0.4–0.7
C	Half round – diameter 0.15 m	0.3–0.3	0.6–0.8
D	Inlet with 45° wingwalls	0.4–0.5	0.6–0.8
E	Groove end inlet	0.3–0.3	0.6–0.8

From Table 10 and Table 11, the following observations are made.

- Inlet-improved profiles (C, D, E) cause a decrease in the inlet loss coefficient and a slight decrease in the outlet loss coefficient.
- Outlet improved profile B shows a decrease in the outlet coefficient and a slight increase in the inlet coefficient.
- The loss coefficients are not influenced by culvert velocity.
- The range of results of the inlet loss coefficient is limited between 0 and 0.2.
- The range of results of the exit loss coefficient is between 0.2 and 0.3.

To address the spread of the results, the same plot is made with a split for the different tailwater depths of 0.6 and 1.1 m, these results are shown in Figure 35.

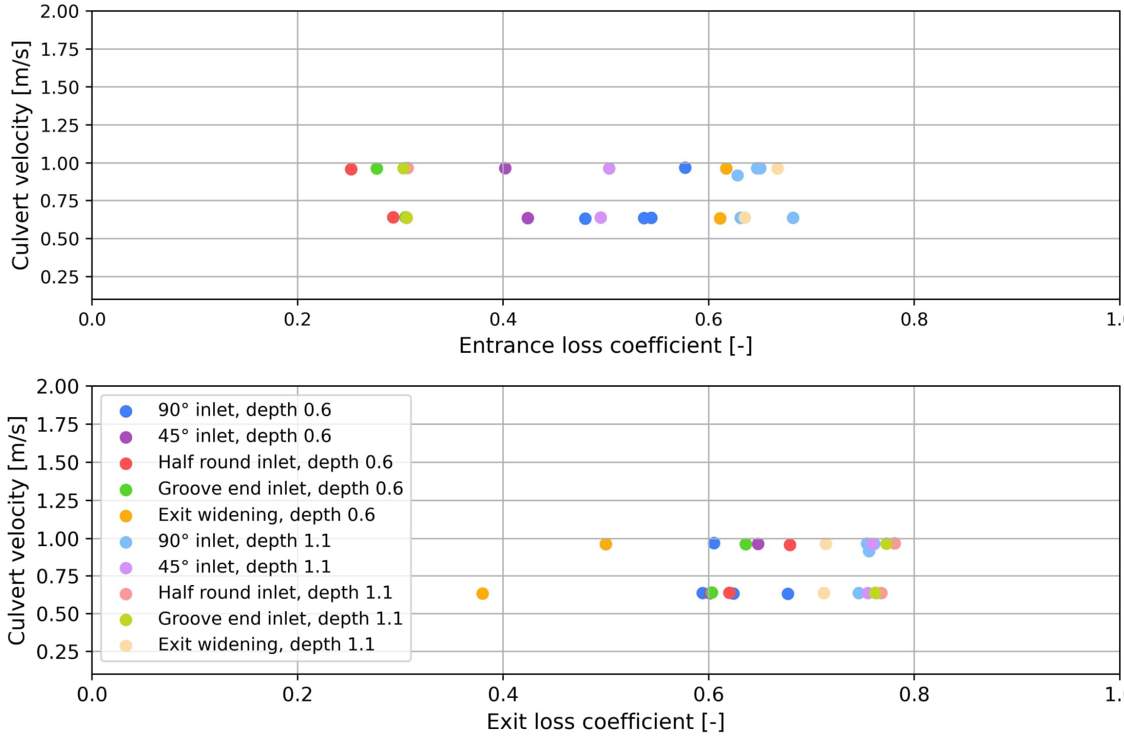

Figure 35: Results of the CFD model of the loss coefficients for the circular culvert, with two different culvert depths, 0.6 and 1.1 m. The top graph shows the entrance loss coefficient plotted against the culvert velocity for various profile shapes. The bottom graph shows the results for the exit loss coefficient. The vertical lines indicate the average loss coefficient per profile shape.

Figure 35 demonstrates the effect of changes in tailwater depth on the loss coefficient, with lighter shades indicating greater depths. This visual suggests a direct correlation, where deeper tailwater levels are associated with an increase in the loss coefficient. The loss coefficients for a tailwater depth of 0.6m are detailed in Table 12, while Table 13 presents the data for a tailwater depth of 1.1m.

Table 12: Results of the loss coefficient for tailwater depth 0.6 m. With the relative influence in comparison to profile A for the CFD model which uses a circular culvert of diameter 500 mm.

	Profile – With tailwater depth 0.6 m	**Average K_e [-], (Percentage difference relative to profile A)**	**Average K_o [-], (Percentage difference relative to profile A)**	**$K_e + K_o$ [-], (Percentage difference relative to profile A)**
A	Square-edged inlet with headwall	0.5	0.6	1.2
B	Gradual widening outlet	0.6, (+15%)	0.4, (-30%)	1.1, (-9%)
C	Half round – diameter 0.15 m	0.3, (-49%)	0.6, (+3%)	0.9, (-21%)
D	Inlet with 45° wingwalls	0.4, (-25%)	0.6, (+3%)	1.1, (-9%)
E	Groove end inlet	0.3, (-45%)	0.6, (-2%)	0.9, (-22%)

Table 13: Results of the loss coefficient for tailwater depth 1.1 m. With the relative influence in comparison to profile A for the CFD model which uses a circular culvert of diameter 500 mm.

	Profile With tailwater depth 1.1 m	**Average K_e [-], (Percentage difference relative to profile A)**	**Average K_o [-], (Percentage difference relative to profile A)**	**$K_e + K_o$ [-], (Percentage difference relative to profile A)**
A	Square-edged inlet with headwall	0.6	0.8	1.4
B	Gradual widening outlet	0.6, (0%)	0.7 (-7%)	1.4, (-3%)
C	Half round – diameter 0.15 m	0.3, (-52%)	0.8, (1%)	1.1, (-23%)
D	Inlet with 45° wingwalls	0.5, (-23%)	0.8, (0%)	1.3, (-10%)
E	Groove end inlet	0.3, (-54%)	0.8, (+1%)	1.1, (-24%)

Comparing the data between Table 12 and Table 13 reveals that the loss coefficients increase with the higher tailwater depth presented in Table 13. In general, the percentage improvements across most cases are within the same magnitude range. An exception is observed in the exit loss coefficient for case B, suggesting that gradually widening the outlet becomes less beneficial at higher tailwater depths. The impact of tailwater depth on these observations will be further investigated in the subsequent section.

[2] Culvert velocity impact on loss coefficient for various culvert diameters
For each diameter (0.3, 0.5 and 0.8m) three different velocities where tested, (0.35, 0.8, and 1.1 m/s). Together with the constant discharge 0.125 m^3/s from Table 8. The results of the loss coefficient are plotted in Figure 36, with the average value noted by the vertical dashed line.

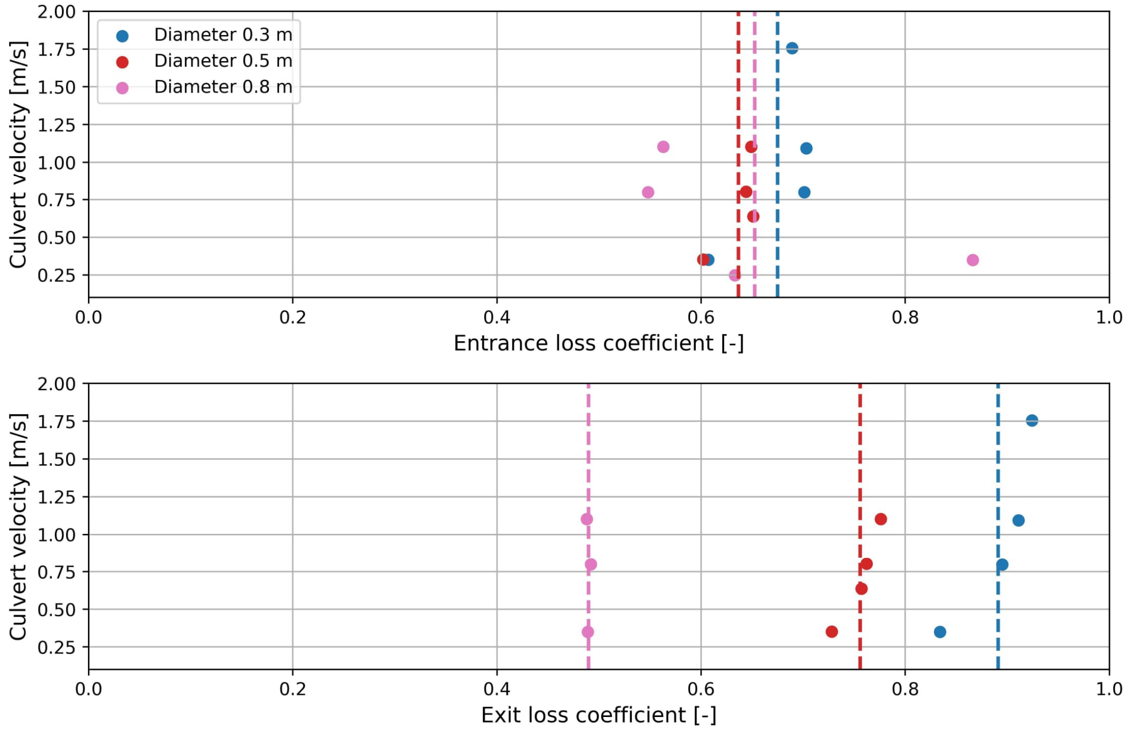

Figure 36: Results of loss coefficient for circular culvert of three velocities (0.35, 0.8, and 1.1 m/s) and the constant culvert discharge 0.125 m^3/s, using the three common culvert diameters (0.3, 0.5 and 0.8m). The vertical dashed lines show the average value.

In Figure 36, the entrance loss exhibits unusual behaviour for the four data points with a velocity below 0.5 m/s. Unlike the higher velocity points, the entrance loss does not remain consistent within this range. A closer examination of these points reveals water level differences across the culvert ranging from 0.2 to 1 cm. This combination of low velocities and small water level differences contributes to the observed anomalies. In contrast, the remaining data points exhibit water level differences of 3 cm or more.

Excluding the anomalous data, it becomes apparent that the entrance loss coefficient is influenced by the diameter, with smaller diameter culverts leading to higher entrance loss coefficients. However, velocity does not significantly impact the loss coefficient.
Regarding the exit loss coefficient, there is less influence from the small water level differences, with the exit loss remaining relatively constant across different velocities.

[3] Diameter and depth influence on loss coefficient for various culvert velocities
To investigate the influence of culvert diameter and tailwater depth the results of Table 9 for profile A are plotted in Figure 37.

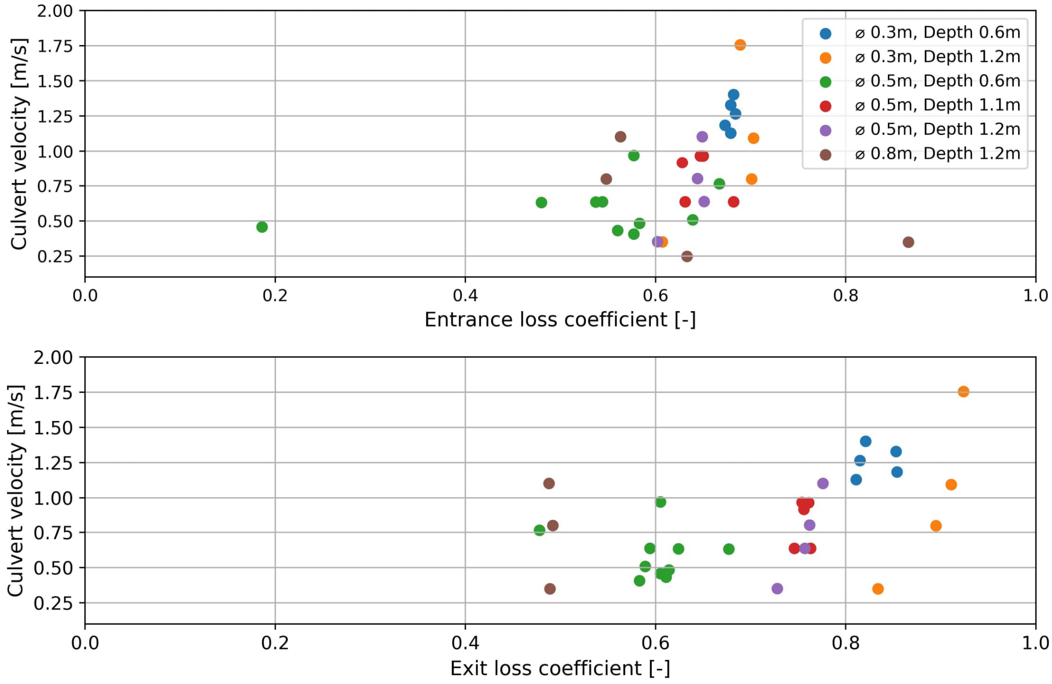

Figure 37: The top graph shows the entrance loss coefficient and culvert velocity for various diameter and tailwater depth combinations. The bottom graph shows the exit loss coefficient for the same combination of diameter and tailwater depths.

Observations drawn from Figure 37 are:

- The entrance loss coefficient reaffirms its correlation with culvert diameter or tailwater depth.
- The exit loss coefficient is dependent on the diameter of the culvert as well as the water depth.
- The exit loss coefficient is highest for the smallest diameter of 300 mm and lowest for the largest diameter of 800 mm. A larger culvert diameter causes a smaller difference in velocity head between the inside and downstream of the culvert. In contrast to a smaller culvert diameter which exhibits a larger difference in velocity head due to higher culvert velocities. As this difference in velocity head diminishes with larger diameters, the exit loss is consequently reduced.
- Increased tailwater depth causes an increase in the exit loss coefficient, this again is caused by the increased difference in velocity head in and downstream of the culvert.

Uncertainty of the model results
From the above results, it becomes evident that the uncertainty in the outcomes for the loss coefficient is minimal for culvert velocities exceeding 0.4 m/s. In such instances, the water level difference across the culvert is notably large enough, with a minimum of 2 to 3 cm. Moreover, the loss coefficients demonstrate consistency across various culvert velocities under these conditions. This implies that a sufficiently substantial water level difference is essential for predicting consistent loss coefficients.

4 Discussion

1) Flume experiment

The use of the flume experiment presents an advantage since it includes all relevant physics. The immediate visualization of the effects of different profiles through streamlines enables rapid insight into their impact. However, accurately measuring the exact discharge in the flume poses challenging. As noted by Le Coz et al. (2014), a deviation of 5-10% in discharge measurements within the flume is expected. To mitigate this, a constant discharge was maintained throughout the experiment phases, allowing for the measurement of water level differences across the culvert with different profiles. This however entails that the loss coefficient was not determined. For future research, a revised measurement setup in the flume, potentially utilizing lasers for precise water depth registration, is recommended. Additionally, to reduce uncertainty in discharge computation using the velocity area method, the Rehbock equation could be employed in tandem (STOWA, 2009). This requires minor adjustments to the experimental setup, given that a weir was already used at the downstream end of the culvert.

Nortier & de Koning (2000) noted that it typically takes 8 to 10 times the width of the channel for flow after a culvert to revert to uniform flow, equivalent to 12 to 15 meters in the context of the flume experiment. However, despite having a 20-meter flume length downstream of the culvert, no uniform flow was detected. This suggests that monitoring water levels at this location should be approached with caution, as they may vary downstream of the now most downstream measured location.

2) CFD model

The CFD model employs equations to simulate the physics of the flume experiment. The key advantage of CFD models lies in their capability to generate output at every location and the ability to make easy adjustments to model dimensions, shapes, and discharges. To minimise the uncertainties a sensitivity analysis on grid size is conducted. Furthermore, the influence of domain length was explored by extending the flume. After fine tuning of the model, the runtime of the model was manageable typically yielding results within 24 to 48 hours.

3) Results uncertainty

Discrepancies between the results from the flume and CFD models are shown, with much of the uncertainty stemming from the measurement outcomes of the flume. Nevertheless, the obtained results give insight into the effects, especially considering the limitations of analytical equations in accurately measuring the effects of different profiles. Understanding the uncertainties in OpenFOAM poses a greater challenge, as the true values remain unknown. To mitigate model result uncertainty, conducting a sensitivity analysis on factors such as cell size and turbulence model parameters is advisable. Additionally, verifying the model against flume results is crucial; however, in the present configuration, the uncertainties are too substantial to permit direct comparison of the results.

4) Limitations of the results

The main findings concern loss coefficients for a variety of smaller culvert types, ranging from 0.3 to 0.8 meters in diameter. These findings might not directly apply to larger-diameter culverts or similar structures. For instance, a 20-meter-wide bridge may not require a 2-meter half-round profile as would follow from the formula $> 0.3 * Width_{culvert}$. Further investigation is necessary for larger culverts or structures. Additionally, the range of culvert velocities tested (0.25-1 m/s) is limited but falls within anticipated values for poorly designed culverts during high discharge scenarios.

To compute the loss coefficient accurately, the culvert velocity must exceed 0.35 m/s to ensure a substantial water level difference (> 1 cm) across the culvert. If these conditions are not met, the loss coefficient may begin to deviate from the anticipated constant value.

5) Application of 45° profile to circular culverts

To maintain simple models, the profile with a 45° angle was positioned vertically (Figure 38, left), rather than being conically placed. A conical inlet could potentially further decrease the inlet loss coefficient as the inlet would be streamlined in all directions of the culvert when considering a drowned culvert. Consequently, this may explain the relatively lower impact of this profile on the inlet loss coefficient (-26%) compared to the -65% reduction observed for the rectangular culvert.

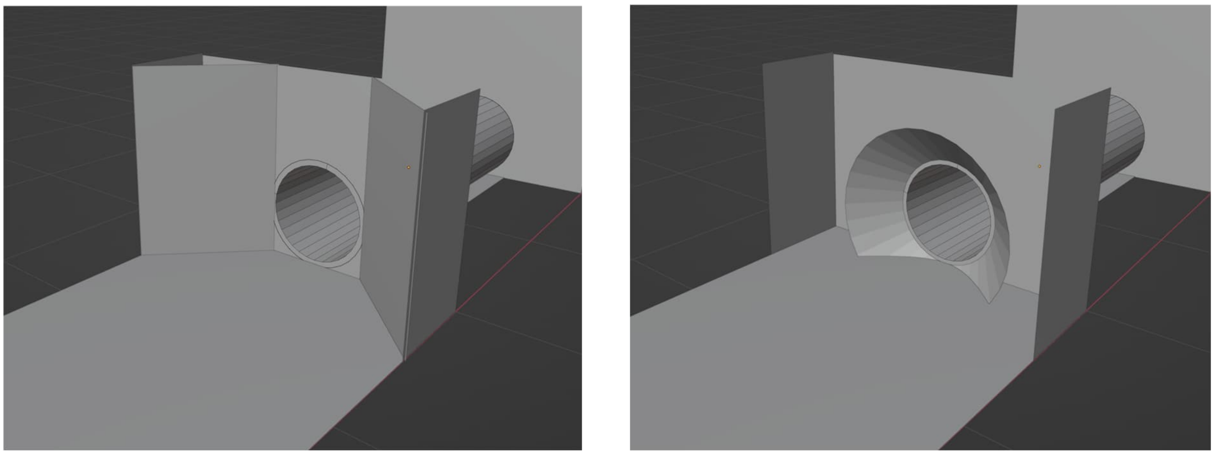

Figure 38: Screenshot of the 3D circular model. The left image shows the simplified model for the 45° profile, right shows the version where a 45° angle is constructed in all directions of the culvert entrance.

6) Comparison of loss coefficient results to literature

Known loss coefficients in literature can be compared to similarly shaped profiles in the CFD model, this can be performed to assess whether the results of the CFD model deviate significantly from the literature. In all CFD results the exit loss coefficient is much smaller than 1, which deviates from the assumed value of 1 in literature, this signals that the exit loss is smaller than assumed.

Rectangular culvert:
In the case of the rectangular culvert, Table 14 compares the entrance loss coefficients with those from literature cases resembling the shape, where the profile is part of the structure rather than an added feature as in the CFD model.

Table 14: Entrance loss coefficient for the rectangular CFD model and literature alternatives resembling the profile.

Profile	CFD entrance loss coefficient [-]	Literature entrance loss coefficient [-]
Square-edged inlet with headwall	0.6	0.5
Half round – diameter 0.05 - 0.1 m	0.2-0.3	0.2
Inlet with 45° wingwalls	0.2	0.4

Table 14 indicates that while the entrance loss coefficients are generally within the same order of magnitude, however, variations exist. These are likely attributed to the dimensions of the profiles. Notably, the CFD model tends to overestimate the entrance loss coefficient for the square-edged inlet. For half-round inlets, the coefficient dependence on radius presents a challenge as the radius is unspecified in the literature case. Similarly, direct comparison of inlets with 45° wingwalls from the CFD model is difficult due to the range in wingwall angles (30-75°) applied in the literature case.

Circular culvert:
In the case of circular culverts, Table 15 compares entrance loss coefficients with literature cases where the profile is part of the structure.

Table 15: Entrance loss coefficient for the circular CFD model and literature alternatives resembling the profile.

Profile	CFD entrance loss coefficient [-]	Literature entrance loss coefficient [-]
Square-edged inlet with headwall	0.5–0.7	0.5
Half round – diameter 0.15 m	0.3–0.3	0.2
Inlet with 45° wingwalls	0.4–0.5	0.2
Groove end inlet	0.3–0.3	0.2

Table 15 suggests that the CFD results tend to overestimate the entrance loss coefficient, possibly due to the added profile being less efficient or due to systemic errors.

Thus, literature-derived entrance loss coefficients offer a rough estimate of efficiency, but the results suggest that the addition of a profile in some cases may be less effective compared to when the profile is an integral part of the construction.

5 Conclusion

The research question of this thesis reads: *"How can the head loss over existing (too tight) culverts be minimised by adding an inlet or outlet profile and does this lead to a substantial enhancement in the performance of these culverts, providing a practical option to postpone the replacement of underperforming culverts?"*
The addition of an inlet profile (groove, 45° or half round) can reduce entrance losses by up to 65% depending on the profile. The exit loss can be reduced by 20% when the outlet is widened. This reduction implies that for a constant discharge, the entrance loss is more than halved. Where possible adjusting the inlet shape is preferred since the footprint of an inlet profile is smaller and more effective for a similar footprint compared to the outlet profile.
Implementing a profile at critical culverts within a polder effectively reduces water level rise upstream, thereby mitigating flooding. Consequently, when applied to a series of culverts, this reduces the cumulative head loss across the structures, thus lowering overall head loss in the system. In conclusion, adding an inlet profile to culverts offers significant enhancements and serves as a viable alternative to the expensive alternative of replacing a culvert for a larger diameter culvert.

1) Data analysis of Dutch culverts

Using the data of the 21 waterboards of The Netherlands the most common culvert was found to have a diameter of 0.5 meters, with a length of 8 meters and constructed of PVC. Furthermore, circular culverts are extensively employed, with over 470,000 applied in Dutch polders (93%), primarily due to their simple installation process. Therefore, optimizing a profile tailored for this type of culvert presents significant potential for market application.

2) Distribution of losses

At a culvert's inlet and exit, friction and exit losses are observed. Friction loss typically accounts for 2–3% of the overall head loss. Meanwhile, without any improvements to the inlet or outlet, the exit and entrance loss of a culvert are comparable in magnitude. In Dutch polder landscapes, this contradicts the literature assumption that the exit loss predominates. This is due to the narrow watercourses where the full velocity head isn't lost at the culvert's outlet.

3) Most effective profiles at the inlet of a circular culvert

Significant reductions in entrance loss are observed for a circular culvert with a diameter of 0.5 meters when employing a groove end and half-round profile. The entrance loss coefficient decreases from $k_e = 0.6$ to 0.3, representing a 50% reduction. The groove end dimensions are illustrated in Figure 39 on the left. Similarly, a half-round profile with a diameter greater than 0.3 times the culvert diameter (as depicted in Figure 39, right) should be employed.

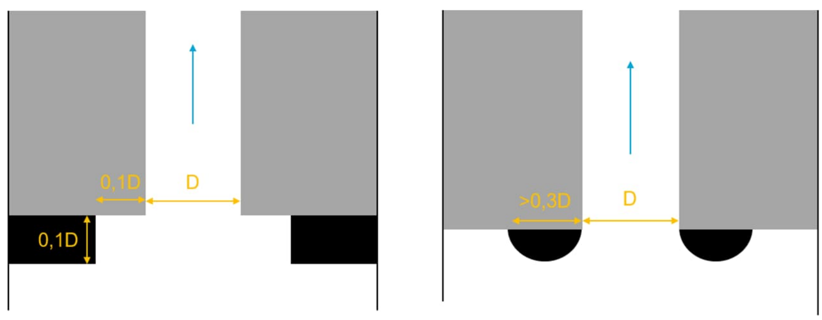

Figure 39: Left: Dimensions of groove end inlet profile for a circular culvert. Right: Dimensions of half-round inlet profile for a circular culvert.

4) Most effective profiles at the inlet of a rectangular culvert

The largest reduction in entrance loss for a rectangular culvert with a width of 0.5 meters is found for an inlet with 45° wingwalls (-65%) and the half-round profile (-68%) with a diameter of $0.4 * Width_{culvert}$ (Figure 40), compared to a culvert with a 90° headwall. This leads to an entrance loss coefficient of $k_e = 0.2$ for both profiles.

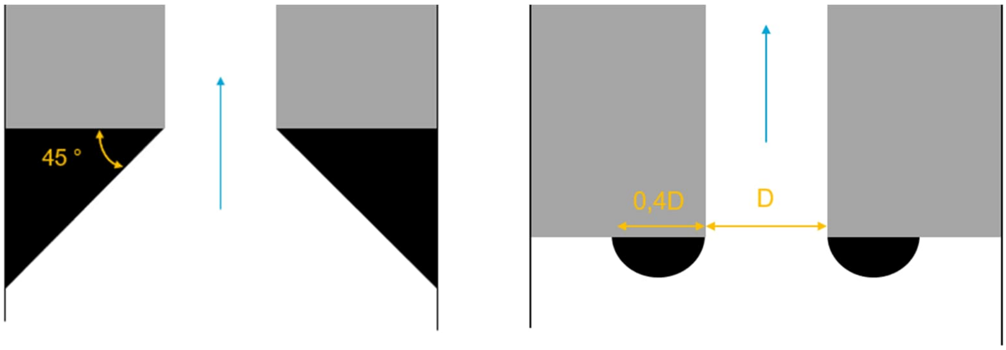

Figure 40: Left: Dimensions of 45° inlet profile. Right: Half-round profile with dimensions relative to the width of the culvert (D).

5) Effective profiles at the outlet of culverts

Adding an outlet widening profile at the exit of a culvert is not considered beneficial when adding a profile to the inlet is feasible. The outlet profile typically has a larger footprint and is less efficient considering its footprint compared to the inlet profile. For a profile with L=1.5 m (Figure 41), the reduction in exit loss is 20% for round and circular culverts. Therefore, achieving a similar reduction as gained from the inlet profile often necessitates an outlet profile length that exceeds the culvert's actual length. However, when the inlet profile alone does not provide the needed loss reduction, the inlet profile can be combined with an outlet profile.

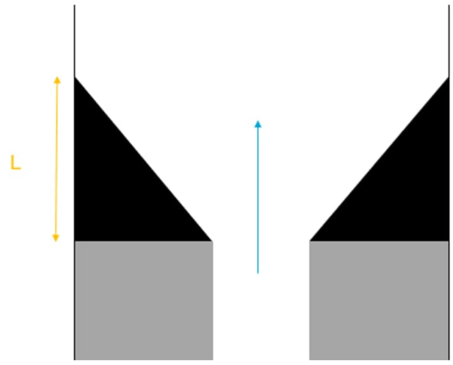

Figure 41: Length of the outlet profile, at the exit of the culvert.

6) Flume and CFD model comparison

The behaviour observed in the flume experiment was replicated in the CFD model, specifically regarding the location of the water level drop at the culvert entrance and the Coanda effect, which diverted the flow toward either the left or right wall downstream of the culvert. The examination of water level differences across the rectangular culvert revealed consistent outcomes when the culvert velocities aligned. However, due to the significant uncertainty in the flume results, achieving a perfect match with the CFD model results was unfeasible. In conclusion, the findings suggest that despite uncertainties, a CFD model can predict water level differences effectively, demonstrating behaviour comparable to that observed in the flume experiment, as the model accurately captures the underlying physics.

7) Influence of culvert velocity on loss coefficients

The loss coefficient for both circular and rectangular culverts is independent of culvert velocity. If the culvert velocity is sufficiently large (0.4 to 1 m/s), the water level difference is at least 2 to 3 cm, which makes that a constant loss coefficient can be applied.

Although the loss coefficient is constant for culvert velocity, the head loss is larger for higher culvert velocities. Therefore, during high discharge events, where the culvert velocity is higher, the decrease in loss coefficient is most effective since the largest reduction in head loss is found.

8) Influence of culvert diameter and tailwater depth

In examining the entrance loss coefficient, a correlation emerged with the culvert diameter, indicating that larger diameter culverts lead to reduced entrance loss coefficients. Similarly for the exit loss coefficient, it was observed that the greatest loss occurred with the smallest diameters. This phenomenon can be attributed to a smaller difference in velocity head between the inside and downstream of the culvert. Additionally, an elevated tailwater depth results in an increased exit loss coefficient, driven again by the decreased difference in velocity head both within and downstream of the culvert.

6 Recommendations

In the recommendations section, a split is made between recommendations for the practical application of the proposed solution to culverts and for further research in the field of culvert streamlining.

Practical recommendations for culverts:

1) Culvert orientation

Large-diameter culverts often consist of concrete sewer pipes due to their widespread availability and scalability in length. They are equipped with a socket end of similar dimensions as suggested for the groove end profile, therefore it is advisable to align the culvert with this end in the direction of flow (Figure 42).

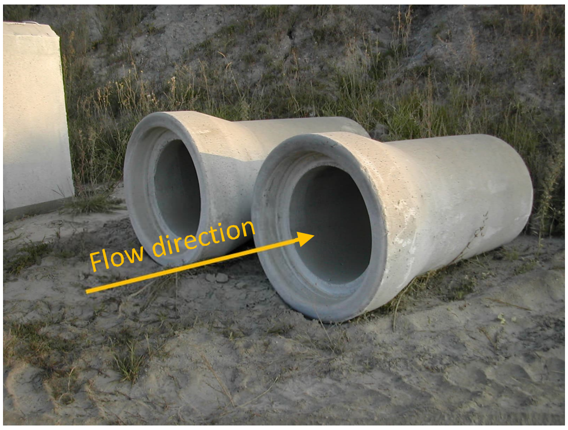

Figure 42: Circular sewer pipe elements with groove end Giverbo (n.d.).

2) Adjusting formwork during concrete pouring

When constructing a new culvert or bridge using in-situ formwork and concrete pouring, it is recommended to integrate a groove or rounded profile into the formwork (Figure 43). This reduces inlet losses in an easy yet cost-effective way.

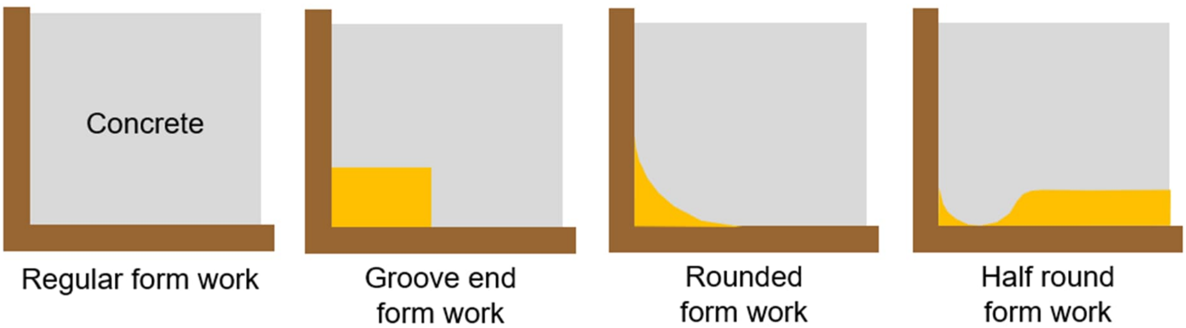

Figure 43: Adjustment to formwork; left shows the standard method of formwork. The other three images show adjusted formwork that integrates the inlet profiles into the structure.

Recommendations for further research:

1) Optimalisation of profile dimensions

The dimensions specified for the groove end, 45° and half-round profile at the inlet of the culvert will decrease the loss coefficient when applied in typical culvert flow velocities of 0.2 to 0.5 m/s. It is recommended to investigate whether further optimization of the profile dimensions is justified and to assess whether the most efficient profile dimensions remain constant for various culvert shapes, sizes, and velocities. The rationale for optimizing the dimensions is twofold: firstly, during the flume experiment, different dimensions were tested to evaluate their impact on flow lines, as illustrated in Figure 44 (left). It was noted that a groove end positioned too close to the culvert had a minor impact on the streamlines, whereas a large distance resulted in the profile performing similarly to the unadjusted culvert. Secondly, the length of the inlet of the 45° profile can be minimized to avoid extending to the entire width of the watercourse, as suggested by Jeager et al. (2020), see Figure 44 right.

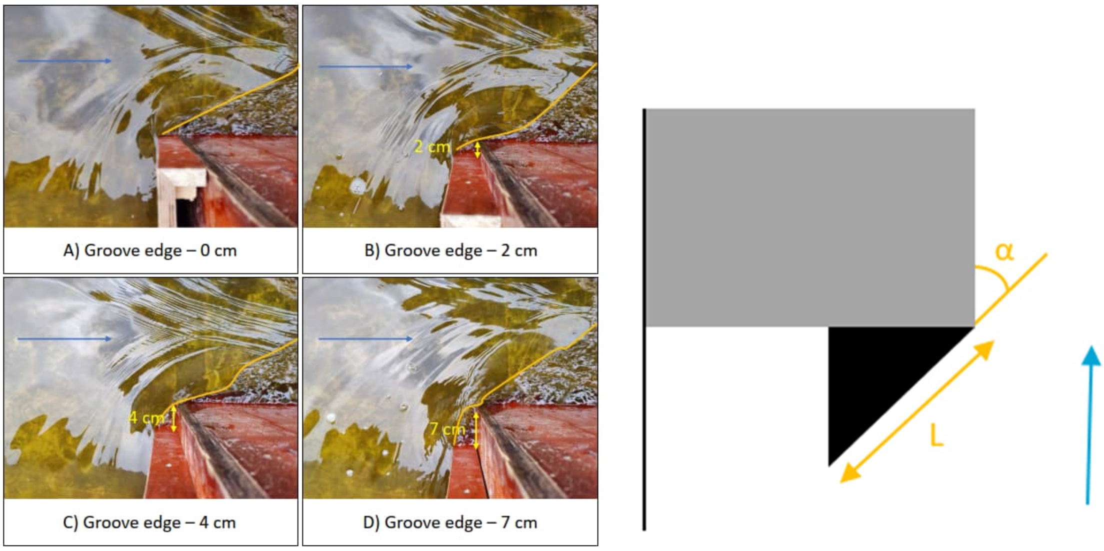

Figure 44: Left: Effect of location of the groove edge inlet on the flow pattern around the inlet, in blue the flow direction is indicated. Right: Reduce the length (L) of the 45° profile as suggested by Jeager et al. (2020).

2) Effect of the culvert entrance on the loss coefficient

In the Dutch landscape often different kind of shape types are found at the culvert entrance. In practice, culverts can be projecting from the fill or mitred to conform to the slope as shown in Figure 45. To extend the understanding of how these profiles apply to different culvert shapes and their influence on the loss coefficient, further investigation through additional CFD modelling is warranted.

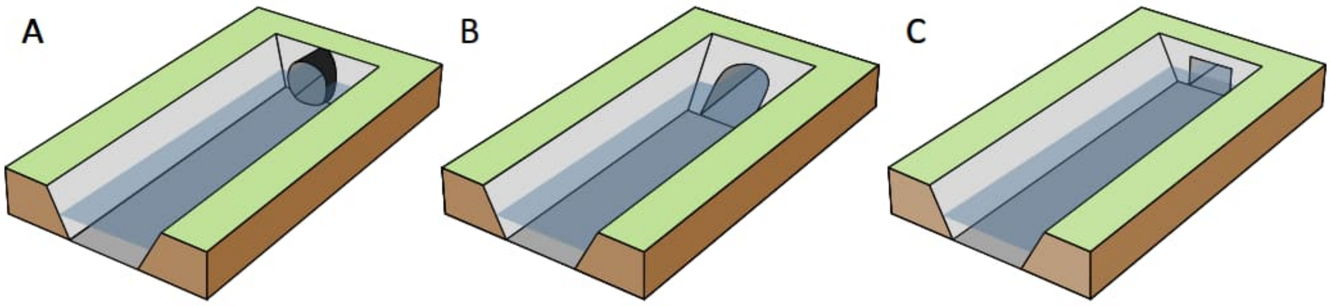

Figure 45: A) Projecting circular shaped culvert. B) Mitred edge of 'Heulprofile'. C) Headwall with a rectangular culvert.

3) Measuring devices

For future research in a flume, it is advisable to explore an alternative measurement setup that incorporates lasers to achieve higher accuracy in water depth measurement. Additionally, the inclusion of a Rehbock weir could be considered, offering an additional method for determining the discharge in the flume alongside the velocity area method utilized in this thesis, as discussed in section 4.

4) Effect of large-scale streamlining on a polder

It would be beneficial to determine the effect of large-scale streamlining of culverts (and bridges) on peak discharge and water levels in a polder using a 1D model (e.g., D-Hydro or Sobek) for a sample polder. This can demonstrate whether the measure achieves the intended effect.

5) Meshing CFD model

During the meshing phase, special attention is required to accurately model non-linear shapes. It is advisable to investigate the alignment of the grid and its impact on the results. The utilization of the *SnappyHexMesh* dictionary is recommended for this purpose.

6) Contraction ratio

The relation between the contraction ratio (culvert width/channel width) and the inlet and outlet coefficients can be investigated. It is assumed that higher contraction ratios result in lower velocities outside the culvert compared to the culvert velocity, thus increasing the loss coefficient.

7) Application of CFD model for realistic culvert conditions

The modelled condition of the flume uses constant friction and a uniform rectangular shape across the flume. In the field, watercourses are filled with plants and the cross-sectional shape varies and is not rectangular, as demonstrated in Figure 46 right. To verify the applicability of the found loss coefficients in the field, additional modelling can be performed using different watercourse profiles and investigate the effect on the loss coefficients.

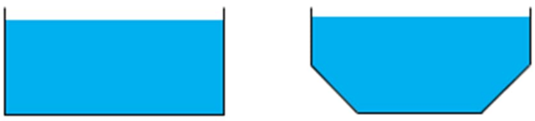

Figure 46: Other watercourse cross sections that simulate a more realistic watercourse shape.

8) Material, method of attachment and costs

It is advisable to explore the integration of the profile into Dutch polders. To achieve this, suitable materials for the profile need to be identified. Additionally, research should be conducted on the attachment methods for the profile, and an estimation of production and installation costs must be made. This is needed for waterboards to assess whether they would consider using a profile instead of a replacement.

Bibliography

Arpan Pradhan, Kishanjit K. Khatua, Saine S. Dash. (2015). Distribution of Depth-Averaged Velocity along a Highly Sinuous Channel. *Aquatic Procedia, 4,* 805-811. https://doi.org/10.1016/j.aqpro.2015.02.100.

Broecker, T., Teuber, K., Gollo, V. S., Nützmann, G., Lewandowski, J., & Hinkelmann, R. (2019). Integral Flow Modelling Approach for Surface Water-Groundwater interactions along a rippled streambed. *Water, 11(7),* 1517. https://doi.org/10.3390/w11071517

Chanson, H. (2004). *The hydraulics of open channel flow: An introduction (2nd ed).* Elsevier. https://doi.org/10.1016/B978-0-7506-5978-9.X5000-4

CFD for everyone. (2022, April 25). *OpenFOAM fvSchemes explained in under 5 mins* [video]. Youtube. https://youtu.be/JlB6y8NSI20?si=SbtW_G68JQ0f2nRn

Delfland. (n.d.). *Leggerkaart*. Retrieved Oktober 17, 2023, from https://www.hhdelfland.nl/over-ons/regelgeving/legger/

DHPC. (2022). *Delft High Performance Computing Centre (DHPC). DelftBlue Supercomputer (Phase 1).* https://www.tudelft.nl/dhpc/ark:/44463/DelftBluePhase1.

Giverbo. (n.d.). Ronde buizen [Photograph]. Retrieved November 26, 2023, from https://www.giverbo.nl/producten-group/1365/ronde-buizen

Hager, W.H. (2010). *Wastewater Hydraulics: Theory and Practice*. Springer. https://doi-org.tudelft.idm.oclc.org/10.1007/978-3-642-11383-3_2

Hemida, H. (2008). *OpenFOAM tutorial: Free surface tutorial using interFoam and rasInterFoam.* https://www.tfd.chalmers.se/~hani/kurser/OS_CFD_2007/HassanHemida/Hassan_Hemida_VOF.pdf

Idel'chik, I.E. (1960). *Handbook of hydraulic resistance* (4th ed.). Begell House, Inc.

IPCC. Seneviratne, S.I., X. Zhang, M. Adnan, W. Badi, C. Dereczynski, A. Di Luca, S. Ghosh, I. Iskandar, J. Kossin, S. Lewis, F. Otto, I. Pinto, M. Satoh, S.M. Vicente-Serrano, M. Wehner, and B. Zhou, 2021: *Weather and Climate Extreme Events in a Changing Climate. In Climate Change 2021: The Physical Science Basis.* Cambridge University Press, Cambridge, United Kingdom and New York, NY, USA, pp. 1513–1766, doi: 10.1017/9781009157896.013.

IBKW. (2023). Installatie rechthoekige duiker [Photograph]. Personal communication November 14th, 2023.

Jaeger, R., Tondera, K., Pather, S., Porter, M., Jacobs, C., Tindale, N. (2020). Hydraulic improvements in culverts for climate change adaptation. *University of the Sunshine Coast, Queensland.* https://doi.org/10.25907/00554

J. Le Coz, B. Camenen, X. Peyrard, Guillaume Dramais. (2012). Uncertainty in open-channel discharges measured with the velocity-area method. *26, 18-29.* https://doi-org.tudelft.idm.oclc.org/10.1016/j.flowmeasinst.2012.05.001

Leakey, S. (2019). *Inlets, outlets, and post-processing for modelling open-channel flow with the volume of fluid method.* http://dx.doi.org/10.17196/OS_CFD#YEAR_2019

Nam, N. V., Archambeau, P., Dewals, B., Pirotton, M., & Erpicum, S. (2013). Local head-loss coefficient at the rectangular transition from a free-surface channel to a conduit. *Journal of Hydraulic Engineering, 139(12),* 1318-1323. https://doi.org/10.1061/(asce)hy.1943-7900.0000790

Nassralla, T. H. (2015). Effect of inlet and outlet geometric shape variations of a pipe culvert on local head-losses. *Journal of Engineering Sciences, 43(6),* 807-822. https://doi.org/10.21608/jesaun.2015.115294

Naudin-Ten Cate, R.,Tjooitink, T., Wentink, M. (2000). *Cultuurtechnisch Vademecum: handboek voor inrichting en beheer van land, water en milieu.* Elsevier

Nortier, I.W., & de Koning P. (1996). *Toegepaste vloeistofmechanica (7th ed.).* Noordhoff.

Openfoam. (n.d.). *WaterChannel.* Retrieved September 1, 2023, from https://develop.openfoam.com/Development/openfoam/-/tree/master/tutorials/multiphase/interFoam/RAS/waterChannel

Ott. (n.d.). Legacy product - OTT ADC [Photograph]. Retrieved September 12, 2023, from https://www.ott.com/products/accessories-109/legacy-product-ott-adc-50/

T. Panitz, D. T. Wasan. (1972). Flow attachment to solid surfaces: The Coanda effect. *AIChE Journal,18(1).* https://doi-org.tudelft.idm.oclc.org/10.1002/aic.690180111

P. Novk and J. Belka (1981). *Models in hydraulic engineering: Physical principles and design applications.* volume 4. Pitman, Boston Mass and London, ISBN 0273084364.

Rahman, M. (n.d.). Culvert - Types of Culvert - Details & Advantages. *Civil today.* https://civiltoday.com/construction/bridge/116-types-of-culvert

Rijkswaterstaat. (n.d.). *Peilbesluiten.* Retrieved January 27, 2023, from https://www.infomil.nl/onderwerpen/lucht-water/handboek-water/wetgeving/waterwet/aanleg-beheer/peilbesluiten/

Scolari, F. (2023). *Multiphase Solver (interFoam Tutorial).* Retrieved September 13, 2023, from https://hydro-informatics.com/numerics/openfoam/of-tutorial-multiphase.html

Smith, C. D. and Oak, A. G. (1995). Culvert inlet efficiency. *Canadian Journal of Civil Engineering, 22(3),* 611-616. https://doi.org/10.1139/l95-069

Stephenson, D. (1981). Stormwater hydrology and drainage, *Elsevier Scientific Publishing company.*

STOWA. 2009. *Handboek debietmeten in open waterlopen.* Retrieved February 15, 2024, from https://www.stowa.nl/publicaties/handboek-debietmeten-open-waterlopen

Swart, S. (2021). Luchtfoto Krimpenerwaard [Photograph]. Retrieved October 6, 2023, from https://www.siebeswart.nl/image/I0000IDlXkBT7qPs

Tec-science. (2020). *Flow separation (boundary layer separation).* https://www.tec-science.com/mechanics/gases-and-liquids/flow-separation-boundary-layer-separation/

Tullis, B. P. (2012). *Hydraulic loss coefficients for culverts.* Transportation Research Board. https://doi.org/10.17226/22673.

U.S. Army Corps of Engineers. (2016). *HEC-RAS River Analysis System.* (5th ed.). 6-26 https://www.hec.usace.army.mil/software/hec-ras/documentation/HEC-RAS%205.0%20Reference%20Manual.pdf

VanEssen. (n.d.). TD Diver [Photograph]. Retrieved September 11, 2023, from https://www.vanessen.com/products/data-loggers/td-diver/

Waterschapshuis. (n.d.). *DAMO - Data- en Asset Management Omgevingswet. Het Waterschapshuis.* Retrieved June 15, 2023, from https://damo.hetwaterschapshuis.nl/

Waterschap AGV. (n.d.). Gemaal Stadwijck [Photograph]. Retrieved Oktober 10, 2023, from https://www.agv.nl/recreatie/watererfgoed/gemalen/gemaal-stadwijck/

Appendix A: Energy losses around a culvert

In this appendix background information is given on energy losses occurring around culverts. First, a general introduction to local losses is given in appendix A.1. Appendix A.1.1 and A.1.2 deal with the derivation of the formulas used to describe the entrance and exit loss. Appendix A.2 introduces the friction loss and the formulas to calculate this loss. Lastly, appendix A.3 employs the formulas derived in a sample calculation using the average culvert to gain insight into their contribution to the total energy loss caused by a culvert.

A.1: Local losses

In fluid flow, local losses occur due to components such as bends, fittings, valves, contraction, and expansion. Local losses occur around culverts at the inlet and exit of the pipe. Local losses in fluid flow are predominantly caused by decelerating flow, which is the effect of a change in geometry (Hager, 2010). In culverts, this happens at the upstream end of the culvert where a sudden contraction causes an opposing pressure gradient along the surface which decelerates the flow in the boundary layer. The difference in flow velocities perpendicular to the primary flow axis leads to momentum exchange and the dissipation of turbulent kinetic energy, known as entrance loss (Tec-science, 2020). The other local loss that can be found in a culvert is the exit loss, which is located at the end of the culvert where a sudden expansion decelerates the flow. Moreover, the development of flow zones with eddies and vortices is found at the exit. These extract energy from the main flow, as depicted in Figure 47.

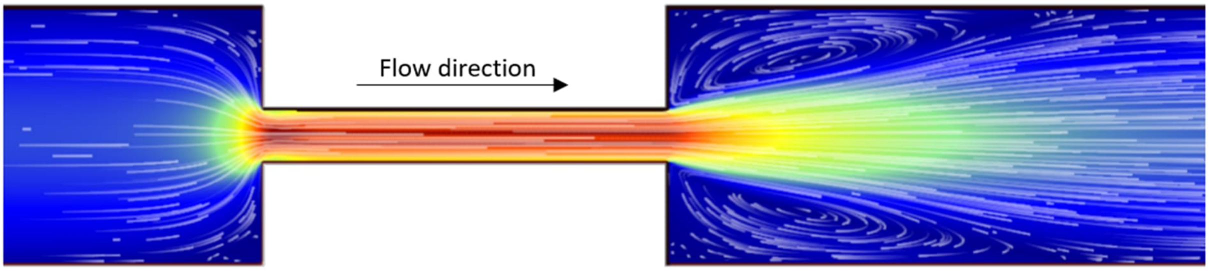

Figure 47: The left side shows a sudden contraction of the flow. The right-hand side shows a sudden expansion with secondary flow zones indicated by the eddies (Hoes, n.d.).

A.1.1: Entrance loss

As a result of a sudden contraction, flow velocity increases reaching its peak at the vena contracta. In instances of accelerating flows, only friction losses act on the culvert (Nortier & de Koning, 2000). The entrance loss is found downstream of the vena contracta, attributable to the deceleration of flow induced by the expansion to the complete width of the culvert. To quantify the entrance loss the extended Bernoulli equation (4) is used between sections 3 and 4 after the vena contracta of Figure 4.

$$z_3 + h_3 + \frac{v_3^2}{2g} = z_4 + h_4 + \frac{v_4^2}{2g} + \Delta H_e \qquad (4)$$

With

$z_{3,4}$:	Height above reference at locations 3 and 4	[m]
$h_{3,4}$:	Hydrostatic head at locations 3 and 4	[m]
$v_{3,4}$:	Average velocity at cross-section 3 and 4	[m/s]
g:	Acceleration due to gravity	[m/s^2]
ΔH_e:	Entrance energy loss	[m]

The assumption is made that the height above the reference point is zero since the culvert is placed horizontally. Rewriting for the entrance energy loss results in:

$$\Delta H_e = (h_3 - h_4) + (\frac{v_3^2}{2g} - \frac{v_4^2}{2g}) \quad (5)$$

Using the momentum equation (6) between sections 3 and 4, results in the momentum forces F_3 and F_4 as shown in Figure 48. Assuming the flow area at location 3 to be the cross-sectional flow area of the culvert ($A_3 = \mu A_4$) and the hydrostatic pressure at location 3 to be acting on the cross-sectional flow area (A_4) (Nortier & de Koning, 2000).

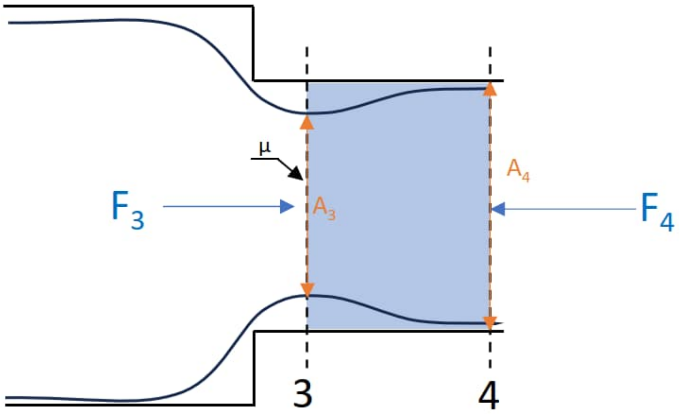

Figure 48: Momentum forces at cross sections 3 and 4 after sudden contraction (own work).

$$\vec{\Sigma}F_x = \rho Q \Delta v_x \quad (6)$$

$$F_3 - F_4 = \rho Q \Delta v_x \quad (7)$$

$$\rho g h_3 A_4 - \rho g h_4 A_4 = \rho Q_4 (v_4 - v_3) \quad (8)$$

$$g A_4 (h_3 - h_4) = v_4 A_4 (v_4 - v_3) \quad (9)$$

$$h_3 - h_4 = \frac{v_4 A_4 (v_4 - v_3)}{g A_4} \quad (10)$$

$$h_3 - h_4 = \frac{v_4}{g}(v_4 - v_3) \quad (11)$$

With:

$A_{3,4}$:	Cross-sectional area at locations 3 and 4	[m^2]
ρ:	Fluid density	[kg/m^3]

When equation (11) is substituted into equation (5), this yields the equation of Carnot (15):

$$\Delta H_e = \frac{v_4}{g}(v_4 - v_3) + (\frac{v_3^2}{2g} - \frac{v_4^2}{2g}) \quad (12)$$

$$\Delta H_e = \frac{2v_4^2 - 2v_3 v_4}{2g} + \frac{v_3^2}{2g} - \frac{v_4^2}{2g} \quad (13)$$

$$\Delta H_e = \frac{v_4^2 - 2v_3 v_4 + v_3^2}{2g} \quad (14)$$

$$\Delta H_e = \frac{(v_3 - v_4)^2}{2g} \quad (15)$$

Using continuity: $v_3 A_3 = v_4 A_4 \rightarrow v_3 = \frac{v_4 A_4}{A_3}$ and substituting into (15).

$$\Delta H_e = \frac{\left(\frac{v_4 A_4}{A_3} - v_4\right)^2}{2g} \quad (16)$$

$$\Delta H_e = \left(\frac{A_4}{A_3} - 1\right)^2 * \frac{v_4^2}{2g} \quad (17)$$

From Figure 48, $A_3 = \mu A_4$ substituted into (17).

$$\Delta H_e = \left(\frac{A_4}{\mu A_4} - 1\right)^2 * \frac{v_4^2}{2g} = \left(\frac{1}{\mu} - 1\right)^2 * \frac{v_4^2}{2g} \quad (18)$$

Rewriting k_e as the unknown entrance loss coefficient:

$$k_e = \frac{\Delta H_e}{\frac{v_4^2}{2g}} = \left(\frac{1}{\mu} - 1\right)^2 \quad (19)$$

A.1.2: Exit loss

The exit loss occurs a small distance downstream of the sudden expansion (Nortier & de Koning, 2000). Using the conservation of energy and momentum between sections 5 and 6 from Figure 49, the exit loss can be calculated. Assuming the flow area at location 5 to be the cross-sectional flow area of the culvert exit (A_5) and the hydrostatic pressure at location 5 to be acting on the channel cross-sectional flow area (A_6). Using these for the momentum equation (20).

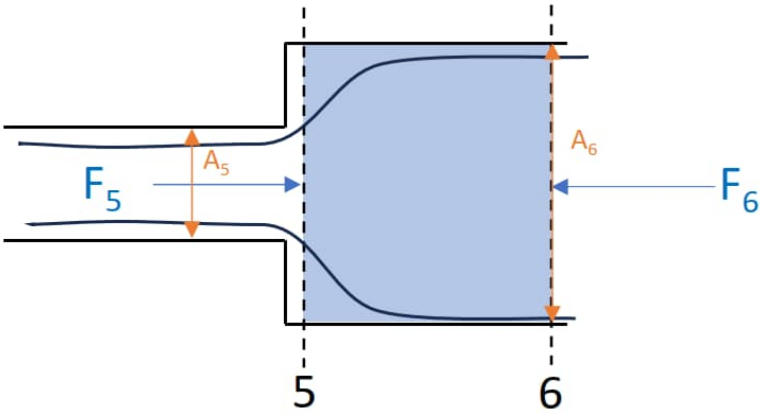

Figure 49: Momentum forces acting on the sudden expansion (own work)

$$\vec{\Sigma} F_x = \rho Q \Delta v_x \quad (20)$$

$$F_5 - F_6 = \rho Q \Delta v_x \quad (21)$$

Using the forces in Figure 49 this yields:

$\rho g h_5 A_6 - \rho g h_6 A_6 = \rho Q_6 (v_6 - v_5)$ rewritten to (22)

$$h_5 - h_6 = \frac{v_6}{g}(v_6 - v_5) \quad (23)$$

With:

$h_{5,6}$:	Water level at locations 5 and 6	[Pa]
$v_{5,6}$:	Average velocity at locations 5 and 6	[m/s]
$A_{5,6}$:	Cross-sectional area at locations 5 and 6	[m^2]

The energy equation is given by the extended Bernoulli equation (24):

$$h_5 + \frac{v_5^2}{2g} = h_6 + \frac{v_6^2}{2g} + \Delta H_o \quad (24)$$

Rewritten for exit loss (ΔH_o):

$$\Delta H_o = h_5 - h_6 + \frac{v_5^2}{2g} - \frac{v_6^2}{2g} \quad (25)$$

When equation (23) is substituted into equation (25), this yields equation (26):

$$\Delta H_o = \frac{v_6}{g}(v_6 - v_5) + \frac{v_5^2}{2g} - \frac{v_6^2}{2g} \tag{26}$$

$$\Delta H_o = \frac{2v_6^2 - 2v_5 v_6}{2g} + \frac{v_5^2}{2g} - \frac{v_6^2}{2g} \tag{27}$$

$$\Delta H_o = \frac{v_6^2 - 2v_5 v_6 + v_5^2}{2g} \tag{28}$$

$$\Delta H_o = \frac{(v_5 - v_6)^2}{2g} \tag{29}$$

Using continuity: $v_5 A_5 = v_6 A_6 \rightarrow v_6 = \frac{v_5 A_5}{A_6}$ and substituting into (29).

$$\Delta H_o = \frac{\left(v_5 - \frac{v_5 A_5}{A_6}\right)^2}{2g} \tag{30}$$

$$\Delta H_o = \left(1 - \frac{A_5}{A_6}\right)^2 * \frac{v_5^2}{2g} = k_o * \frac{v_5^2}{2g} \tag{31}$$

Thus, the exit loss coefficient k_o is equal to:

$$k_o = \frac{\Delta H_o}{\frac{v_5^2}{2g}} = \left(1 - \frac{A_5}{A_6}\right)^2 \tag{32}$$

A.2: Friction loss

Friction losses are losses resulting from the development of a boundary layer between the moving fluid and the wall surface. This interaction creates a resistance to the flow, resulting in energy dissipation. A simplified depiction of this principle has been depicted in Figure 50.

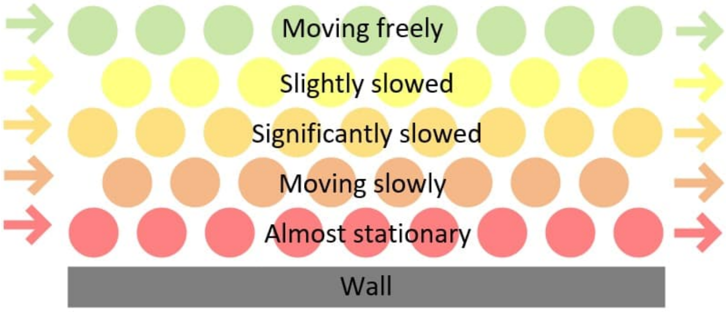

Figure 50: Friction loss near a wall shown by a schematisation of water particles. The particles near the wall are slowed due to friction with the wall, the adjacent particles stick to this slower-moving layer until the influence of the wall is negligible (own work).

In the case of pressurised full culvert flow the Darcy Weisbach equation can be used to calculate the friction losses in full pipe flow. The Darcy Weisbach equation is given by equation (33).

$$\Delta H_f = f * \frac{L}{D_5} * \frac{v_5^2}{2g} \qquad (33)$$

With:

ΔH_f:	Head loss due to friction	[m]
f:	Darcy-Weisbach friction factor	[-]
L:	Length of the pipe	[m]
D_5:	Diameter of the pipe	[m]
v_5:	Average velocity of the fluid in the pipe	[m/s]
g:	Acceleration due to gravity	[m/s^2]

The Darcy-Weisbach friction factor (f) depends on the Reynolds number and relative roughness of the culvert. Where from experiments conducted by Osborne Reynolds the Reynolds number was established to describe the flow regime.

$$Re = \frac{v_5 D_5}{\nu} \qquad (34)$$

With:

Re:	Reynolds number	[-]
v_5:	Average velocity of the fluid in the pipe	[m/s]
D_5:	Diameter of the pipe	[m]
ν:	Kinematic viscosity	[m^2/s]

The Reynolds number (Re) has three regimes with laminar, transitional, and turbulent flows. Laminar flows are below $Re = 2300$ and turbulent flows are above $Re = 3500$. The relative roughness is of importance in turbulent flow, for fully developed flow in smooth pipes the friction factor can be estimated using the Colebrook-White equation (35).

$$\frac{1}{\sqrt{f}} = -2\log\left(\frac{\varepsilon/D_5}{3.7} + \frac{2.51}{Re\sqrt{f}}\right) \qquad (35)$$

Where:

f:	Darcy-Weisbach friction factor	[-]
ϵ:	pipe roughness	[m]
D_5:	Diameter pipe	[m]
Re:	Reynolds number	[-]

A.3: Implications of loss formula on a common circular culvert

By employing equations (19), (32) and (35) along with the most common culvert dimensions outlined in Section 2.2, it is possible to compute the entrance, exit and friction losses. The common culvert has a diameter of 0.5 meters, measures 8 meters in length, and is composed of PVC material. This methodology enables an evaluation of the factors that contribute to total head loss within a circular culvert.

Example calculation of entrance loss

The entrance loss calculated in equation (19) is dependent on the contraction of the Vena Contracta as well as the velocity in the culvert. By using the contraction coefficient $\mu = 0.6$ (Nortier & de Koning, 2000) and a discharge of Q=0.08 m^3/s the entrance loss can be calculated. This velocity in the culvert represents a realistic yet upper limit of the velocities encountered in the field.

$$v_4 = \frac{Q}{A_4} = \frac{0.08}{\frac{1}{4} * \pi * 0.5^2} = \frac{0.08}{0.196} = 0.4\ m/s$$

$$\Delta H_e = \left(\frac{1}{\mu} - 1\right)^2 \frac{v_4^2}{2g} = \left(\frac{1}{0.6} - 1\right)^2 \frac{0.4^2}{2g} = 0.44\ \frac{0.4^2}{2g} = 0.0036\ m = 0.36\ cm$$

Example calculation of exit loss

Looking at equation (31), which describes the exit loss, the assumption can be made that the culvert ends in a large reservoir that has an area $A_6 >> A_5$, this leads to $k_o = 1$.

$$\Delta H_o = \left(1 - \frac{A_5}{\infty}\right)^2 * \frac{v_5^2}{2g}$$

$$\Delta H_o = k_o * \frac{v_5^2}{2g} = 1 * \frac{0.4^2}{2g} = 0.0082m = 0.82\ cm \qquad (36)$$

When the exit loss coefficient is equal to 1, the exit loss is equal to the full velocity head in the barrel which means that all velocity head is lost. However, in Dutch polders culverts are employed in small watercourses and therefore equation (36) is not used in practice as A_6 is almost equal to A_5. Using the most common dimensions for the circular culvert and a channel width of 1.5 meters and a water depth of 0.7 the exit loss coefficient is calculated.

$$k_o = \left(1 - \frac{A_5}{A_6}\right)^2 = \left(1 - \frac{\left(\frac{1}{4} * \pi * 0.5^2\right)}{(1.5 * 0.7)}\right)^2 = 0.66$$

$$v_5 = v_4 = 0.4\, m/s$$

$$\Delta H_o = k_o * \frac{v_5^2}{2g} = 0.66 \frac{0.4^2}{2g} = 0.0056 \text{ meters} = 0.56 \text{ cm}$$

The exit loss is 5.6 mm whilst using $k_o = 1$ results in an exit loss of 8.2 mm, thus overestimating the head loss compared to using the real channel dimensions (Tullis, 2012). To conclude, the exit loss is reduced when the assumption is made that not all kinetic energy is dissipated, as there is still some water flow downstream of the culvert. According to HEC-14 (Thompson and Kilgore, 2006), this is caused by not accounting for a conversion of a portion of the kinetic energy in the culvert to potential energy in the channel.

Example calculation of friction loss

The Reynolds number can be calculated using the average velocity in the culvert, which was equal to 0.4 m/s.

$Re = \frac{vD}{\nu} = \frac{0.4*0.5}{1E-6} = 205000$, thus flow in the culvert is very turbulent. Laminar situations are unlikely since velocity must be 90 times lower to be laminar.

Next the friction factor is calculated, for this the pipe roughness is needed. The pipe roughness of a PVC pipe is 0.015 mm Chanson (2004, p. 74).

$$\frac{1}{\sqrt{f}} = -2\log\left(\frac{\frac{\varepsilon}{D}}{3.7} + \frac{2.51}{Re\sqrt{f}}\right) => \frac{1}{\sqrt{f}} = -2\log\left(\frac{\frac{1.5 * 10^{-5}}{0.5}}{3.7} + \frac{2.51}{205000\sqrt{f}}\right)$$

This results in $f = 0.0035\, m$. The head loss is estimated using equation (35):

$$\Delta H_f = f * \frac{L}{D} * \frac{v^2}{2g} = 0.0035 * \frac{8}{0.5} * \frac{0.4^2}{2 * 9.81} = 0.00045 \text{ m} = 0.045 \text{ cm}$$

Thus, the head loss due to friction is 0.045 cm.

Summary example calculations

To summarize, head losses around a culvert can be calculated using analytical equations, Table 16 shows a summary of the results. These equations provide a reference framework for typical shapes and conditions. The example calculations reveal that the friction loss accounts for 5 % of the total loss and is less significant compared to entrance and exit losses. Therefore, minimizing local losses is advantageous for reducing the overall head loss in a culvert, as these losses typically contribute significantly to the total energy loss.

Table 16: Summary of results of the sample calculations of the losses around a culvert.

Loss type	**Calculated head loss [cm]**
Friction loss	0.045
Entrance loss	0.36
Exit loss, using $k_o = \left(1 - \frac{A_5}{A_6}\right)^2$	0.56
Exit loss, using $k_o = 1$	0.82

Appendix B: Culvert statistics

This appendix showcases additional outcomes from the culvert analysis in Section 2.2, which covers the predominant culvert data. Additional results and graphs are presented and explored in B.1. The prevalence of circular culverts is explained by delving into installation variations between round and rectangular culverts in B.2.

B.1: Additional results of culvert data

From the 21 waterboards in The Netherlands, relevant data on culverts was downloaded which included culvert shape, length, width, height, material, and location. Shape data was originally indexed using two distinct methods, DAMO and Geonis Blaeu, which vary across the waterboards. Consequently, an initial step involved standardizing this data (Waterschapshuis, n.d). Next, the data is sorted and presented in the graphs and figures below.

Figure 51 presents a bar graph depicting the distribution of various diameters of circular culverts. The analysis reveals that the most prevalent diameters are 0.3 m (16%), 0.5 m (28%), and 0.6 m (13%).

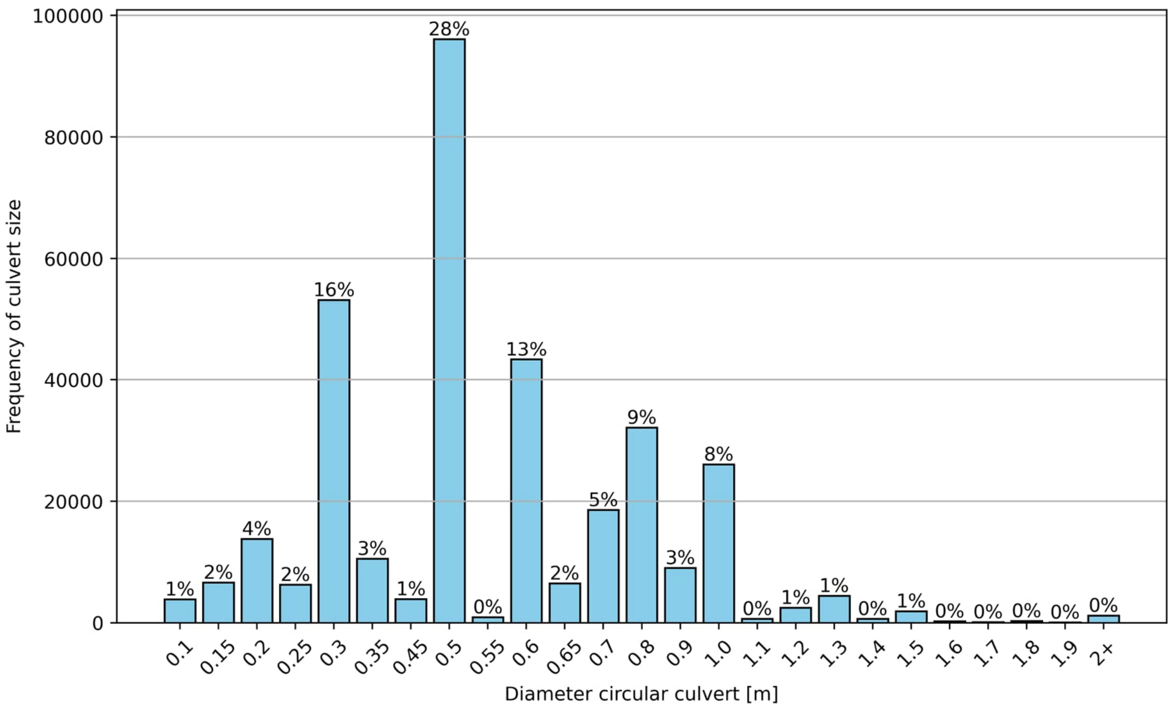

Figure 51: Frequency diagram of circular culverts with different diameters. The most common diameters are 0.3 m (16%), 0.5 m (28%) and 0.6 m (13%).

The following Figure 52 illustrates the distribution of culverts for each waterboard as a percentage of the total culverts. Additionally, the right image depicts the density of culverts per km.

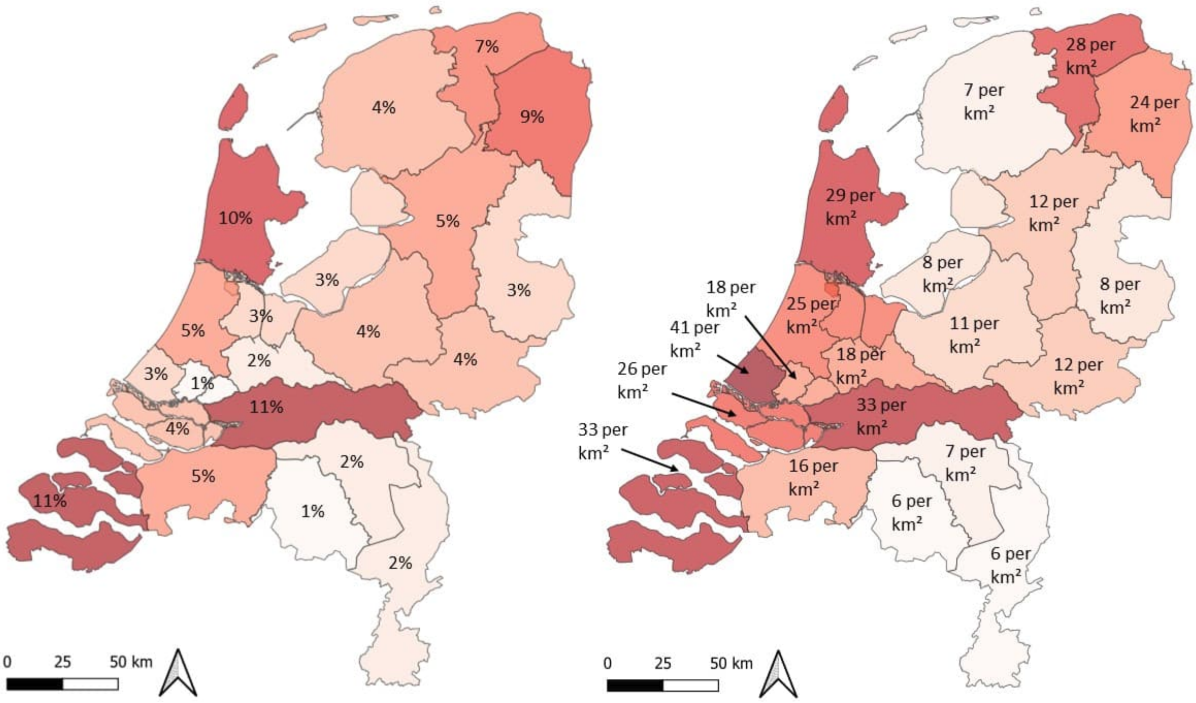

Figure 52: Left map shows distribution of culverts for each waterboard as a percentage of the total culverts. Right map shows density of culverts for each of the waterboards, with the number of culverts per km².

Figure 52 shows that the locations with a high density of culverts also have a high number of culverts, it can be found that most culverts are found in the west and in waterboards with rivers. Next, a histogram for the median length of circular and non-circular culverts has been plotted in Figure 53, followed by Figure 54 , which shows the total length of all culverts for each waterboard.

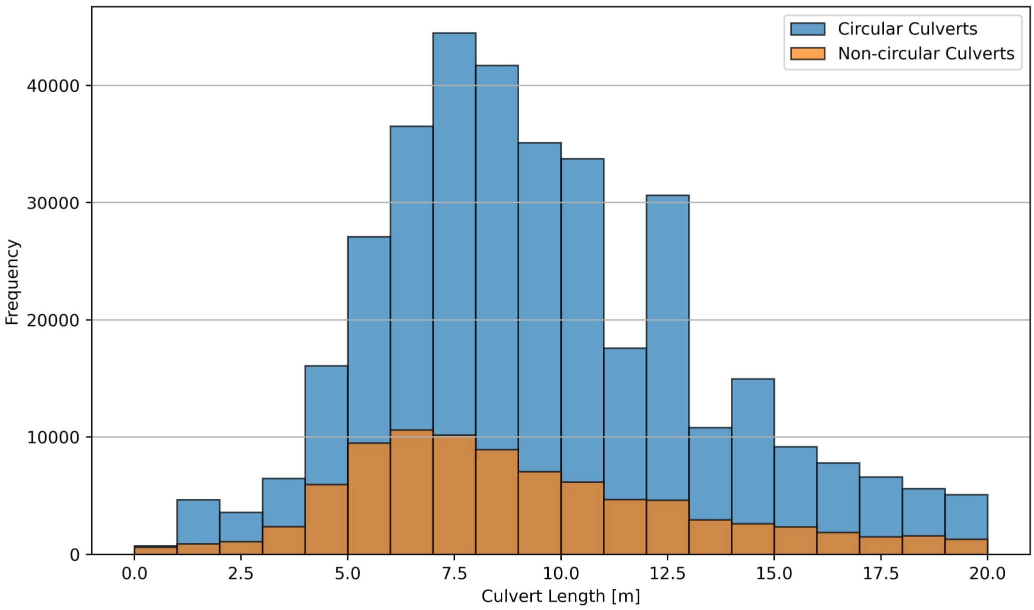

Figure 53: Histogram of median culvert length for circular and non-circular culverts.

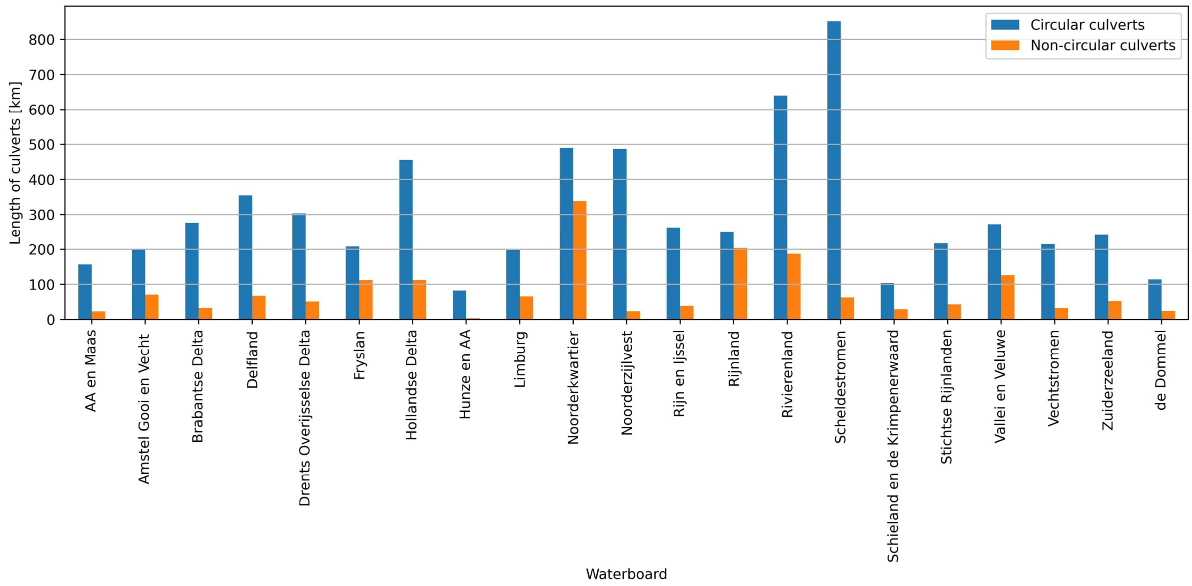

Figure 54: Total length of all culverts per waterboard in kilometres, separated between circular and non-circular culverts.

Figure 53 shows that the most common non-circular culvert length is found in the range of 6-8 meters, whereas for the circular culvert the range is between 6 and 12.5 meters. Figure 54 indicates that the waterboard Scheldestromen has a network of over 800 km of circular culverts, making it the longest. In contrast, Noorderkwartier holds the record for the longest length of non-circular culverts, exceeding 300 km.

B.2: Circular and rectangular culvert installation

From the culvert analysis (Section 2.2), it is found that circular culverts are dominant, which is explicable as circular culverts are favoured for their simple installation and cost-effectiveness compared to rectangular culverts. The installation of circular culverts is straightforward, as they can be placed in situ without emptying the watercourse. First, the watercourse is excavated at the correct location, indicated in Figure 55A. Next, the foundation is reinforced to prevent sinking. This is done by removing sludge and adding soil or sand to the intended elevation. Next, the culvert is installed, in the case of a PVC culvert this can be manually done by rolling as shown in Figure 55B. Larger diameter (more than 1 m) culverts often require concrete pipe elements that need to be handled using machinery. Once the culvert is in place and at the intended elevation, the surrounding soil is backfilled shown in Figure 55C. Lastly, a timber revetment can be placed when this is required as seen in Figure 55D.

Figure 55: Installation steps of round PVC culvert in a watercourse. A) Excavation of watercourse. B) Placement of culvert in excavated area. C) Backfilling of soil. D) Optional installation of timber revetment (Own work).

Installing rectangular concrete culverts poses greater challenges. Firstly, the work site must be prepared for dry installation of the culvert by halting the water flow. Subsequently, excavation and dewatering of the site are necessary as shown in Figure 56A. Depending on local conditions, a bypass might need to be constructed to allow some flow. Ensuring a stable foundation becomes crucial to support the weight of the rectangular culvert and prevent settling or misalignment of concrete sections. Depending on soil conditions and the weight of the structure, the installation may require a pile foundation upon which the installation can be placed, Figure 56B. For less heavy structures a sand foundation is used, in combination with wooden beams to facilitate the sliding of elements into position. Unlike round PVC culverts that can be simply rolled into place, the delivery and installation of rectangular culverts require cranes due to their substantial weight. Once in position, the various sections must be meticulously aligned and joined to create a uniform structure. This involves the precise positioning of heavy subcomponents, necessitating the use of heavy machinery, Figure 56C. Finally, backfilling and finishing are required to complete the installation of the rectangular culvert.

Figure 56: Installation of a concrete rectangular culvert. A) Drained work area with concrete foundation with pile foundation of 20 meters. B) Installation of a concrete element by crane. C) Sliding of concrete element into place using a digger. (IBKW, 2023)

Appendix C: Introduction to the Dutch polders

This appendix aims to deepen the understanding of Dutch polders by offering supplementary details discussed in Section 2.3, regarding a friction head loss of 4 cm/km and a per-structure head loss of 5 mm. These specified losses serve as a guide for designing a polder system, and they are not rigid and may fluctuate based on local conditions. When a smaller water level compartment is considered, larger losses from friction and structures can be accommodated without negative consequences, provided the allowable head loss remains constant.

By providing an example calculation, which illustrates the impact of head loss attributable to culverts and friction, a better understanding of the influence of available head loss in a water level compartment is gained. Equation (37) presents a simplified formula for calculating the maximum allowable head loss in a compartment, excluding the consideration of the height required for weirs to remain in free flow.

$$Maximum\ headloss = L_{watercourse} * 0.04 + N_{structures} * 0.005 \qquad (37)$$

With

$Maximum\ headloss$	Maximum head loss height	[m]
$L_{watercourse}$:	Length of the watercourse	[km]
$N_{structures}$:	Number of culverts in the watercourse	[-]

If the maximum head loss is restricted to 20 cm, it becomes possible to calculate the maximum number of culverts for varying ditch lengths. Table 17 shows the outcomes, while including an additional calculation where the maximum allowable head loss is extended to 30 cm. This highlights the delicate balance between available head loss and the number of structures.

Table 17: Ditch length and maximum number of structures in a fictitious watercourse. In which the loss due to a structure is 5 mm and has a water level slope of 4 cm/km as indicated in equation (37).

Length watercourse [km]	Maximum number of structures with a maximum allowable head loss of 20 cm	Maximum number of structures with a maximum allowable head loss of 30 cm
2	24	44
3	16	36
4	8	28

Table 17 demonstrates that the length of the watercourse is an influential factor in the maximum number of culverts allowed. Moreover, an additional 10 cm of allowable head loss increases the maximum number of structures significantly.

Appendix D: Literature review

In this appendix the results of the works of Idel'chik (1960), the U.S. Army Corps of Engineers (2016) are shown. These works present the loss coefficients for various culvert shapes when the profile is incorporated into the structure. Table 18 shows the entrance coefficient for circular culverts and Table 19 for rectangular box culverts. Exit loss coefficients (k_o) are assumed to be constant at k_o=1. In Figure 57 six cross-sectional images are shown of the different culvert shapes.

Table 18: Summarised standard entrance coefficients for circular culverts.

Circular pipe culverts		**Entrance loss coefficient K_e**
Projecting from fill	Socket end	0.2
	Square edge	0.5
Headwall	Socket end	0.2
	Rounded edge	0.2
	Square edge	0.5
Bevelled edges 33,7° or 45°		0.2
End-section conforming to fill slope		0.5
Mitred to conform to fill slope		0.7

Table 19: Summarised standard entrance coefficients for rectangular boxed culverts.

Rectangular Boxed culverts		**Entrance loss coefficient K_e**
Headwall without wingwalls	Rounded edge	0.2
	Square edge	0.5
Headwall with wingwalls at 30-75°	top rounded to a radius of 1/12	0.2
	Square edge	0.4
Headwall with wingwalls at 10-25°	Square edge	0.5
Wingwalls parallel (extension of sides) Square edge		0.7
Side or slope tapered inlet		0.2

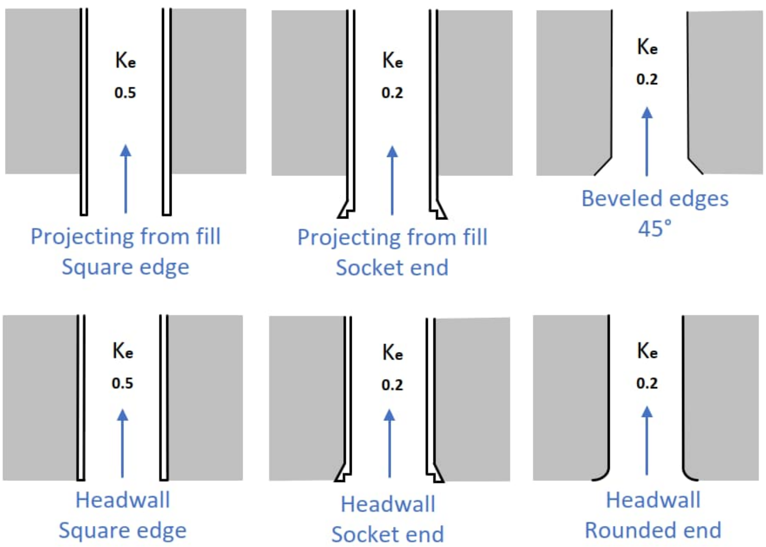

Figure 57: Example cross sections of the different shapes mentioned in Table 18 and Table 19.

Appendix E: Results of the flume experiment

In this appendix the results of the flume experiment are shown, this provides a more in-depth view of the results. First, a schematic of the flows in the flume experiment is shown in Figure 58.

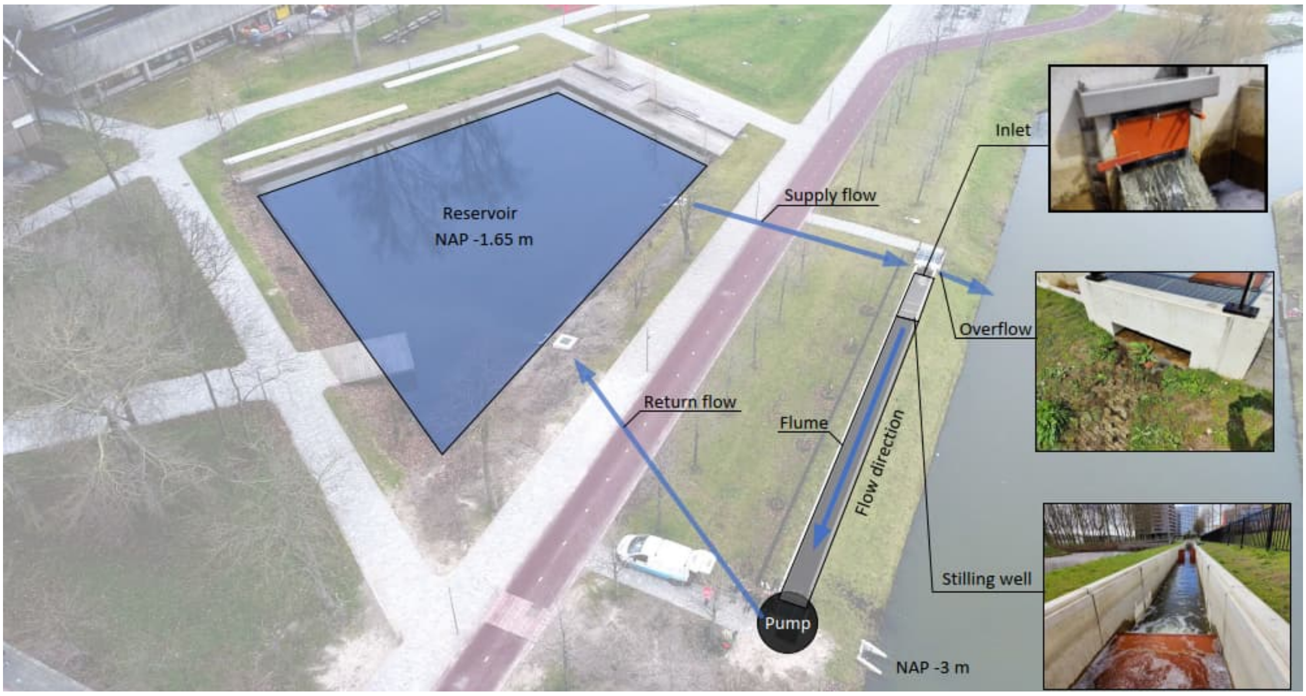

Figure 58: Schematic representation of the flows in and around the flume. Included are images of the stilling well at the beginning of the flume. An overflow into the adjacent watercourse to maintain a stable water level in the reservoir and the inlet construction is shown.

Figure 58 shows an aerial shot of the flume experiment, where water is let into the flume from the reservoir which is fed with water from the flume and neighbouring watercourse. To maintain a stable water level in the reservoir an overflow to the watercourse was used which made sure that a constant discharge was let into the flume.

Table 20: Results of the flume experiment, where the results of the different experiments are shown. Locations indicated originate from Figure 19.

Profile	**Water depth location 1.0 [cm]**	**Velocity measured at location 3 [m/s]**	**Water depth location 3 [cm]**	**Weir height [cm]**	**Discharge Velocity area method [m3/s]**	**WL difference location 1.1 - 5.1 [cm]**	**WL difference location 1.0 – 5.0 [cm]**	**WL difference location 1.0 – 5.1 [cm]**	**WL difference location 1.1 – 5.0 [cm]**	**WL difference location average [cm]**
90° inlet	27.2	0.8	24.5	0	0.09	3.6	3.4	3.5	3.4	3.5
45° inlet	26.8	0.8	24	0	0.09	2.9	2.8	3	2.7	2.9
Groove end inlet - 7,5cm	27	0.8	24	0	0.09	2.9	2.9	3.1	2.7	2.9
Groove end inlet - 3cm	27	0.8	25	0	0.10	2.8	2.7	3	2.5	2.7
Groove end inlet +45°		0.8	25	0	0.10	2.7	2.6	2.7	2.6	2.7
Exit widening	27.5	0.8	23.8	0	0.09	3.1	2.8	3.1	2.8	3
45° inlet + exit widening	26.5	0.8	23.5	0	0.09	2.4	2.2	2.3	2.3	2.3
90° inlet	22.5	0.7	20.5	0	0.10	3.1	2.6	3.1	2.6	2.9
45° inlet	22	0.7	20.6	0	0.07	2.7	2.2	2.8	2.2	2.5
Groove end inlet - 7,5cm	22.5	0.7	20.7	0	0.07	3.0	2.1	2.6	2.5	2.6
Groove end inlet -7,5cm+45°	22	0.7	20.7	0	0.07	2.6	2.1	2.5	2.1	2.3
Exit widening	23	0.7	21	0	0.08	3.4	2.5	2.6	3.3	2.9
45° inlet + exit widening	22.5	0.7	21	0	0.08	2.5	1.9	2.1	2.3	2.2
Half round inlet	23	0.7	20.6	0	0.08	2.8	2.1	2.3	2.7	2.5
Half round inlet	26.8	0.6	25.7	10	0.08	2.1	1	1.4	1.6	1.5
90° inlet	27.9	0.6	26.7	10	0.07	2.4	1.6	2.1	2	2
45° inlet	27.5	0.6	26.8	10	0.08	2.1	1.3	1.8	1.6	1.7
45° inlet + exit widening	27	0.6	26.5	10	0.07	1.7	1	1.4	1.3	1.3
Exit widening		0.6		10	0.07	2.2	1	1.4	1.8	1.6
Groove end inlet -3cm+half round	27.4	0.6	27	10	0.07	2.1	1	1.7	1.4	1.6
Groove end inlet - 3cm	27.3	0.6	27	10	0.08	1.7	1.2	1.3	1.7	1.5

Profile	Water depth location 1.0 [cm]	Velocity measured at location 3 [m/s]	Water depth locatio n 3 [cm]	Weir height [cm]	Discharge Velocity area method [m3/s]	WL difference location 1.1 - 5.1 [cm]	WL difference location 1.0 – 5.0 [cm]	WL difference location 1.0 – 5.1 [cm]	WL difference location 1.1 – 5.0 [cm]	WL differenc e location average [cm]
Groove end inlet +45°		0.6	27	10	0.08	1.9	1.1	1.4	1.5	1.5
90° inlet	34	0.7	30	10	0.08	2.8	1.9	2	2.7	2.3
45° inlet		0.7	30	10	0.10	2.3	1.6	1.8	2.1	1.9
Groove end inlet - 3cm		0.6	31	10	0.10	2.4	1.2	1.7	1.9	1.8
90° inlet	37	0.7	34	10	0.10	3.1	2.1	2.5	2.7	2.6
45° inlet	37	0.7	34.8	10	0.12	2.9	1.6	2.2	2.3	2.2
45° inlet+ exit widening		0.7	34	10	0.12	2.3	1.4	1.9	1.9	1.9
Groove end inlet - 3cm	36	0.7	34	10	0.12	2.6	1.7	2.2	2.1	2.2
Groove end inlet -3cm+ Half round		0.7	34	10	0.11	1.2	-0.6	-0.6	1.1	0.3

Appendix F: CFD model setup

This paragraph provides an overview of the basics of the CFD software "OpenFOAM", including the parameters and assumptions necessary to replicate results.
Computational fluid dynamics (CFD) serves as a versatile tool for simulating a wide range of water-related processes. It enables the analysis of fundamental principles, including mass continuity, momentum conservation, and energy conservation. Fluid motion is solved using the Navier-Stokes equations.
Section F.1 introduces the used software. Next, Section F.2 walks through the simulation workflow. Where Section F.3 shows the geometry and mesh, followed by Section F.4 which discusses the boundary and initial conditions. Lastly, in Sections F.5 and F.6 the turbulence model, solver selection and numerical schemes are discussed.

F.1: Software selection

Open-source Field Operation and Manipulation (OpenFOAM) is a free opensource software package which is mainly used for CFD. The version used is OpenFOAM version 2106. OpenFOAM is written in the C++ language and is pre-programmed with pre- and post-processing utilities. The geometry of the structures is made in Blender Version 3.4 which can be used to construct complex designs in 3D. For the visualisation of the flow and mesh another open-source software is used, ParaView version 5.7.0. ParaView is used to display the text-generated result of OpenFOAM in a Graphical User Interface (GUI). The solution of the calculations can be visualised in ParaView, and different kinds of analysis can be performed. Lastly, python scripts have been developed to automatically visualise the calculated results and watch the convergence of the relevant parameters.

F.2: Navigating the Simulation Workflow: From geometry to post-processing

Running a successful simulation involves several key steps: geometry setup, meshing, solving, and post-processing as summarised in Figure 59.

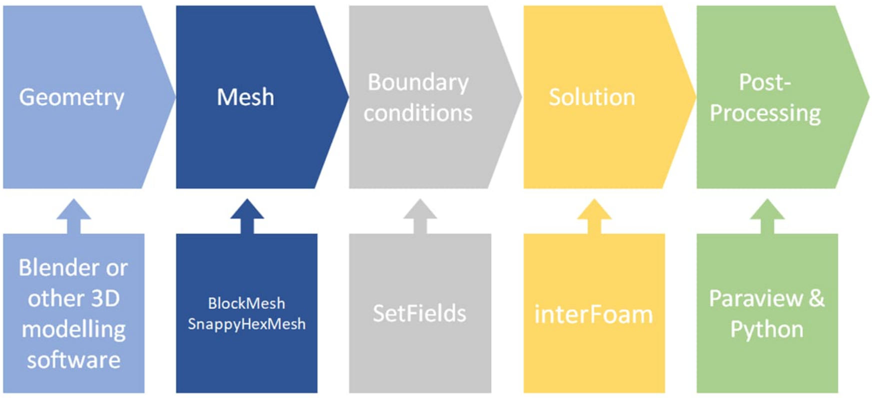

Figure 59: From left to right; Blender or any other 3D modelling software is used to make a model, using dictionaries BlockMesh and SnappyHexMesh this is turned into a mesh. Using the Setfield utility the boundary conditions are applied to the mesh and interFoam is used to run the simulation. Lastly, Paraview and Python are used to post-process the simulation results.

- First, the geometry of the model must be sketched in Blender or any other 3D modelling software. Following that patches can be joined into distinct groups. A basic model needs at least the following groups: inlet, outlet, walls, and atmosphere. Since these groups are

essential for adding the correct boundary conditions to the model. The patches must be exported as ASCII files with the STL file format.
- Secondly, the geometry is turned into a mesh by OpenFOAM, this is needed since the domain must be subdivided into multiple cells in which all the equations can be calculated. By changing the parameters of the meshing utility, it can be made coarse or fine. The shape of the mesh can also be changed, and zones that are of interest can be meshed with larger detail, these actions are performed using dictionaries such as *blockMesh* and *snappyHexMesh*.
- The third step is to set up the boundary conditions for the distinct groups and parameters needed for the solver. For this case, the incompressible *InterFoam* solver is used.
- The fourth step is to run the simulation, here the runtime of the simulation must be set and the number of cores to perform the calculation.
- The last step is to post-process the results using the Graphical User Interface (GUI) ParaView. Moreover, a Python script is developed to check the convergence of model parameters such as the water level and velocity.

F.3: Geometry and mesh

The initial phase of this study involves the creation of a three-dimensional (3D) model. The various materials in the model are of paramount importance, as each material category necessitates separate labelling and property assignment based on its inherent physical characteristics. Consequently, the first step involves defining these material patches when configuring the model.
To facilitate a direct comparison with the empirical data acquired from the flume experiment, the dimensions are replicated in the model. The physical dimensions of the flume encompass a length of 40 meters, a width of 1.5 meters, and a depth of expected water level + 20 cm.

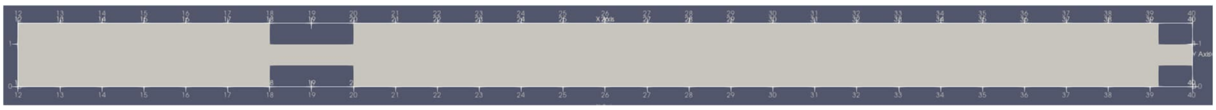

Figure 60: Top view of the model construction

The first 6 meters of the model are situated before the structure. The initial part of the inlet displays a developing flow, after which a fully developed flow occurs. The first section is kept as short as possible to reduce the number of computational cells and is thus shorter than in the flume. Once the flow has developed the structure is placed in the model. The structure has a length of 2 meters and obstructs two-thirds of the flume width, resulting in an opening of 0.5 meters. After the structure a 20-meter section is modelled, this is due to the reattachment length after the sudden expansion. Nortier & de Koning (2000) indicates a length of $8-10 * width\ of\ the\ channel$ which results in roughly 12 and 15 meters downstream of the structure.
To account for different material properties the mesh is subdivided into different patches. These patches can be used to apply material properties such as friction coefficient. Furthermore, they can be used to assign physical properties such as the discharge of the model. The patches used are *Inlet*, *outletAir, outletWater, atmosphere, walls, bottom, wallsDitch* and *profile*, shown in Figure 61.

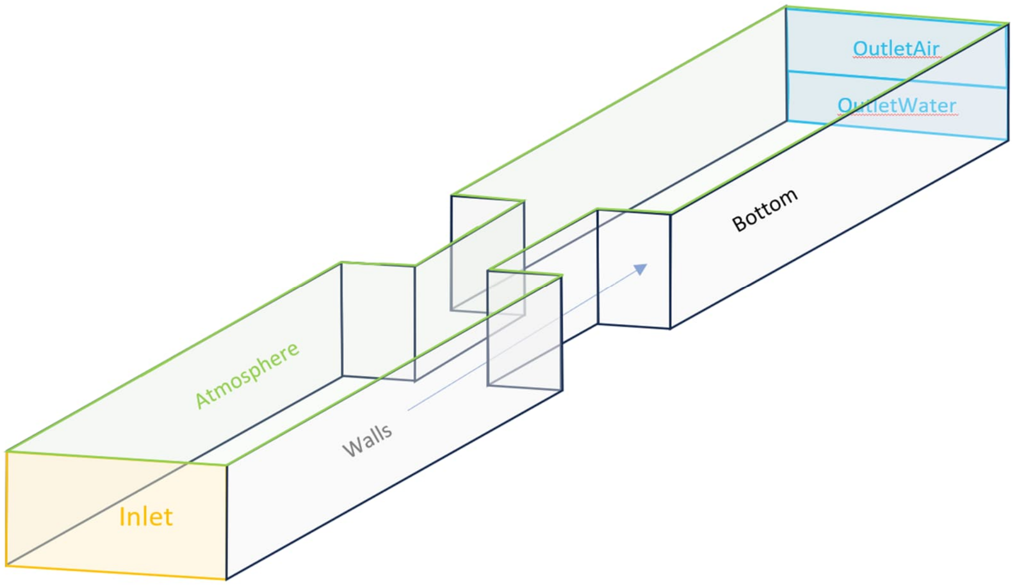

Figure 61: Image of 3D model, with the different patches shown in the model

After setting up the 3D model and dividing it into sections, we need to decide how to create the mesh for the model. Research by Keyes et al. (2000) and Bayón (2017) suggests that a structured mesh is the best choice for handling multiphase flows. For entirely rectangular models, using hexahedral cells for the mesh is the most suitable option. However, if the model includes circular or slanted shapes, polyhedral cells are needed to follow the shape precisely. Determining the ideal mesh size is specific to each case and involves a mesh sensitivity analysis. In this case, a mesh of 10 cm in the X-direction, 5 cm in the Y-direction and 2 cm in the Z-direction was found to be adequate, as shown in Figure 62. In areas around the profile and for the circular culvert the mesh size is increased to add detail to the mesh. This is performed to ensure a high resolution in the areas of interest which better simulates the relevant processes.

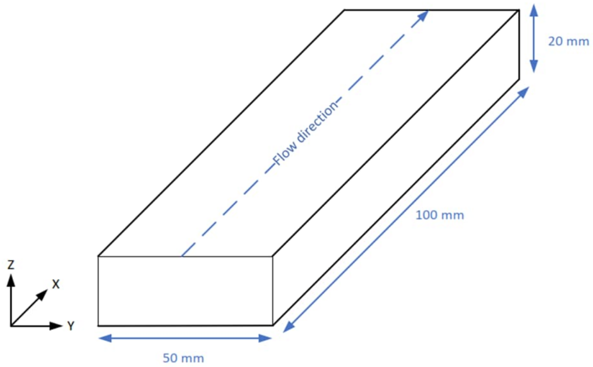

Figure 62: Element size of 100 mm in the X-direction (the direction of flow), 50 mm in the Y-direction, and 20 mm in the Z-direction.

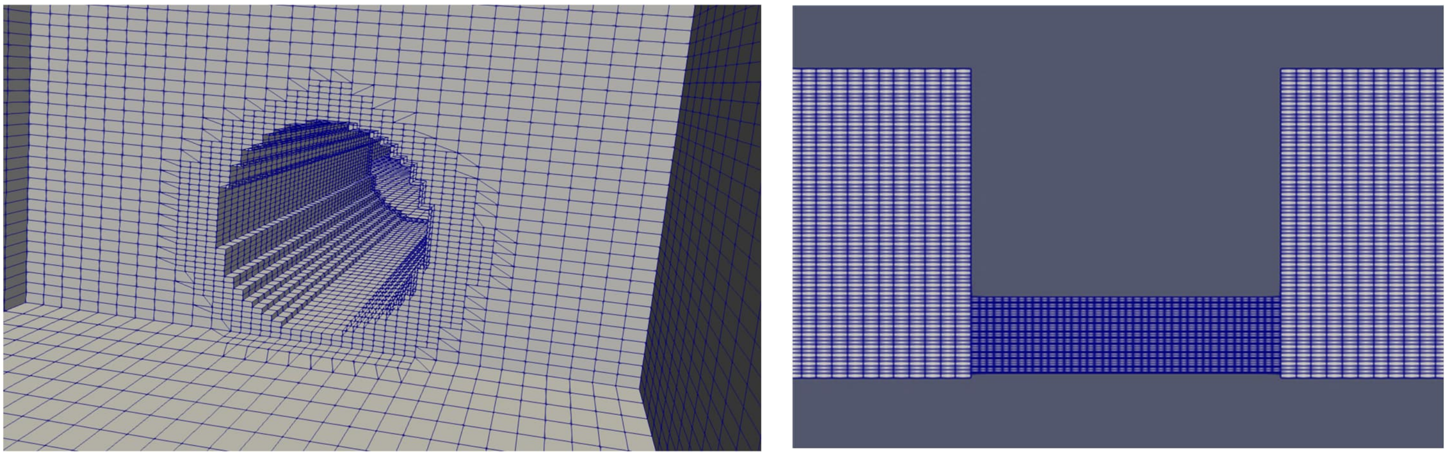

Figure 63: Left shows the entrance of the circular culvert, where mesh refinement is applied. The right image shows a side view at the location of the culvert that demonstrated mesh refinement along the culvert.

F.4: Boundary conditions initial conditions and runtime

Based on insights from Broecker et al. (2019) it is advisable to divide the outlet into separate water and air sections. This division helps maintain a fixed downstream water level while allowing the upstream water level to fluctuate.

Boundary patches

Inlet:

The inlet patch is used to let water enter the model domain. The boundary condition employs a constant discharge into the domain, whilst the water level is allowed to fluctuate over time. This is done to ensure that the unknown upstream water level can develop, a graphical representation is shown in Figure 64.

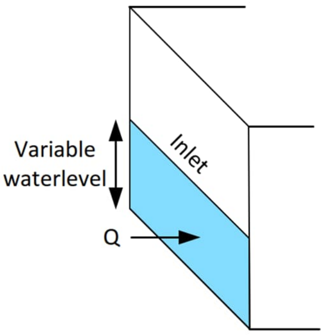

Figure 64: Schematisation of inlet patch in which the discharge in the model is constant and the water level is variable and unknown depending on conditions in the model.

Outlet:
The outlet patch is split into a water and air phase, *outletWater* and *outletAir* respectively. The purpose is to regulate the water level on the outlet side by determining the height of the *outletWater* patch, the discharge is matched to the inlet, see Figure 65. This mirrors real-life situations where large bodies of water experience minimal disturbance.

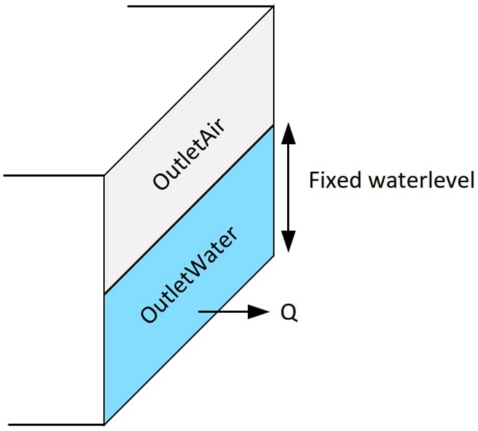

Figure 65: Schematisation of outlet patch in which the discharge out of the model is constant and the water level is fixed depending on downstream conditions.

Walls:
The walls patch is subdivided into, *bottom*, *walls*, *WallsDitch* and *profile*. Wall functions are used to describe these patches to reduce the computational cost of resolving flow close to the wall by making approximations based on the boundary layer theory.

Atmosphere:
The use of an atmosphere patch is needed, as the water-air interface can undergo vertical shifts. The *Atmosphere* patch maintains a constant atmospheric air pressure, permitting the ingress and egress of air as required.

A summarised overview of all boundary conditions employed for each variable is given in Table 21.

Table 21: CFD model parameters employed for the different patches, ZG: zeroGradient, VHFRIV: variableHeightFlowRateInletVelocity, VHFR:variableHeightFlowRate, FFP: fixedFluxPressure, nkRWF: nutkRoughWallFunction.

Variable	Inlet	OutletAir	OutletWater	Atmosphere	Walls/wallsDitch /Bottom/Profile
U	VHFRIV	ZG	flowRate InletVelocity	Pressure InletOutletVelocity	noSlip
k	fixedValue	inletOutlet	inletOutlet	inletOutlet	kqRWallFunction
p_rgh	FFP	FFP	FFP	totalPressure	FFP
nut	calculated	calculated	calculated	calculated	nkRWF
omega	fixedValue	inletOutlet	inletOutlet	inletOutlet	omegaWallFunction
alpha.water	VHFR	inletOutlet	ZG	inletOutlet	ZG

Initial conditions
Moving forward, the following section delves into the initial conditions of the model. To expedite the convergence of the equilibrium water level, the “setFields” dictionary is utilized to pre-fill the model with water, aligning the water level with the desired downstream level. Additionally, the inlet and outlet velocities are established. To initiate the model, the discharge is incrementally increased over a 60-second interval, allowing the model sufficient time to adapt and stabilize.

Model runtime
Model simulations indicate water level convergence usually happens within 1000-1500 seconds. The time step varies based on the Courant number, capped at 0.9, yielding an average step of 0.01-0.015 seconds. Utilizing 8 cores on Delftblue servers, simulations typically finish within 24 hours (Delftblue, 2022).

F.5: Turbulence model and solver

OpenFOAM offers various methodologies and models for turbulence modelling, due to its open-source nature. Tutorial cases, like "waterChannel," are customizable to meet individual needs. This thesis utilizes "waterChannel" due to its similarity to the intended model. Prior studies by Bayon (2017), Romagnoli et al. (2009), and Broecker (2021) have also used the solver InterFoam, whilst employing different turbulence models.

In this study, the incompressible multiphase solver known as interFoam is utilised. The selection of an incompressible solver is chosen because a constant fluid density is assumed. The choice of a multiphase solver is motivated by the objective of modelling the dynamic interface between water and air, commonly referred to as the free surface. Notably, interFoam adopts the Volume of Fluid (VOF) method as its principal mechanism for identifying and tracking the water-air interface (Scolari, 2023). Moreover, the interFoam solver is the most popular solver for these types of model simulations, as has been demonstrated in studies by Hemida, (2008); Leakey, (2019) and Scolari, (2023).

Choosing the appropriate turbulence model depends on factors such as geometry, computational resources, and the required level of detail. Common models used with the interFoam solver include Reynolds-Averaged Navier-Stokes (RANS, noted as RAS in OpenFOAM), Large Eddy Simulation (LES), and Detached Eddy Simulation (DES).

In this model, turbulence is represented using the k-ω SST turbulence model, a type of RANS model where turbulent fluctuations is parameterized. This choice aligns with the waterChannel tutorial case. The k-ω SST model is selected for its suitability in modelling flow around structures. It combines the advantages of the k-ω model, which performs well near solid walls, with the strong performance characteristics of the k-ε model at greater distances from walls (Alireza et al., 2018).

F.6: Numerical Schemes

It is chosen to not adapt the tutorial case with regards to the numerical schemes, although choices can be made for each of the schemes by picking the most stable, most accurate or best practice (CFD For Everyone, 2022) this is only necessary when the simulation crashes and other boundary conditions do not converge the model results. The numerical schemes used are shown in Table 22.

Table 22: Numerical schemes and their numerical approximation used in the model.

Numerical Scheme	Numerical approximation
ddtSchemes	Euler
gradSchemes	Gauss Linear
divSchemes	Gauss Linear, vanLeer, Upwind
laplacianSchemes	Gauss linear corrected
interpolationSchemes	Linear
snGradSchemes	Corrected
wallDist	meshWave

Appendix G: Results of CFD model

In this appendix all the individual results of the CFD model simulations are shown, showing information on culvert shape, profile shape, downstream water depth, culvert velocity and the results of the inlet and outlet loss coefficient.

G.1: Rectangular culvert results

For the results of the rectangular culvert, the shape, water depth, discharge, culvert velocity, entrance and exit loss coefficient have been displayed in Table 23.

Table 23: Individual CFD results of the model with a rectangular culvert. Locations indicated originate from Figure 19.

ID	Shape	Water depth loc 3 [m]	Discharge [m3/s]	Culvert velocity [m/s]	Entrance loss coefficient [-]	Exit loss coefficient [-]
1	Inlet 45° + outlet widening	0.35	0.083	0.47	0.21	0.39
2	Inlet 45° + outlet widening	0.35	0.125	0.67	0.22	0.49
3	Gradual widening outlet	0.35	0.083	0.47	0.67	0.36
4	Gradual widening outlet	0.35	0.125	0.68	0.63	0.45
5	Groove end inlet	0.35	0.083	0.47	0.31	0.60
6	Groove end inlet	0.35	0.125	0.67	0.37	0.53
7	Half round inlet	0.35	0.083	0.47	0.21	0.54
8	Half round inlet	0.35	0.083	0.46	0.32	0.58
9	Half round inlet	0.35	0.125	0.66	0.17	0.60
10	Half round inlet	0.35	0.125	0.66	0.27	0.63
11	Inlet with 45° wingwalls	0.27	0.083	0.57	0.18	0.60
12	Inlet with 45° wingwalls	0.27	0.083	0.57	0.20	0.60
13	Inlet with 45° wingwalls	0.35	0.083	0.47	0.20	0.57
14	Inlet with 45° wingwalls	0.31	0.1	0.61	0.20	0.57
15	Inlet with 45° wingwalls	0.35	0.1	0.55	0.21	0.53
16	Inlet with 45° wingwalls	0.35	0.12	0.59	0.26	0.46
17	Inlet with 45° wingwalls	0.35	0.12	0.66	0.23	0.54
18	Inlet with 45° wingwalls	0.35	0.12	0.71	0.19	0.57
19	Inlet with 45° wingwalls	0.35	0.125	0.67	0.22	0.57
20	Square edged in and outlet	0.27	0.075	0.50	0.59	0.53
21	Square edged in and outlet	0.26	0.075	0.59	0.56	0.53

ID	Shape	Water depth loc 3 [m]	Discharge [m3/s]	Culvert velocity [m/s]	Entrance loss coefficient [-]	Exit loss coefficient [-]
22	Square edged in and outlet	0.27	0.083	0.57	0.57	0.54
23	Square edged in and outlet	0.35	0.083	0.47	1.38	0.43
24	Square edged in and outlet	0.31	0.1	0.60	0.58	0.54
25	Square edged in and outlet	0.31	0.1	0.55	0.58	0.54
26	Square edged in and outlet	0.31	0.1	0.60	0.56	0.50
27	Square edged in and outlet	0.31	0.1	0.72	0.33	0.65
28	Square edged in and outlet	0.49	0.1	0.41	0.58	0.52
29	Square edged in and outlet	0.49	0.1	0.41	0.57	0.52
30	Square edged in and outlet	0.35	0.1	0.55	0.57	0.53
31	Square edged in and outlet	0.35	0.12	0.58	0.54	0.55
32	Square edged in and outlet	0.35	0.12	0.66	0.53	0.53
33	Square edged in and outlet	0.35	0.12	0.71	0.50	0.56
34	Square edged in and outlet	0.35	0.125	0.68	0.55	0.53
35	Square edged in and outlet	0.35	0.125	0.62	0.65	0.51
36	Square edged in and outlet	0.35	0.125	0.68	0.56	0.52
37	Square edged in and outlet	0.35	0.125	0.67	0.56	0.54
38	Square edged in and outlet	0.35	0.125	0.59	0.77	0.74

G.2: Circular culvert results

For the circular culvert different model runs have been performed. Table 24 shows the individual results with information on the shape. water depth. discharge. culvert velocity and loss coefficients.

Table 24: Individual CFD results of the model with a circular culvert. Locations indicated from Figure 19.

ID	shape	Discharge [m3/s]	Culvert diameter [m]	Water depth loc 3 [m]	Culvert velocity [m/s]	Entrance loss coefficient [-]	Exit loss coefficient [-]
1	Gradual widening outlet	0.19	0.5	0.6	0.96	0.62	0.50
2	Gradual widening outlet	0.125	0.5	0.6	0.63	0.61	0.38
3	Gradual widening outlet	0.125	0.5	1.1	0.64	0.64	0.71
4	Gradual widening outlet	0.19	0.5	1.1	0.97	0.67	0.71
5	Groove end inlet	0.19	0.5	0.6	0.96	0.28	0.64
6	Groove end inlet	0.125	0.5	0.6	0.64	0.31	0.60
7	Groove end inlet	0.125	0.5	1.1	0.64	0.31	0.76
8	Groove end inlet	0.19	0.5	1.1	0.97	0.30	0.77
9	Half round inlet	0.19	0.5	0.6	0.96	0.25	0.68
10	Half round inlet	0.125	0.5	0.6	0.64	0.29	0.62
11	Half round inlet	0.125	0.5	1.1	0.64	0.31	0.77
12	Half round inlet	0.19	0.5	1.1	0.97	0.31	0.78
13	Inlet with 45 deg wingwalls	0.19	0.5	0.6	0.97	0.40	0.65
14	Inlet with 45 deg wingwalls	0.125	0.5	0.6	0.64	0.42	0.60
15	Inlet with 45 deg wingwalls	0.125	0.5	1.1	0.64	0.50	0.76
16	Inlet with 45 deg wingwalls	0.19	0.5	1.1	0.97	0.50	0.76
17	Square edged in and outlet	0.19	0.5	0.6	0.97	0.58	0.61
18	Square edged in and outlet	0.125	0.5	0.6	0.64	0.54	0.59
19	Square edged in and outlet	0.125	0.5	0.6	0.63	0.48	0.68
20	Square edged in and outlet	0.125	0.5	0.6	0.63	0.54	0.62
21	Square edged in and outlet	0.125	0.5	1.1	0.64	0.68	0.76
22	Square edged in and outlet	0.125	0.5	1.1	0.64	0.63	0.75
23	Square edged in and outlet	0.19	0.5	1.1	0.97	0.65	0.76
24	Square edged in and outlet	0.19	0.5	1.1	0.97	0.65	0.75

ID	shape	Discharge [m3/s]	Culvert diameter [m]	Water depth loc 3 [m]	Culvert velocity [m/s]	Entrance loss coefficient [-]	Exit loss coefficient [-]
25	Square edged in and outlet	0.19	0.5	1.1	0.92	0.63	0.76
26	Square edged in and outlet	0.08	0.3	0.6	1.13	0.68	0.81
27	Square edged in and outlet	0.085	0.3	0.6	1.18	0.67	0.85
28	Square edged in and outlet	0.09	0.3	0.6	1.27	0.68	0.82
29	Square edged in and outlet	0.095	0.3	0.6	1.33	0.68	0.85
30	Square edged in and outlet	0.1	0.3	0.6	1.40	0.68	0.82
31	Square edged in and outlet	0.105	0.3	0.6	2.11	0.69	0.81
32	Square edged in and outlet	0.08	0.5	0.6	0.41	0.58	0.58
33	Square edged in and outlet	0.085	0.5	0.6	0.43	0.56	0.61
34	Square edged in and outlet	0.09	0.5	0.6	0.46	0.19	0.61
35	Square edged in and outlet	0.095	0.5	0.6	0.48	0.58	0.61
36	Square edged in and outlet	0.1	0.5	0.6	0.51	0.64	0.59
37	Square edged in and outlet	0.105	0.5	0.6	0.77	0.67	0.48
38	Square edged in and outlet	0.025	0.3	1.2	0.35	0.61	0.83
39	Square edged in and outlet	0.057	0.3	1.2	0.80	0.70	0.90
40	Square edged in and outlet	0.078	0.3	1.2	1.09	0.70	0.91
41	Square edged in and outlet	0.069	0.5	1.2	0.35	0.60	0.73
42	Square edged in and outlet	0.157	0.5	1.2	0.80	0.64	0.76
43	Square edged in and outlet	0.216	0.5	1.2	1.10	0.65	0.78
44	Square edged in and outlet	0.176	0.8	1.2	0.35	0.87	0.49
45	Square edged in and outlet	0.402	0.8	1.2	0.80	0.55	0.49
46	Square edged in and outlet	0.553	0.8	1.2	1.10	0.56	0.49
47	Square edged in and outlet	0.125	0.3	1.2	1.76	0.69	0.92
48	Square edged in and outlet	0.125	0.5	1.2	0.64	0.65	0.76
49	Square edged in and outlet	0.125	0.8	1.2	0.25	0.63	0.75